Min-Bias Data: Jet Evolution and Event Shapes

Rick Field and David Stuart

July 1, 1999

Abstract

The Min-Bias data are used to study the transition between "soft" and "hard" collisions. We study this transition by plotting a variety of observables versus PTmax (*leading charged particle*) and PT(jet#1) (*leading jet*). The data are compared with "soft" scattering Monte-Carlo models and "hard" scattering QCD Monte-Carlo models. The data contain a lot of "hard" scattering and exhibit "jet structure" even for PT values as small as 1 GeV. We define "jets" as simple circular regions in η-ϕ space with R = 0.7 and watch the growth and development of "jets" from 0.5 to 50 GeV. "Jets" are "born" somewhere around PT(jet) of about 1 GeV with, on the average, about 2 charged particles and grow to, on the average, about 10 charged particles at 50 GeV. The QCD "hard" scattering Monte-Carlo models are in qualitative agreement with the properties of "jets" and agree as well with 2 GeV "jets" as they do with 50 GeV "jets". We also examine carefully the growth and development of the "underlying event" in "hard" scattering. None of the QCD Monte-Carlo models describe properly the behavior of the underlying event. Accurate predictions of detector occupancies and physics backgrounds in Run II depend on the correct modeling of min-bias interactions and the underlying event.

I. Introduction

The total proton-antiproton cross section is the sum of the elastic and inelastic cross sections. The inelastic cross section consists of a single-diffractive, double-diffractive, and "hard core" component. The "hard core" component is everything non-diffractive, it is what is left after one removes the single-diffractive and the double-diffractive events. The CDF minimum bias trigger selects predominately the "hard core" component of the inelastic cross section. "Hard core", of course, does not necessarily imply "hard scattering". A "hard scattering"

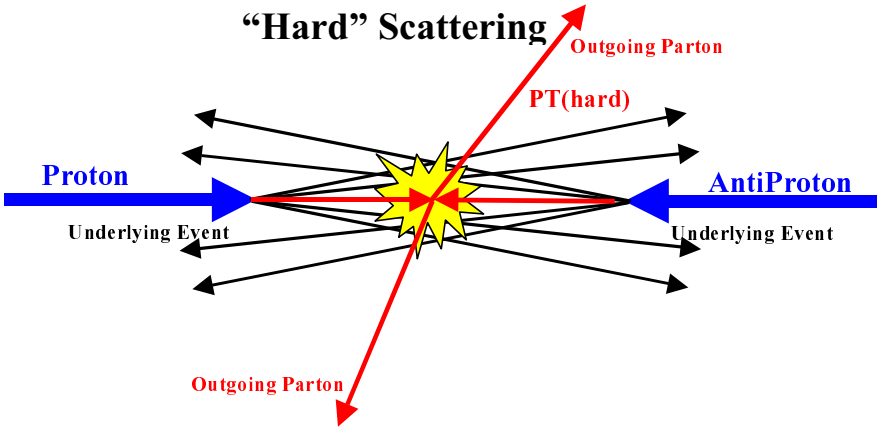

Fig. 1.1. Illustration of a proton-antiproton collision in which a "hard" 2-to-2 parton scattering with transverse momentum, P_T(hard), has occurred. The resulting event contains particles that originate from the two outgoing partons and particles that come from the

breakup of the proton and antiproton (*i.e.* "beam-beam remnants") that contribute to the "underlying event".

collision, such as that illustrated in Fig. 1.1, is one in which a "hard" (*i.e.* large transverse momentum, PT(hard)) 2-to-2 parton-parton subprocess has occurred. "Soft" hard core collisions, such as the one shown in Fig. 1.2, corresponds to events in which no "hard" interaction has occurred. When there is no large transverse momentum subprocess in the collision one is not probing short distance and it probably does not make any sense to talk about partons.

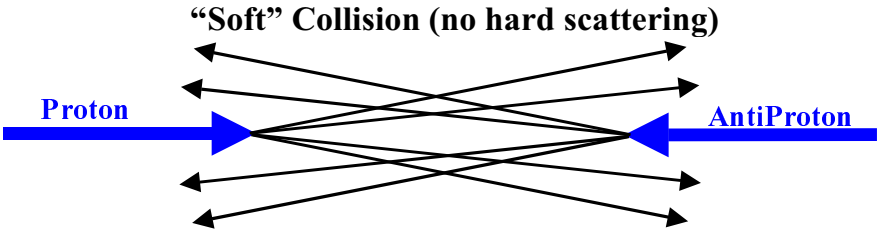

Fig. 1.2. Illustration of a "soft" proton-antiproton collision in which no hard scattering has occurred. The proton and antiproton ooze through each other and fall apart.

The minimum bias data is an excellent place to study the transition between "soft" and "hard" collisions. Ultimately, the goal is to find a Monte-Carlo generator that will fit the entire "hard core" inelastic cross section. To do this one will have to combine a model for the "soft" collisions with a QCD perturbative Monte-Carlo model for the "hard" collisions. The QCD perturbative 2-to-2 parton-parton differential cross section diverges as PT(hard) goes to zero. One must set a minimum PT(hard) large enough so that the resulting cross section is not larger that the total entire "hard core" inelastic cross section, and large enough to ensure that QCD perturbation theory is accurate. A non-perturbative "soft" model would then be used to describe (*or parameterize*) the remaining "hard core" inelastic cross section (*i.e.* all collisions in which PT(hard) is less than the cut-off). We do not attempt such a superposition of "soft" and "hard" models here. In this note on the physics of the min-bias data we simply compare the data with the models, "soft" and "hard scattering". We find that at 1.8 TeV that there is a lot of "hard scattering" in the min-bias data and we will be able to examine the evolution of "jets" from low to high transverse momentum.

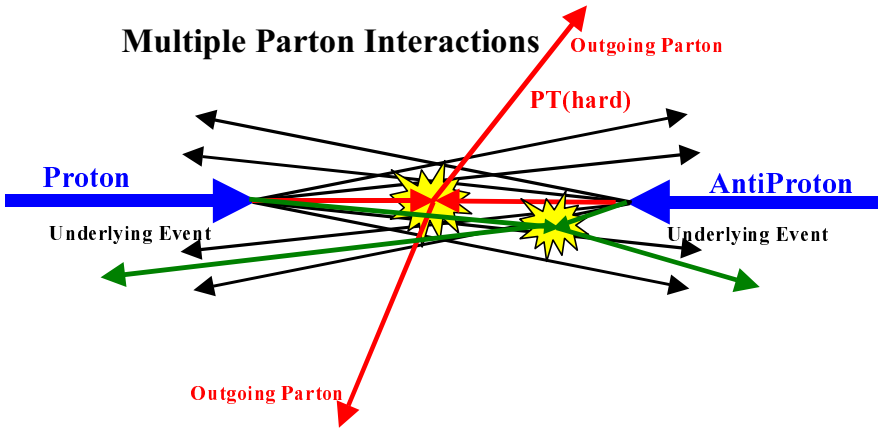

Fig. 1.3. Illustration of a proton-antiproton collision in which a multiple parton interaction has occurred. In addition to the "hard" 2-to-2 parton scattering with transverse momentum, $P_T(hard)$, there is a "semi-hard" parton-parton scattering that contributes particles to the "underlying event".

A "hard scattering" event, like that shown in Fig. 1.1 consists of large transverse momentum outgoing hadrons that originate from the large transverse momentum partons (*i.e.* outgoing "jets") and also hadrons that originate from the break-up of the proton and antiproton (*i.e.* the "beam-beam remnants"). The "underlying event" is an interesting object that is not very well understood. In addition to hadrons from the break-up of the initial proton and antiproton, it may contain hadrons resulting from initial state gluon radiation. Also, it is possible that the underlying event contains hadrons that originate from multiple parton interactions as illustrated in Fig. 1.3. Pythia, for example, uses multiple parton interactions as a way to enhance the activity of the underlying event. Since we are attempting to describe entire min-bias events, we will be able to examine closely the growth and structure of the underlying event. We find that the underlying "hard" scattering event is not the same as the "soft" collision illustrated in Fig. 1.2. For the same available energy the underlying event in a "hard" scattering is considerable more active (*i.e.* higher charge particle density and more transverse momentum) than a "soft" collision. This is not surprising since a violent "hard" scattering has occurred! We find that none of the QCD Monte-Carlo models describe properly the behavior of the underlying event.

A good way to watch the transition between "hard" and "soft" collisions is to plot observables versus the maximum transverse momentum particle in the event, PTmax. If PTmax is large then clearly a "hard" scattering has occurred and if PTmax is small there was no "hard" scattering. After we discuss the data selection and Monte-Carlo models in Section II, we study the overall event structure of the Min-Bias data as a function of PTmax in Section III. We use the TRACK12 data to extend the range of PTmax. Combining the Min-Bias and the TRACK12 allows us to examine events with PTmax from 0.5 GeV to 25 GeV. We do not define "jets" in Section III, nevertheless the "jet" structure in the data is clearly seen, even for PTmax values as low as 1 GeV. Furthermore, we examine carefully the growth and development of the underlying event as a function of PTmax.

In Section IV, we define "jets" as simple circular regions in η-ϕ space with R = 0.7 and watch the growth and development of "jets" from 0.5 to 50 GeV. We use the JET20 data to extend the range of P_T(jet#1) (*leading jet*). In addition, we examine carefully the growth and development of the underlying event as a function of P_T(jet#1). We reserve Section IV for summary and conclusions. There are many more interesting Min-Bias data plots than we can put in the this note. We plan to write a second CDF note on the physics of the Min-Bias data that examines the differential cross sections in P_T, PTmax, PTsum, P_T(jet), and P_T(jet#1).

II. Data Selection and Monte-Carlo Models

In this analysis we use the three sets of data listed in Table 1. The minimum bias (min-bias) data were selected by requiring at least two interactions in the beam-beam counters located at high pseudo-rapidity (at least one forward *and* at least one backward) as illustrated in Fig. 2.1. We

consider only charged particles with $P_T > 0.5$ GeV and $|\eta| < 1$ where the CTC efficiency is high. Also, to improve the purity we select events with zero or one vertex and in addition require that the intercept of the charged track with the beam axis, z_c, lies within 2 cm of the vertex, z_v, which reduces fakes and helps remove secondary interactions.

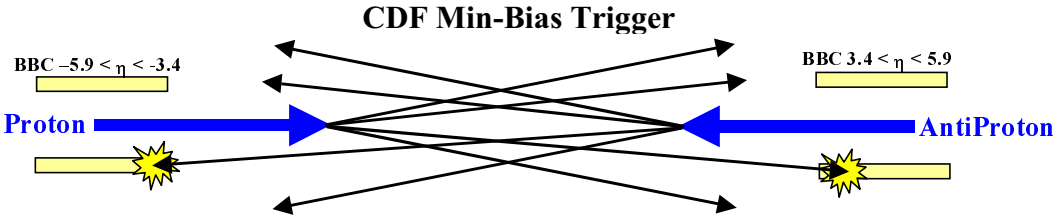

Fig. 2.1. Illustration of the CDF min-bias trigger in which at least one charge particle must interact with the forward beam-beam counter BBC ($3.4 < \eta < 5.9$) *and* at least one charge particle must interact with the backward BBC ($-5.9 < \eta < -3.4$).

Table 1. Data sets and selection criterion used in this analysis.

CDF Data Set	Trigger	Events	Selection
Min-Bias	Min-Bias Trigger (Fig. 2.1)	634,800	zero or one vertex in $\|z\| < 100$ cm $\|z_c - z_v\| < 2$ cm $P_T > 0.5$ GeV, $\|\eta\| < 1$
TRACK12	Charged particle track in the with $P_T > 12$ GeV (ONE_CFT_NTRK_12)	60,884	zero or one vertex $\|z_c - z_v\| < 2$ cm $P_T > 0.5$ GeV, $\|\eta\| < 1$
JET20	Calorimeter tower cluster with $E_T > 20$ GeV	32,874	zero or one vertex $\|z_c - z_v\| < 2$ cm $P_T > 0.5$ GeV, $\|\eta\| < 1$

The three "soft" Monte-Carlo models considered in this analysis are listed in Table 2. There is no theory for "soft" collisions (perturbation theory is not valid). All the "soft" models are essentially parameterizations. Isajet's soft "min-bias" generator [1] uses a model based on a "cut Pomeron" with Poisson fluctuations. At 1.8 TeV it produces 7.8 charged particles in the range $P_T > 0$ and $|\eta| < 1$, or roughly 3.9 charged particles per unit rapidity with a $\langle P_T \rangle$ of around 400 MeV. Herwig's "min-bias" generator [2] also produces 7.8 charged particles in the range $P_T > 0$ and $|\eta| < 1$ with a $\langle P_T \rangle$ of 430 MeV.

Table 2. "Soft" theoretical Monte-Carlo models studied in this analysis.

Monte-Carlo Model	Subprocess	Comments
Herwig 5.9	"Soft" collisions: IPROC = 8000	Herwig's soft "min-bias" generator
Isajet 7.32	"Soft" collisions: MINBIAS	Isajet's soft "min-bias" generator
MBR	"hard core" component: iproc = 1	Rockefeller's "min-bias" generator version 2

MBR is a "soft" Monte-Carlo generator written by the Rockefeller group [3], that conserves energy, momentum, and charge. At 1.8 TeV it produces 7.6 charged particles in the range $P_T > 0$ and $|\eta| < 1$, or roughly 3.8 charged particles per unit rapidity with a $\langle P_T \rangle$ of 530 MeV. MBR agrees well with the overall multiplicity and P_T distributions of the Min-Bias data. All the "soft" models have no correlations (except for resonances and momentum conservation) and, as we will see, the data have strong correlations associated with "jets" and hard scattering.

The "hard" scattering QCD Monte-Carlo models used in this analysis are listed in Table 3. Each of the QCD Monte-Carlo models handle the "beam-beam remnants" (Fig. 1.1) in a similar fashion. A hard scattering event is basically the superposition of a hard parton-parton interaction on top of a "soft" min-bias type collision. Herwig [2] assumes that the underlying event is a soft collision between the two "beam clusters". Isajet [1] uses a model similar to the one it uses for soft "min-bias" events (*i.e.* "cut Pomeron"), but with different parameters, to describe the underlying beam-beam remnants. Pythia [4] assumes that each incoming beam hadron leaves behind a "beam remnant", which do not radiate initial state radiation, and simply sail through unaffected by the hard process. However, unlike Herwig and Isajet, Pythia also uses multiple parton interactions to enhance the activity of the underlying event as illustrated in Fig. 1.3.

Table 3. Theoretical QCD "hard" scattering Monte-Carlo models studied in this analysis. In all cases we take PT(hard) > 3 GeV.

Monte-Carlo Model	Subprocesses	Comments
Herwig 5.9	QCD 2-to-2 parton scattering: IPROC = 1500	Default values for all parameters
Herwig EN2	QCD 2-to-2 parton scattering: IPROC = 1500	Underlying event multiplicity enhancement factor: ENSOF = 2.0
Herwig EN4	QCD 2-to-2 parton scattering: IPROC = 1500	Underlying event multiplicity enhancement factor: ENSOF = 4.0
Isajet 7.32	QCD 2-to-2 parton scattering: TWOJET	Default values for all parameters
Pythia 6.115	QCD 2-to-2 parton scattering: MSEL = 1	Default values for all parameters: PARP(81) = 1.4
Pythia 6.125	QCD 2-to-2 parton scattering: MSEL = 1	Default values for all parameters: PARP(81) = 1.9
Pythia No MS	QCD 2-to-2 parton scattering: MSEL = 1	Pythia 6.125 with no multiple parton interactions : MSTP(81) = 0
Pythia 4097	QCD 2-to-2 parton scattering: MSEL = 1	Pythia 6.115 with the multiple scattering parameters set according to CDF Note #4097: MSTP(81) = 1 MSTP(82) = 3 PARP(81) = 1.4 PARP(82) = 1.55 PARP(85) = 1.0 PARP(86) = 1.0 MSTP(33) = 1 PARP(31) = 1.69 PARJ(21) = 0.613

In this analysis we examine four versions of Pythia including Pythia 6.115 and Pythia 6.125 both with the default values for all the parameters. The default values changed in going from version 6.115 to 6.125. In particular, the effective minimum transverse momentum for multiple parton interactions, PARP(81), changed from 1.4 GeV in version 6.115 to 1.9 GeV in version 6.125.

Increasing this cut-off decreases the multiple parton interaction cross section which reduces the amount of multiple parton scattering. Pythia 4097 is Pythia 6.115 with the multiple parton interaction parameters set according to the "tuned" fit from CDF Note #4097 [5]. In this note, a set of Pythia parameters were tuned to fit the structure of the underlying event in reactions with B candidates. The high statistics B^+ to lepton D^0 data set was used and a comparison with the W data was also made. Pythia 4097 has a tremendous amount of multiple parton scattering and does not agree with the data presented here. For completeness, we also consider a version of Pythia with no multiple scattering (MSTP(81)=0).

Isajet and Herwig do not include multiple parton interactions. In Isajet and Herwig the underlying event arises solely from the breakup of the beams (i.e. beam-beam remnants) and from initial state radiation. If a QCD Monte-Carlo model does not describe correctly the underlying event, it is very difficult to say if this due to the lack of multiple parton interactions or due to a poor parameterization of the beam-beam remnants. We investigate this a bit by considering three versions of Herwig. The default version of Herwig 5.9, plus a version with ENSOF =2 and a version with ENSOF = 4. ENSOF is a Herwig parameter that effects the multiplicity of the underlying event by changing the energy, W_{cm}, at which the underlying event multiplicity is calculated. The underlying event is assigned the multiplicity of a "soft" hadron-hadron collision an energy of ENSOF times W_{cm}.

In comparing the Monte-Carlo models with the Min-Bias data, we require that the Monte-Carlo events satisfy the CDF min-bias trigger (see Fig. 2.1) and we apply an 8% correction for the CTC efficiency. The CTC efficiency can vary substantially for very low P_T tracks and in dense high P_T jets ($PT(jet) > 125$ GeV). To avoid this we consider only the region $P_T > 0.5$ GeV and $|\eta| < 1$ where the CTC efficiency is high and stable (assumed to be 92% efficient) and we restrict ourselves to jets less the 50 GeV. Our conclusions are not sensitive to variations in the tracking efficiency.

III. Studying the Event Structure as a Function of PTmax

It is instructive to examine collider observables as a function of the charged particle with the maximum transverse momentum in the event (called PT_{max}). There is just one PT_{max} per event. Here it is not necessary to define "jets" and PT_{max} is an excellent probe that distinguishes between "hard" and "soft" scattering. Clearly if PT_{max} is large, a "hard" scattering has occurred. We will plot observables versus PT_{max} and examine the transition from "soft" to "hard" scattering.

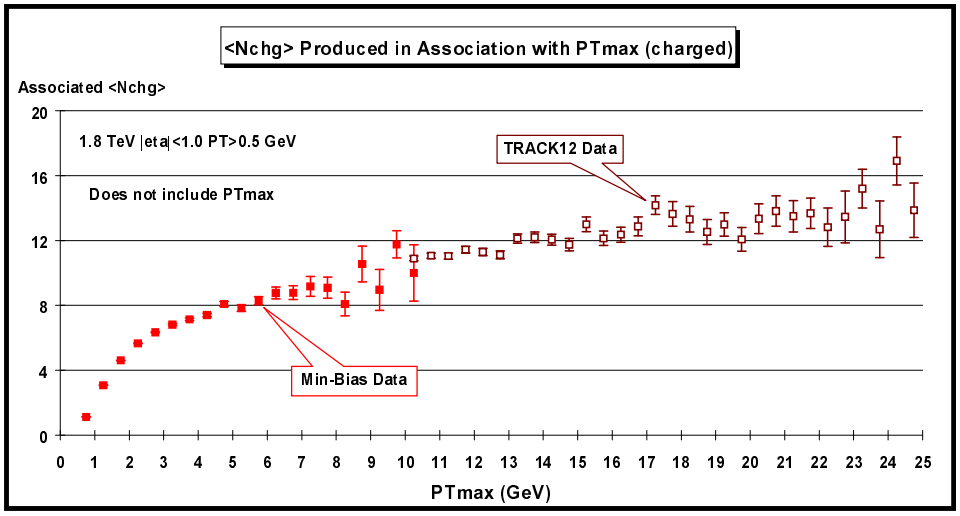

Fig. 3.1. Average number of "associated" charged particles ($P_T > 0.5$ GeV and $|\eta| < 1$) as a function of PTmax (*leading charged particle*). Each point corresponds to the <Nchg> in a 0.5 GeV bin (*not including PTmax*). The solid (open) points are the Min-Bias data (TRACK12 data). The data have not been corrected for efficiency.

(1) "Associated" Nchg and "Associated" PTsum versus PTmax

Fig. 3.1 shows the average number of "associated" charged particles ($P_T > 0.5$ GeV and $|\eta| < 1$) as a function of PTmax (*leading charged particle*) for the Min-Bias and TRACK12 data. Here one plots <Nchg> not including PTmax. It is the number of charged particles that are produced in association with PTmax. The TRACK12 data connect on smoothly to the Min-Bias data and allows us to study observables over the range $0.5 < PTmax < 25$ GeV. There is a small overlap region where the Min-Bias and TRACK12 data agree. The errors are only statistical and the data have not been corrected for efficiency (*the true multiplicities are about 9% larger*). Fig. 3.1 shows a fast rise in the "associated" multiplicity at low PTmax and then a flattening out at high PTmax. For events with PTmax around 0.5 GeV, the "associated" charge particle multiplicity is about 1 ($P_T > 0.5$ GeV and $|\eta| < 1$) and for PTmax around 2 GeV it is about 6.

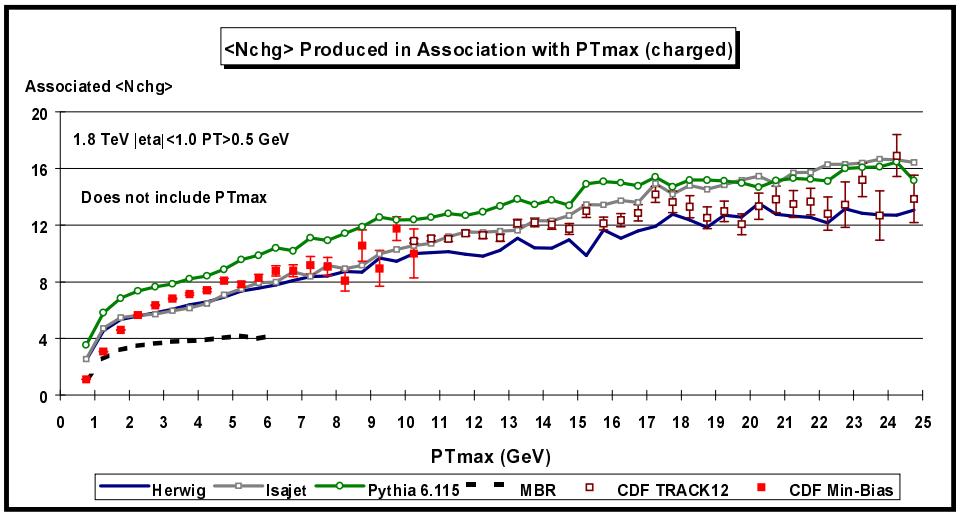

Fig. 3.2. Data on the average number of "associated" charged particles ($P_T > 0.5$ GeV and $|\eta| < 1$) as a function of PTmax (*leading charged particle*) from Fig. 3.1 compared with the QCD "hard" scattering Monte-Carlo predictions of Herwig 5.9, Isajet 7.32, Pythia 6.115, and the "soft" scattering predictions of MBR. Each point corresponds to the <Nchg> in a 0.5 GeV bin (*not including PTmax*). The theoretical predictions have been corrected for the CTC efficiency.

Fig. 3.2 compares the theoretical Monte-Carlo predictions of Herwig 5.9, Pythia 6.115, Isajet 7.32, and MBR with the data on the average number of "associated" charged particles as a function of PTmax from Fig. 3.1. The wiggles in the theoretical curves are due to limited statistics. It is not easy to generate the theoretical predictions over this large range of PTmax. Each theory curve contains 2,000,000 events corresponding to four 500,000 event runs with PT(hard) > 3, 5, 10, and 20 GeV, which then are carefully fitted together to form the curves. The "hard" scattering Monte-Carlo models describe the data qualitatively but not precisely. The "soft" MBR model does not describe correctly the "associated" multiplicity. It is interesting to note that the MBR model does fit the overall multiplicity and transverse momentum distribution of the Min-Bias data, however, it does not fit the "associated" multiplicity shown in Fig. 3.2. This is because the MBR model has no hard scattering and thus no "jets" and, as we will see, there are "jets" in the Min-Bias data. It will become clear that PTmax is part of a "jet" of charged particles that accompany it, even for very low PTmax values!

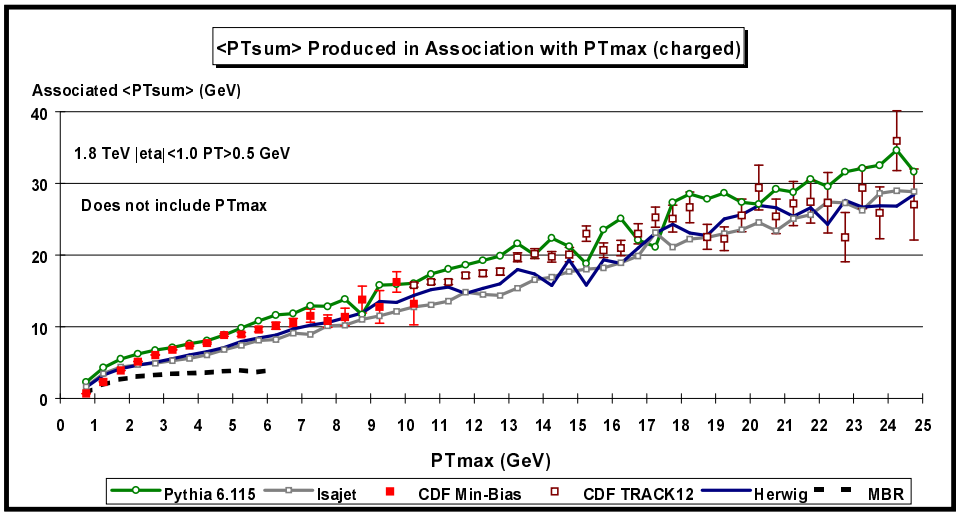

Fig. 3.3. Data on the "associated" *scalar* P_T sum of charged particles ($P_T > 0.5$ GeV and $|\eta| < 1$)as a function of PTmax (*leading charged particle*) compared with the QCD "hard" scattering Monte-Carlo predictions of Herwig 5.9, Isajet 7.32, Pythia 6.115, and "soft" scattering predictions of MBR. Each point corresponds to the <PTsum> in a 0.5 GeV bin (*not including PTmax*). The theoretical predictions have been corrected for the CTC efficiency.

Fig. 3.3 compares the theoretical Monte-Carlo predictions of Herwig 5.9, Pythia 6.115, Isajet 7.32, and MBR with the data on the average *scalar* PT sum of the "associated" charged particles ($P_T > 0.5$ GeV and $|\eta| < 1$) as a function of PTmax. In each event one constructs the scalar sum of the transverse momentum of all the charged particles produced in association with PTmax (*not including PTmax*). Again, the TRACK12 data connects on smoothly to the Min-Bias data. The

"hard" scattering Monte-Carlo models describe the data qualitatively but not precisely and the "soft" MBR model does not correctly describe the data.

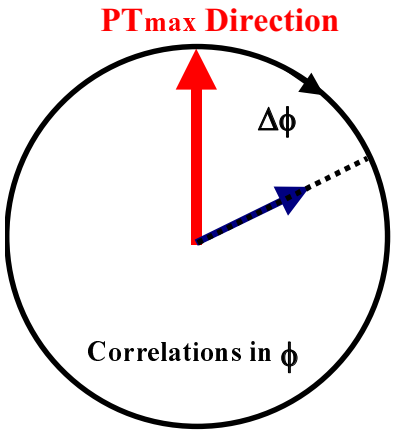

Fig. 3.4. Illustration of correlations in the azimuthal angle $\Delta\phi$ relative to the direction of the leading charged particle in the event, PTmax. The angle $\Delta\phi = |\phi - \phi_{max}|$ is the relative azimuthal angle between charged particles produced in "association" with PTmax and the direction of PTmax. Plots of <Nchg> and <PTsum> as a function of $\Delta\phi$ are referred to as "associated multiplicity flow in ϕ" relative to PTmax and "associated transverse momentum flow in ϕ" relative to PTmax, respectively. PTmax itself is not included in these plots.

(2) Correlations in $\Delta\phi$ relative to PTmax and "Jet" Structure

To see the "jet" structure in the data we examine correlations in the azimuthal angle $\Delta\phi$ relative to the direction of the leading charged particle in the event, PTmax. As illustrated in Fig. 3.4, the angle $\Delta\phi = |\phi - \phi_{max}|$ is the relative azimuthal angle between charged particles produced in "association" with PTmax and the direction of PTmax. Plots of <Nchg> and <PTsum> as a function of $\Delta\phi$ are referred to as "associated multiplicity flow in ϕ" relative to PTmax and "associated transverse momentum flow in ϕ" relative to PTmax, respectively. PTmax itself is not included in these plots.

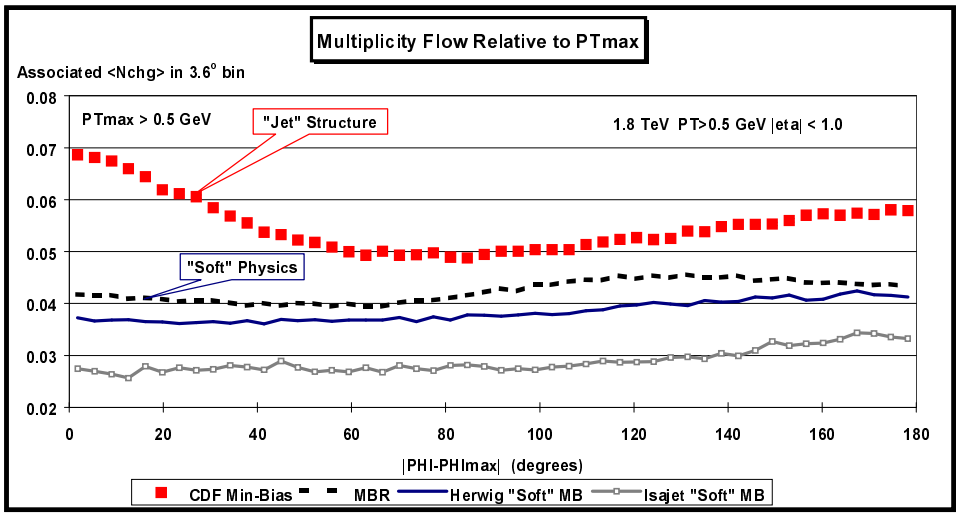

Fig. 3.5. Associated charged particle multiplicity flow in ϕ relative to PTmax as a function of $|\phi - \phi_{max}|$. Each point corresponds to the $\langle N_{chg} \rangle$ in a 3.6^o bin (*not including PTmax*). The solid squares are the Min-Bias data (PTmax > 0.5 GeV, $P_T > 0.5$ GeV, $|\eta| < 1$) and the curves correspond to the Monte-Carlo predictions of MBR, Herwig soft "min-bias", and Isajet soft "min-bias". The Monte-Carlo predictions have been corrected for the CTC efficiency.

Fig. 3.5 shows the data on the "associated" multiplicity flow in ϕ relative to PTmax for PTmax > 0.5 GeV. Each point corresponds to the $\langle N_{chg} \rangle$ ($P_T > 0.5$ GeV, $|\eta| < 1$) in a 3.6^o bin (*not including PTmax*). The solid squares are the Min-Bias data and the curves correspond to the theoretical Monte-Carlo predictions of MBR, Herwig soft "min-bias", and Isajet soft "min-bias". Clearly, the "soft" models do not show the structure seen in the data. The data show additional particles in the direction of PTmax (*i.e.* "jet" structure). In the data, quite often PTmax is the leading particle within a jet and the enhancement of particles following PTmax correspond to the accompanying particles within the jet. The soft models have no "hard scattering" and no jets. Any correlations in the "soft" models come from resonances and momentum conservation. Clearly there is a lot of hard scattering in the Min-Bias data even for PTmax > 0.5 GeV! It is interesting to note that although the MBR program fits the overall multiplicity and P_T distribution of the Min-Bias data, it does not fit the "associated" multiplicity flow shown in Fig. 3.5.

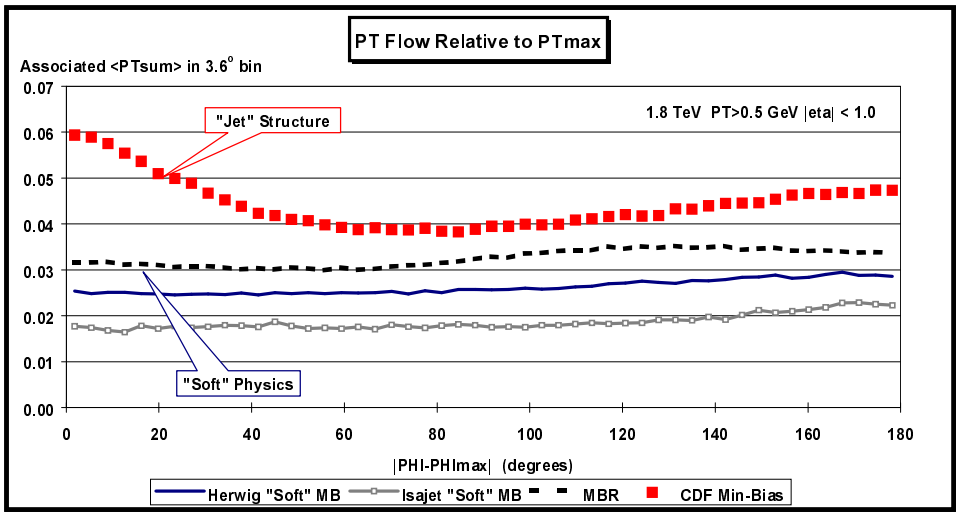

Fig. 3.6. Associated transverse momentum flow in ϕ relative to PTmax, as a function of $|\phi - \phi_{max}|$. Each point corresponds to the *scalar* $\langle PT_{sum} \rangle$ in a 3.6^o bin (*not including PTmax*). The solid squares are the Min-Bias data (PTmax > 0.5 GeV, $P_T > 0.5$ GeV, $|\eta| < 1$) and the curves correspond to the Monte-Carlo predictions of MBR, Herwig soft "min-bias", and Isajet soft "min-bias". The theoretical predictions have been corrected for the CTC efficiency.

Fig. 3.6 shows the data on the "associated" transverse momentum flow in ϕ relative to PTmax for PTmax > 0.5 GeV. Each point corresponds to the $\langle PT_{sum} \rangle$ ($P_T > 0.5$ GeV, $|\eta| < 1$) in a 3.6^o bin (*not including PTmax*). The solid squares are the Min-Bias data and the curves correspond to the theoretical Monte-Carlo predictions of MBR, Herwig "soft" min-bias, and Isajet "soft" min-bias. Again, the "soft" models do not show the structure seen in the data.

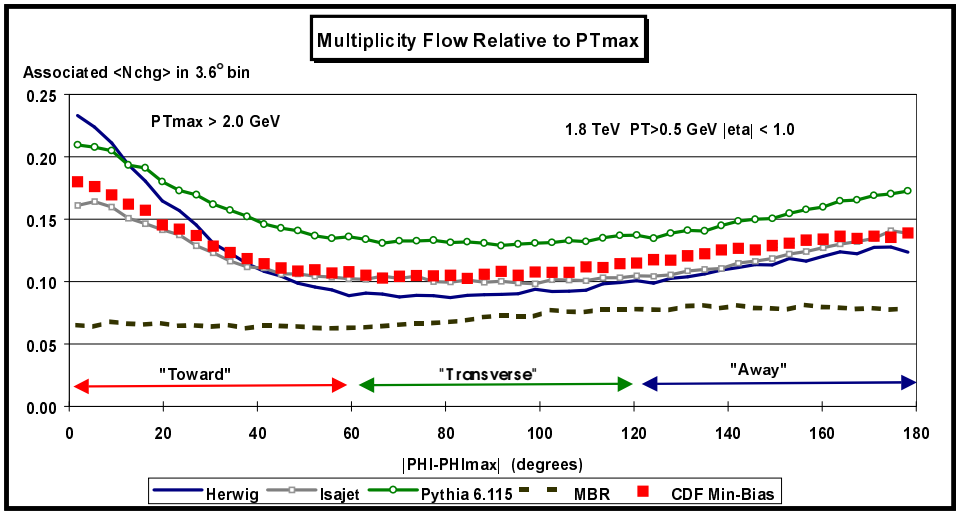

Fig. 3.7. Average number of charged particles (*not including PTmax*) produced in association with PTmax as a function of $|\phi - \phi_{max}|$, where PTmax is the maximum P_T charged particle in the event and $|\phi - \phi_{max}|$ | is the relative azimuthal angle between the particle and PTmax. Each point corresponds to the <Nchg> in a 3.6^o bin. The solid squares are the Min-Bias data (PTmax > 2.0 GeV, $P_T > 0.5$ GeV, $|\eta| < 1$) and the curves correspond to the QCD "hard" scattering Monte-Carlo predictions of Herwig 5.9, Isajet 7.32, Pythia 6.115, and the "soft" scattering predictions of MBR. The theoretical predictions have been corrected for the CTC efficiency.

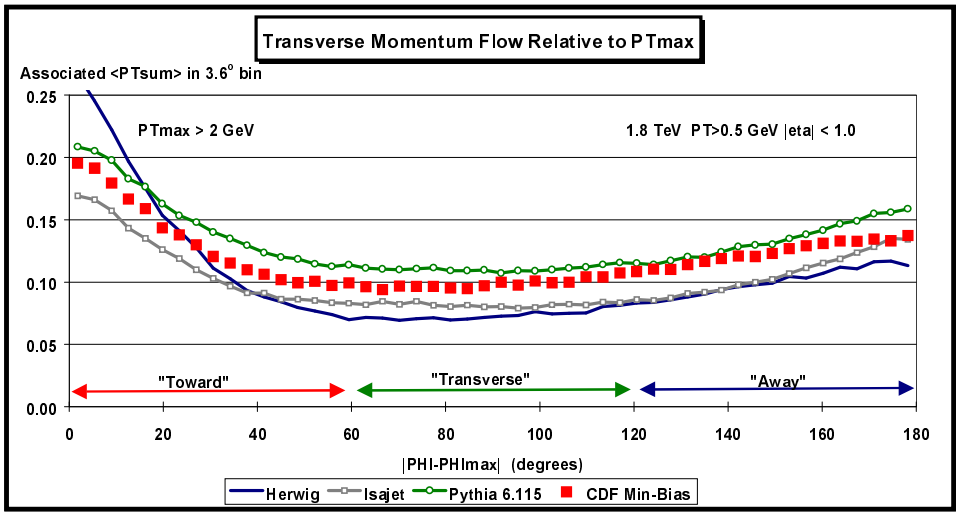

Fig. 3.8. Average charged particle *scalar* P_T sum (*not including PTmax*) produced in association with PTmax as a function of $|\phi - \phi_{max}|$, where PTmax is the maximum P_T charged particle in the event and $|\phi - \phi_{max}|$ | is the relative azimuthal angle between the particle and PTmax. Each point corresponds to the <PTsum> in a 3.6^o bin. The solid squares are the Min-Bias data (PTmax > 2.0 GeV, $P_T > 0.5$ GeV, $|\eta| < 1$) and the curves correspond to the QCD "hard" scattering Monte-Carlo predictions of Herwig 5.9, Isajet 7.32, and Pythia 6.115. The theoretical predictions have been corrected for the CTC efficiency.

Fig. 3.7. and Fig. 3.8 shows the data on the "associated" multiplicity flow and transverse momentum flow, respectively, in ϕ relative to PTmax for PTmax > 2.0 GeV. The solid squares are the Min-Bias data and the curves correspond to the theoretical Monte-Carlo "hard" scattering predictions of Herwig 5.9, Isajet 7.32 and Pythia 6.115. The "hard" scattering Monte-Carlo models describe the data qualitatively but not precisely. Below PTmax for around 2 GeV that data is a mixture of "hard" and "soft" collisions.

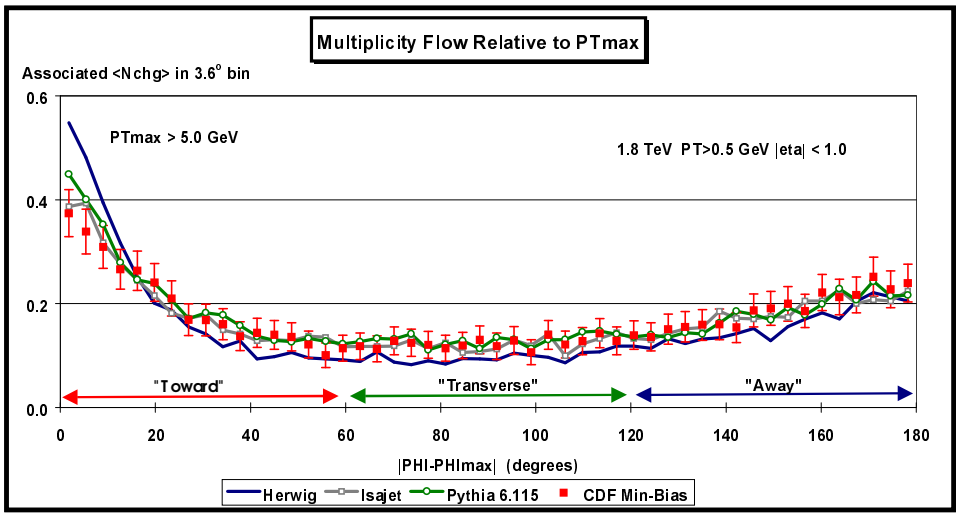

Fig. 3.9. Average number of charged particles (*not including PTmax*) produced in association with PTmax as a function of $|\phi - \phi_{max}|$, where PTmax is the maximum P_T charged particle in the event and $|\phi - \phi_{max}|$ | is the relative azimuthal angle between the particle and PTmax. Each point corresponds to the <Nchg> in a 3.6^o bin. The solid squares are the Min-Bias data (PTmax > 5.0 GeV, P_T > 0.5 GeV, $|\eta| < 1$) and the curves correspond to the QCD "hard" scattering Monte-Carlo predictions of Herwig 5.9, Isajet 7.32, and Pythia 6.115. The theoretical predictions have been corrected for the CTC efficiency.

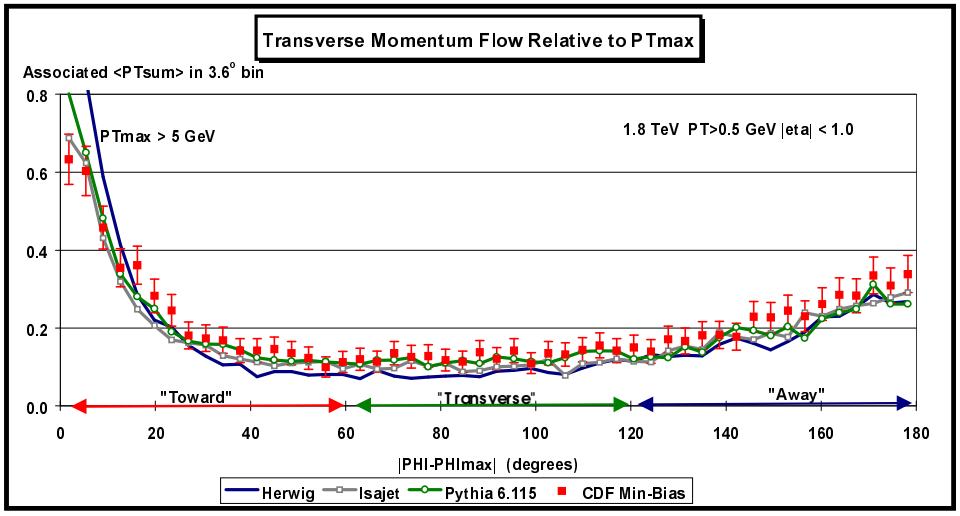

Fig. 3.10. Average charged particle *scalar* P_T sum (*not including PTmax*) produced in association with PTmax as a function of $|\phi - \phi_{max}|$, where PTmax is the maximum P_T charged

particle in the event and $|\phi - \phi max|$ | is the relative azimuthal angle between the particle and PTmax. Each point corresponds to the <PTsum> in a 3.6^o bin. The solid squares are the Min-Bias data (PTmax > 5.0 GeV, $P_T > 0.5$ GeV, $|\eta| < 1$) and the curves correspond to the QCD "hard" scattering Monte-Carlo predictions of Herwig 5.9, Isajet 7.32, and Pythia 6.115. The theoretical predictions have been corrected for the CTC efficiency.

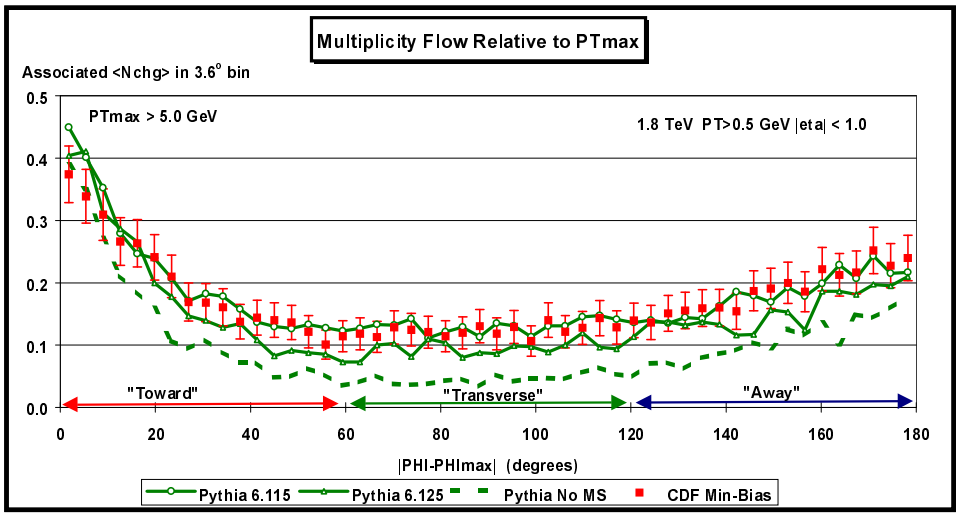

Fig. 3.11. Average number of charged particles (*not including PTmax*) produced in association with PTmax as a function of $|\phi - \phi max|$, where PTmax is the maximum P_T charged particle in the event and $|\phi - \phi max|$ | is the relative azimuthal angle between the particle and PTmax. Each point corresponds to the <Nchg> in a 3.6^o bin. The solid squares are the Min-Bias data (PTmax > 5.0 GeV, $P_T > 0.5$ GeV, $|\eta| < 1$) and the curves correspond to the QCD "hard" scattering Monte-Carlo predictions Pythia 6.115, Pythia 6.125, and Pythia (*no multiple scattering*). The theoretical predictions have been corrected for the CTC efficiency.

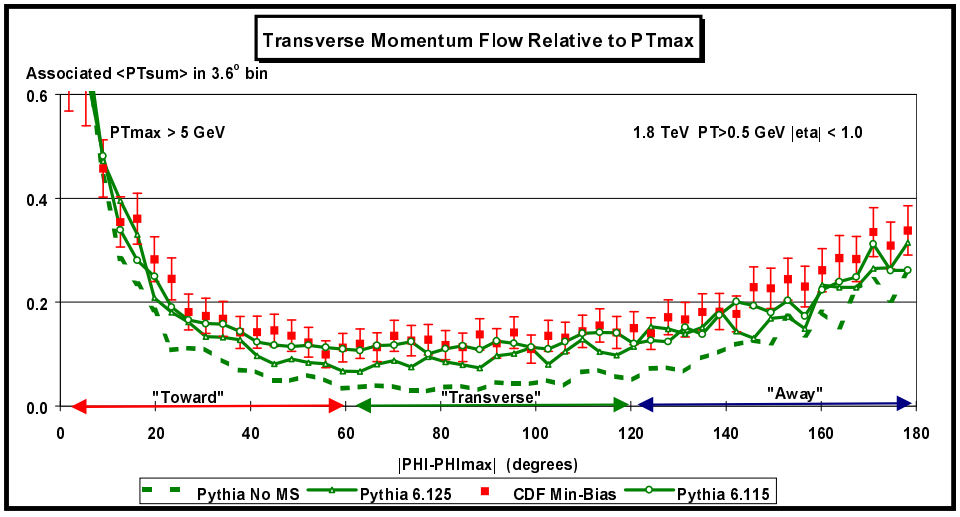

Fig. 3.12. Average charged particle *scalar* P_T sum (*not including PTmax*) produced in association with PTmax as a function of $|\phi - \phi max|$, where PTmax is the maximum P_T charged

particle in the event and $|\phi - \phi_{max}|$ | is the relative azimuthal angle between the particle and PTmax. Each point corresponds to the <PTsum> in a 3.6^o bin. The solid squares are the Min-Bias data (PTmax > 5.0 GeV, $P_T > 0.5$ GeV, $|\eta| < 1$) and the curves correspond to the QCD "hard" scattering Monte-Carlo predictions of Pythia 6.115, Pythia 6.125, and Pythia (*no multiple scattering*). The theoretical predictions have been corrected for the CTC efficiency.

Fig. 3.9 and Fig. 3.10 shows the data on the "associated" multiplicity flow and transverse momentum flow, respectively, in ϕ relative to PTmax for PTmax > 5.0 GeV. The solid squares are the Min-Bias data and the curves correspond to the theoretical Monte-Carlo "hard" scattering predictions of Herwig 5.9, Isajet 7.32, and Pythia 6.115. The "hard" scattering Monte-Carlo models describe the data quite well but not precisely. These plots are sensitive to the entire event structure both the "underlying event" and the outgoing parton "jets". This is seen clearly in Fig. 3.11 and Fig. 3.12 which show the data for PTmax > 5.0 GeV compared with three versions of Pythia (Pythia 6.115, Pythia 6.125, and Pythia with no multiple scattering). These three version of Pythia differ in the amount of activity in the underlying event.

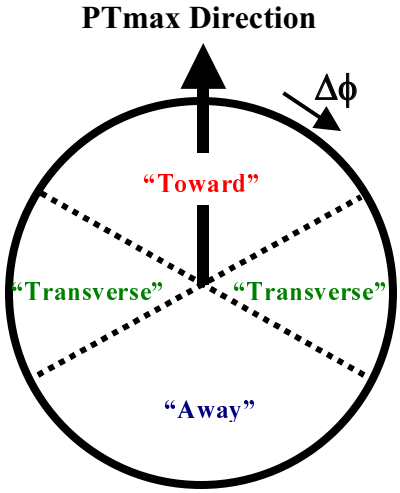

Fig. 3.13. Illustration of correlations in azimuthal angle $\Delta\phi$ relative to the direction of the leading charged particle in the event, PTmax. The angle $\Delta\phi = |\phi - \phi_{max}|$ is the relative azimuthal angle between charged particles produced in "association" with PTmax and the direction of PTmax. The region $|\phi - \phi_{max}| < 60^o$ is referred to as "toward" PTmax and the region $|\phi - \phi_{max}| > 120^o$ is called "away" from PTmax. The "transverse" to PTmax region is defined by $60^o < |\phi - \phi_{max}| < 120^o$. Each region, "toward", "transverse", and "away" covers the range $|\Delta\eta| \times |\Delta\phi| = 2 \times 120^o$.

(3) Event "Shape" versus PTmax

In Fig. 3.7 – Fig. 3.12 we have labeled the region $|\phi - \phi_{max}| < 60^o$ as "toward" PTmax and the region $|\phi - \phi_{max}| > 120^o$ is as "away" from PTmax. The "transverse" to PTmax region is defined by $60^o < |\phi - \phi_{max}| < 120^o$. As illustrated in Fig. 3.13, each region, "toward", "transverse", and "away" covers the range $|\Delta\eta| \times |\Delta\phi| = 2 \times 120^o$. The "toward" region contains the "jet" of

particles associated with PTmax. The "transverse" region is very sensitive to the underlying event. The "away" region is a mixture of the underlying event and the "away-side" jet. Fig. 3.14 shows the data on the average number of "associated" charged particles ($P_T > 0.5$ GeV and $|\eta| < 1$) as a function of PTmax for the three regions. Each point corresponds to the "toward", "transverse", or "away" <Nchg> in a 1 GeV bin (*not including PTmax*). The solid points are the Min-Bias data and the open points are the TRACK12 data. The data in Fig. 3.14 define the average event "shape". This is illustrated in Fig. 3.15 which shows an "average" proton-antiproton collider event at 1.8 TeV with PTmax = 10 GeV. There are, on the average, 4.4 charged particles "toward" PTmax (*not including PTmax*), 2.2 "transverse" to PTmax, and 4.2 "away" from PTmax. These numbers are not corrected for CTC efficiency (*the true multiplicities are about 9% higher*).

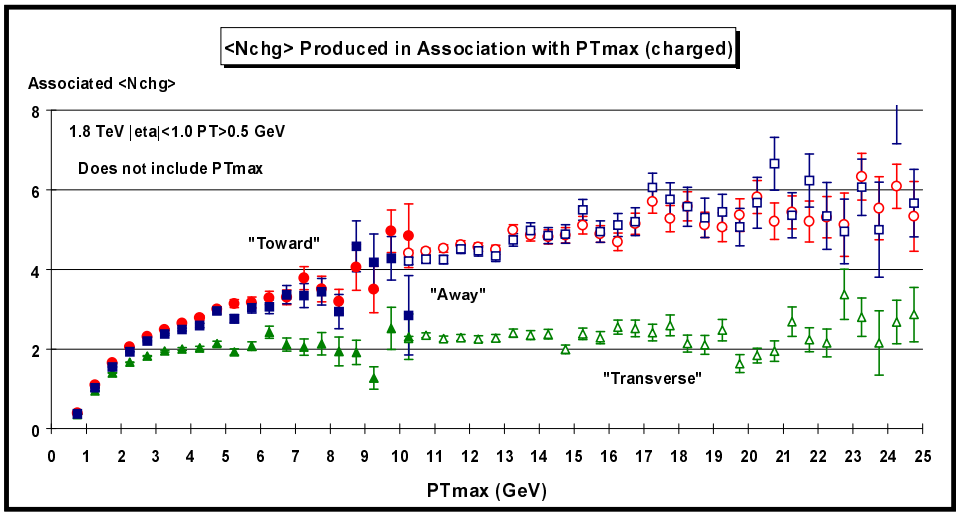

Fig. 3.14. Average number of "associated" charged particles with $P_T > 0.5$ GeV and $|\eta| <$ 1as a function of PTmax (*leading charged particle*) for the three regions defined in Fig. 3.13. Each point corresponds to the "toward", "transverse", or "away" <Nchg> in a 0.5 GeV bin (*not including PTmax*). The solid (open) points are the Min-Bias data (TRACK12 data). The data have not been corrected for efficiency.

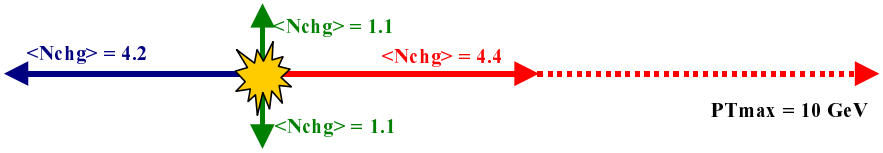

Fig. 3.15. Illustration (*drawn to scale*) of an "average" proton-antiproton collider event at 1.8 TeV with PTmax = 10 GeV. The data in Fig. 3.14 show that the average number of "associated" charged particles with $P_T > 0.5$ GeV and $|\eta| < 1$ for the three regions defined in Fig. 3.13 is 4.4 charged particles "toward" PTmax (*not including PTmax*), 2.2 "transverse" to PTmax, and 4.2 "away" from PTmax. The data have not been corrected for efficiency (*the true multiplicities are about 9% higher*).

For 0.5 < PTmax < 25 GeV the "associated" charged multiplicity in the "toward" region (*not including PTmax*) is about the same as in the "away" region and although there is much more charged multiplicity in the "forward" and "away" region (*i.e.* the event shape is "flat"), there is a

lot of activity in the "transverse" region. If we suppose that the "transverse" multplicity is uniform in azimuthal angle ϕ and rapidity η, the observed 2.2 charged particles translates to 3.6 charged particles per unit rapidity with $P_T > 0.5$ GeV (multiply by 3 to get 360^o, divide by 2 for the two units of rapidity, multiply by 1.09 to correct for the CTC efficiency). We know that if we include all P_T then there are roughly 4 charged particles per unit rapidity which is not much different than the 3.6 we see with $P_T > 0.5$ GeV! If we further assume that the P_T distribution is an exponential at small P_T with a mean of 500 MeV then the 3.6 charged particles extrapolates to 9.7 charged particles per unit rapidity (multiply by 2.7), which is about a factor of two larger than the 4 charged particles per unity rapidity seen in "soft" parton-antiproton collisions at this energy. The underlying event in a "hard" collision is considerably more active (by at least a factor of two) than a "soft" collision. Furthermore, the particle density in the underlying event is a function of PTmax and as can be seen in Fig. 3.14 it rises very rapidly as PTmax increases. The "transverse" charged multiplicity doubles in going from PTmax = 0.75 GeV to PTmax = 1.25 GeV and forms an approximately constant "plateau" for PTmax > 4 GeV.

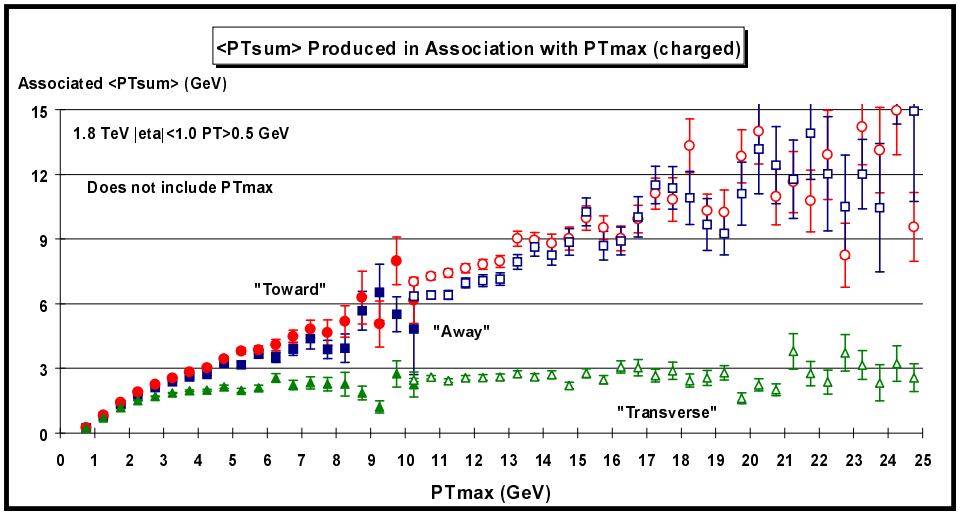

Fig. 3.16. Average "associated" *scalar* P_T sum of charged particles ($P_T > 0.5$ GeV and $|\eta| < 1$)as a function of PTmax (*leading charged particle*) for the three regions defined in Fig. 3.13. Each point corresponds to the "toward", "transverse", or "away" <PTsum> in a 0.5 GeV bin (*not including PTmax*). The solid (open) points are the Min-Bias data (TRACK12 data). The data have not been corrected for efficiency.

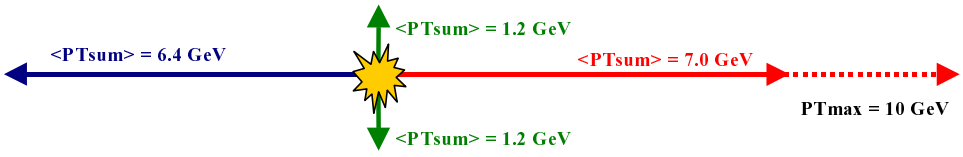

Fig. 3.17. Illustration (*drawn to scale*) of an "average" proton-antiproton collider event at 1.8 TeV with PTmax = 10 GeV. The data in Fig. 3.16 show that the average "associated" scalar PT sum of charged particles ($P_T > 0.5$ GeV and $|\eta| < 1$) for the three regions defined in Fig. 3.13 is 7.0 GeV "toward" PTmax (*not including PTmax*), 2.4 GeV "transverse" to PTmax, and 6.4 GeV "away" from PTmax. The numbers have not been corrected for efficiency.

Fig. 3.16 shows the data on the average *scalar* P_T sum of "associated" charged particles as a function of PTmax for the three regions. Each point corresponds to the "toward", "transverse", or "away" <PTsum> in a 1 GeV bin (*not including PTmax*). The solid points are the Min-Bias data and the open points are the TRACK12 data. The event "shape" in transverse momentum is illustrated in Fig. 3.17 which shows an "average" proton-antiproton collider event with PTmax = 10 GeV. There are, on the average, 7.0 GeV "toward" PTmax (*not including PTmax*), 2.4 GeV "transverse" to PTmax, and 6.4 GeV "away" from PTmax. As was the case with the charged multiplicity, the "associated" <PTsum> in the "toward" region (*not including PTmax*) is about the same as in the "away" region. The "transverse" <PTsum> also rises rapidity as a function of PTmax and forms an approximately constant "plateau" for PTmax > 4 GeV.

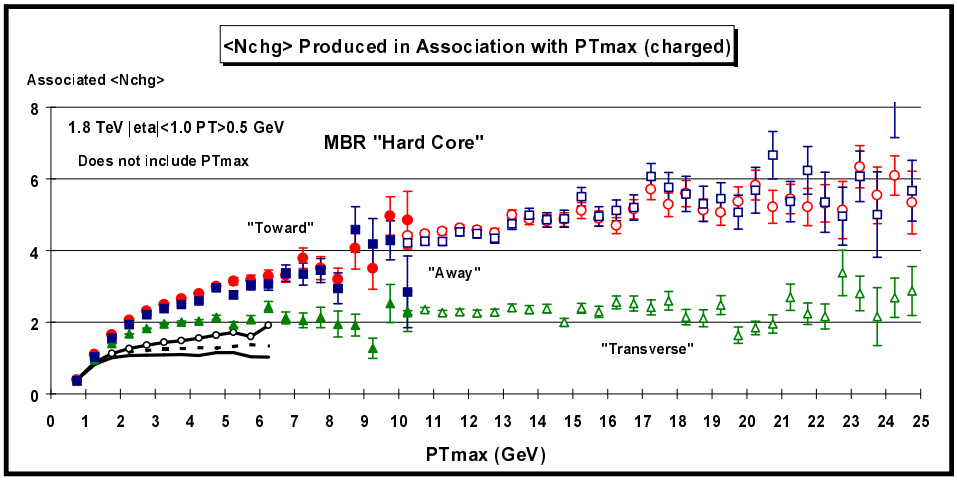

Fig. 3.18. Data from Fig. 3.14 on the average number of "associated" charged particles (P_T > 0.5 GeV and $|\eta| < 1$) as a function of PTmax (*leading charged particle*) for the three regions defined in Fig. 3.13 compared with the theoretical Monte-Carlo predictions of MBR (solid = "toward", dashed = "transverse", circles = "away"). Each point corresponds to the "toward", "transverse", or "away" <Nchg> in a 0.5 GeV bin (*not including PTmax*). The theoretical predictions have been corrected for the CTC efficiency.

In Fig. 3.18 data on the average number of "associated" charged particles as a function of PTmax for the three regions is compared with the Monte-Carlo predictions of the "soft" MBR model. We have already seen in Fig. 3.2 that the model does not produce sufficient "associated" charge particle multiplicity. Here we see that the behavior of the "toward", "transverse" and "away" multiplicity is opposite to that seen in the data. In the MBR model the "toward" charged multiplicity is the smallest of the three regions and the "transverse" multiplicity is larger than the "toward" multiplicity. The "away" multiplicity is the largest of the three due to the way the model conserves momentum.

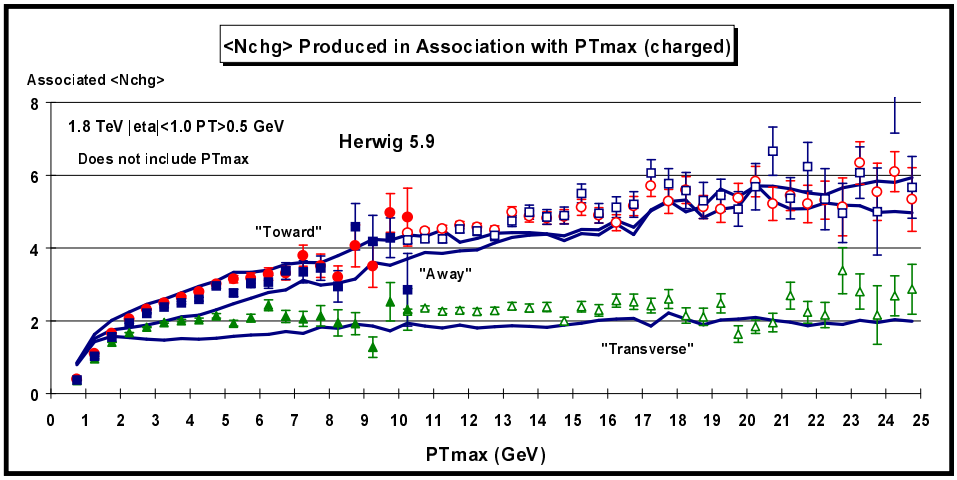

Fig. 3.19. Data from Fig. 3.14 on the average number of "associated" charged particles ($P_T > 0.5$ GeV and $|\eta| < 1$as a function of PTmax (*leading charged particle*) for the three regions defined in Fig. 3.13 compared with the theoretical Monte-Carlo predictions of Herwig 5.9. Each point corresponds to the "toward", "transverse", or "away" <Nchg> in a 0.5 GeV bin (*not including PTmax*). The theoretical predictions have been corrected for the CTC efficiency.

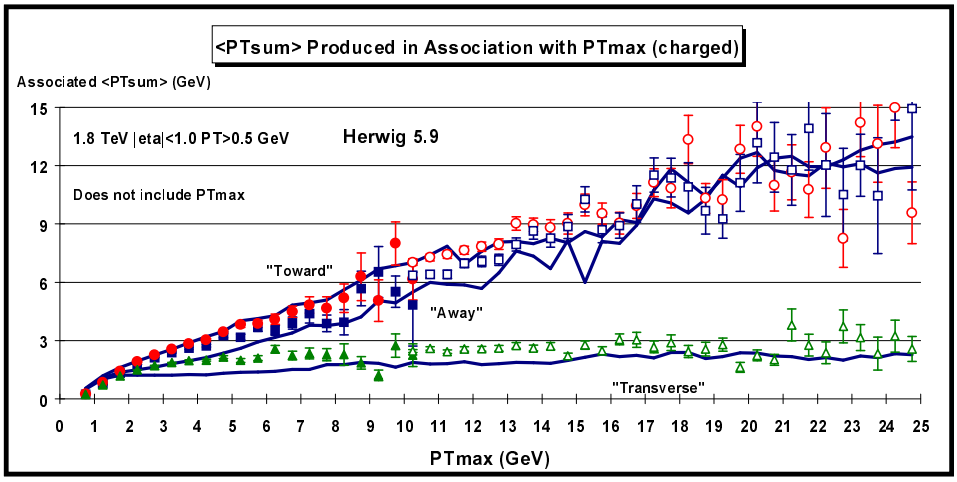

Fig. 3.20. Data from Fig. 3.16 on the average "associated" *scalar* P_T sum of charged particles ($P_T > 0.5$ GeV and $|\eta| < 1$) as a function of PTmax (*leading charged particle*) for the three regions defined in Fig. 3.13 compared with the theoretical Monte-Carlo predictions of Herwig 5.9. Each point corresponds to the "toward", "transverse", or "away" <PTsum> in a 0.5 GeV bin (*not including PTmax*). The theoretical predictions have been corrected for the CTC efficiency.

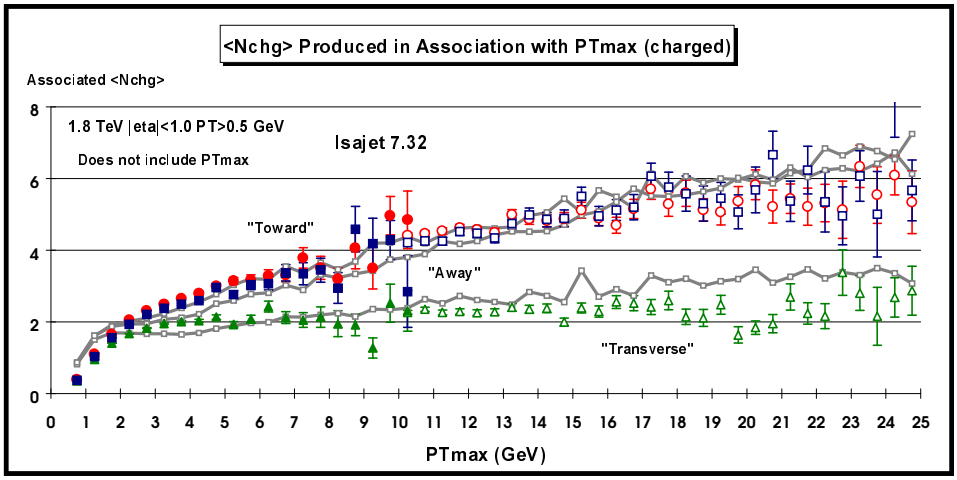

Fig. 3.21. Data from Fig. 3.14 on the average number of "associated" charged particles ($P_T > 0.5$ GeV and $|\eta| < 1$) as a function of PTmax (*leading charged particle*) for the three regions defined in Fig. 3.13 compared with the theoretical Monte-Carlo predictions of Iasjet. Each point corresponds to the "toward", "transverse", or "away" <Nchg> in a 0.5 GeV bin (*not including PTmax*). The theoretical predictions have been corrected for the CTC efficiency.

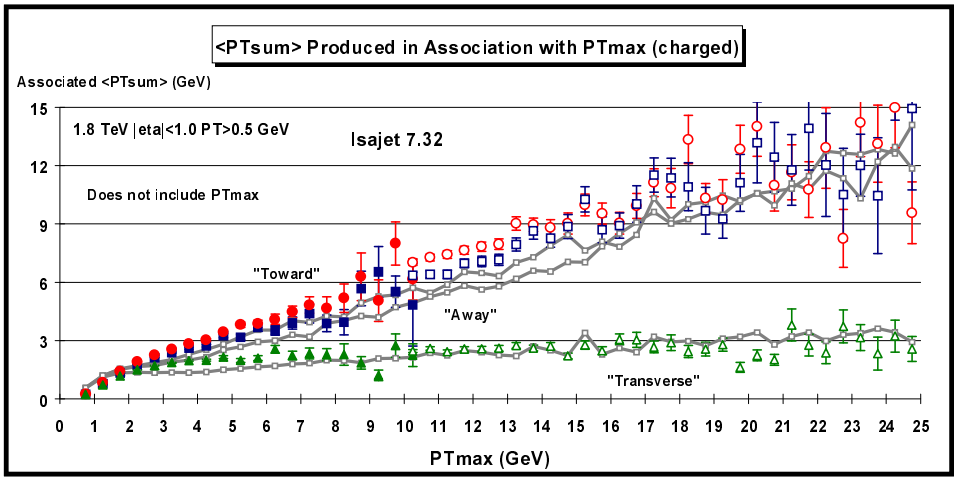

Fig. 3.22. Data from Fig. 3.16 on the average "associated" *scalar* P_T sum of charged particles ($P_T > 0.5$ GeV and $|\eta| < 1$) as a function of PTmax (*leading charged particle*) for the three regions defined in Fig. 3.13 compared with the theoretical Monte-Carlo predictions of Isajet 7.32. Each point corresponds to the "toward", "transverse", or "away" <PTsum> in a 0.5 GeV bin (*not including PTmax*). The theoretical predictions have been corrected for the CTC efficiency.

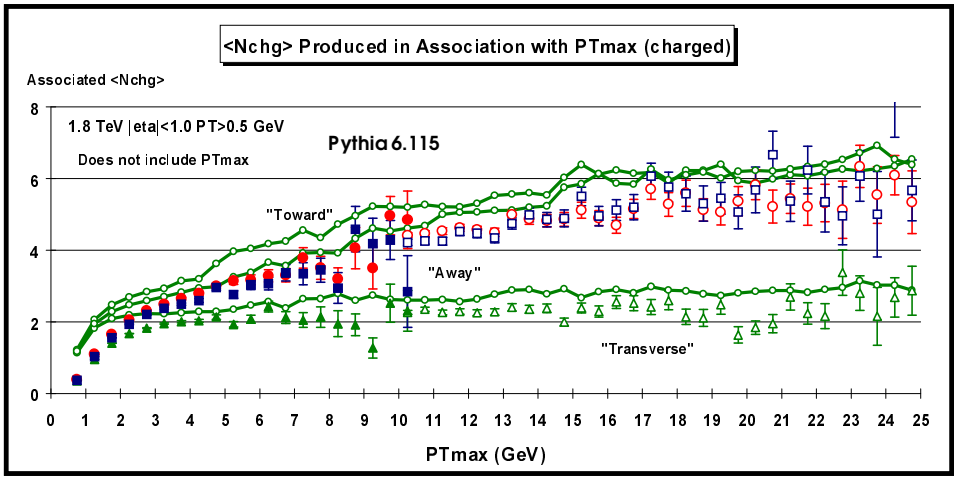

Fig. 3.23. Data from Fig. 3.14 on the average number of "associated" charged particles ($P_T > 0.5$ GeV and $|\eta| < 1$) as a function of PTmax (*leading charged particle*) for the three regions defined in Fig. 3.13 compared with the theoretical Monte-Carlo predictions of Pythia 6.115. Each point corresponds to the "toward", "transverse", or "away" <Nchg> in a 0.5 GeV bin (*not including PTmax*). The theoretical predictions have been corrected for the CTC efficiency.

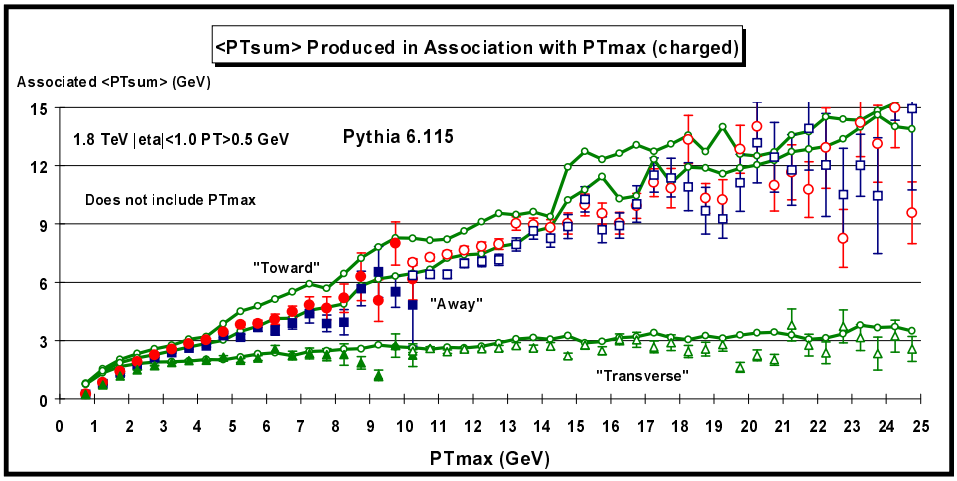

Fig. 3.24. Data from Fig. 3.14 on the average "associated" *scalar* P_T sum of charged particles ($P_T > 0.5$ GeV and $|\eta| < 1$)as a function of PTmax (*leading charged particle*) for the three regions defined in Fig. 3.13 compared with the theoretical Monte-Carlo predictions of Pythia 6.115. Each point corresponds to the "toward", "transverse", or "away" <PTsum> in a 0.5 GeV bin (*not including PTmax*). The theoretical predictions have been corrected for the CTC efficiency.

In Fig. 3.19 and Fig. 3.20 data on the "associated" <Nchg> and <PTsum>, respectively, as a function of PTmax for the three regions is compared with the "hard" scattering Monte-Carlo predictions of Herwig 5.9. Fig. 3.21 and Fig. 3.22 show the same comparison for Isajet 7.32, while Fig. 3.23 and Fig. 3.24 show the predictions of Pythis 6.115.

The "hard" scattering Monte-Carlo models shown in Fig. 3.19 – Fig. 3.24 agree qualitatively but not precisely with the data. You can see that Herwig does not have enough activity in the underlying event. Pythia 6.115 has more activity in the underlying event but as a result of this produces too much "toward" <Nchg> and <PTsum>. Isajet has a lot of activity in the underlying event but the dependence on PTmax is not quite right. The "transverse" <Nchg> rises with PTmax rather than forming the constant "plateau" seen in the data.

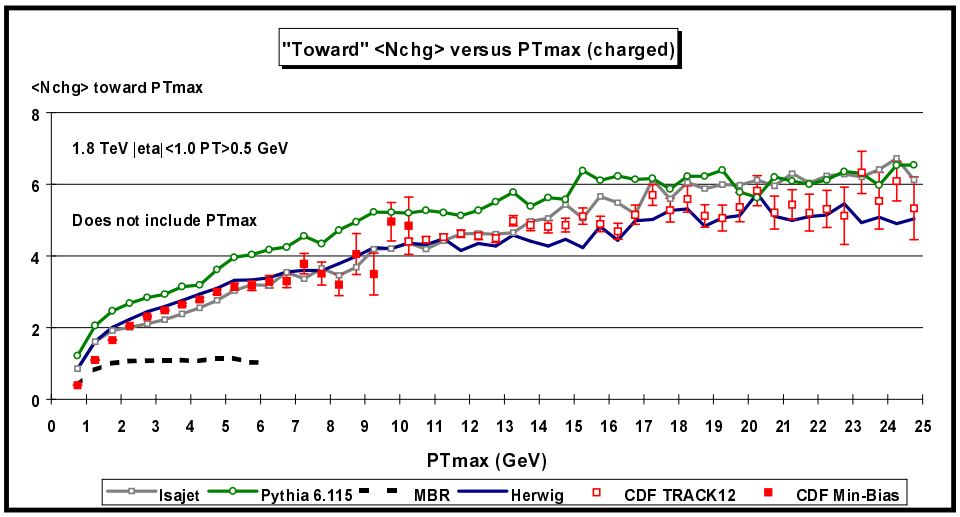

Fig. 3.25. Data from Fig.3.14 on the average number of "associated" charged particles (P_T > 0.5 GeV and |η| < 1) as a function of PTmax (*leading charged particle*) for the "toward" region defined in Fig. 3.13 compared with the QCD "hard" scattering Monte-Carlo predictions of Herwig 5.9, Isajet 7.32, Pythia 6.115, and the "soft" scattering predictions of MBR. Each point corresponds to the "toward" <Nchg> in a 0.5 GeV bin (*not including PTmax*). The theoretical predictions have been corrected for the CTC efficiency.

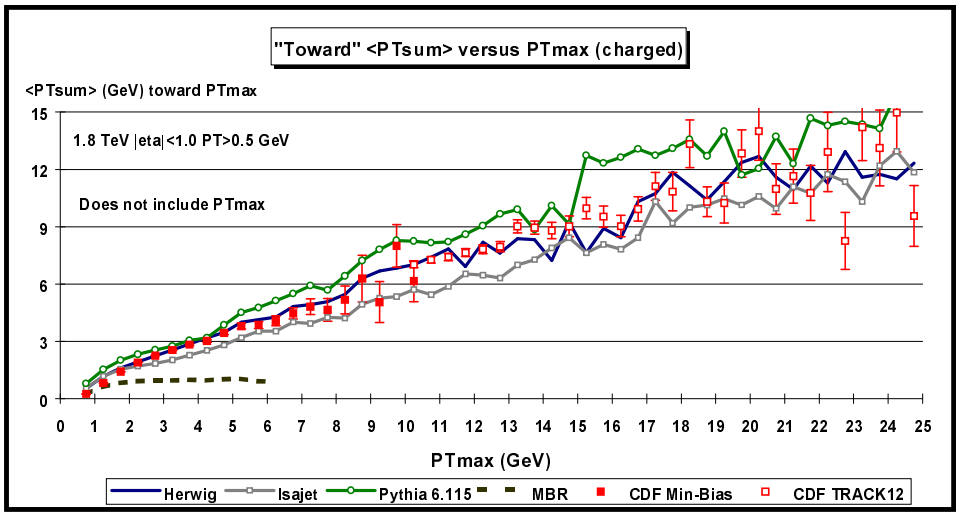

Fig. 3.26. Data from Fig. 3.16 on the average "associated" *scalar* P_T sum of charged particles (P_T > 0.5 GeV and |η| < 1) as a function of PTmax (*leading charged particle*) for the "toward" region defined in Fig. 3.13 compared with the QCD "hard" scattering Monte-Carlo predictions of Herwig 5.9, Isajet 7.32, Pythia 6.115, and the "soft" scattering

predictions of MBR. Each point corresponds to the "toward" <PTsum> in a 0.5 GeV bin (*not including PTmax*). The theoretical predictions have been corrected for the CTC efficiency.

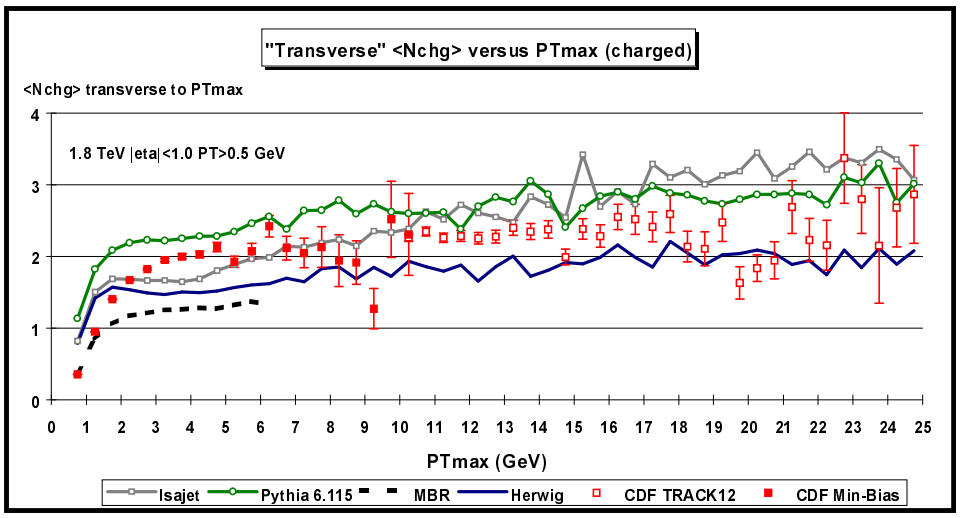

Fig. 3.27. Data from Fig.3.14 on the average number of "associated" charged particles (P_T > 0.5 GeV and $|\eta| < 1$) as a function of PTmax (*leading charged particle*) for the "transverse" region defined in Fig. 3.13 compared with the QCD "hard" scattering Monte-Carlo predictions of Herwig 5.9, Isajet 7.32, Pythia 6.115, and "soft" scattering predictions of MBR. Each point corresponds to the "transverse" <Nchg> in a 0.5 GeV bin (*not including PTmax*). The theoretical predictions have been corrected for the CTC efficiency.

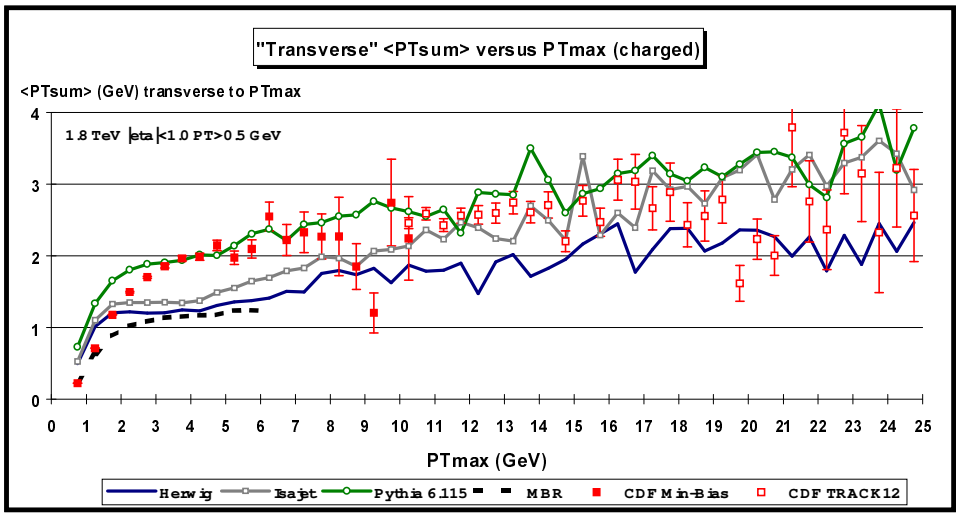

Fig. 3.28. Data from Fig. 3.16 on the average "associated" *scalar* P_T sum of charged particles (P_T > 0.5 GeV and $|\eta| < 1$) as a function of PTmax (*leading charged particle*) for the "transverse" region defined in Fig. 3.13 compared with the QCD "hard" scattering Monte-Carlo predictions of Herwig 5.9, Isajet 7.32, Pythia 6.115, and "soft" scattering predictions of MBR. Each point corresponds to the "transverse" <PTsum> in a 0.5 GeV bin (*not including PTmax*). The theoretical predictions have been corrected for the CTC efficiency.

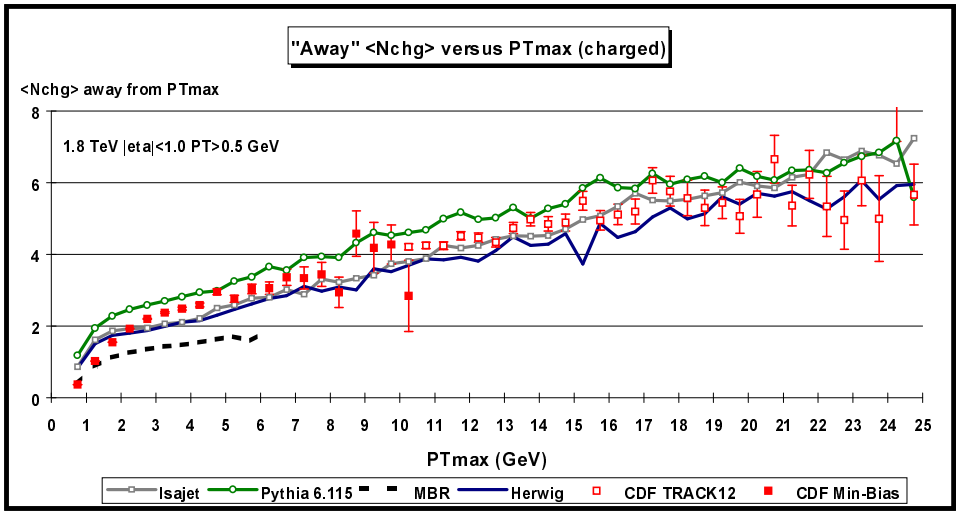

Fig. 3.29. Data from Fig.3.14 on the average number of "associated" charged particles (P_T > 0.5 GeV and $|\eta| < 1$) as a function of PTmax (*leading charged particle*) for the "away" region defined in Fig. 3.13 compared with the QCD "hard" scattering Monte-Carlo predictions of Herwig 5.9, Isajet 7.32, Pythia 6.115, and "soft" scattering predictions of MBR. Each point corresponds to the "away" <Nchg> in a 0.5 GeV bin (*not including PTmax*). The theoretical predictions have been corrected for the CTC efficiency.

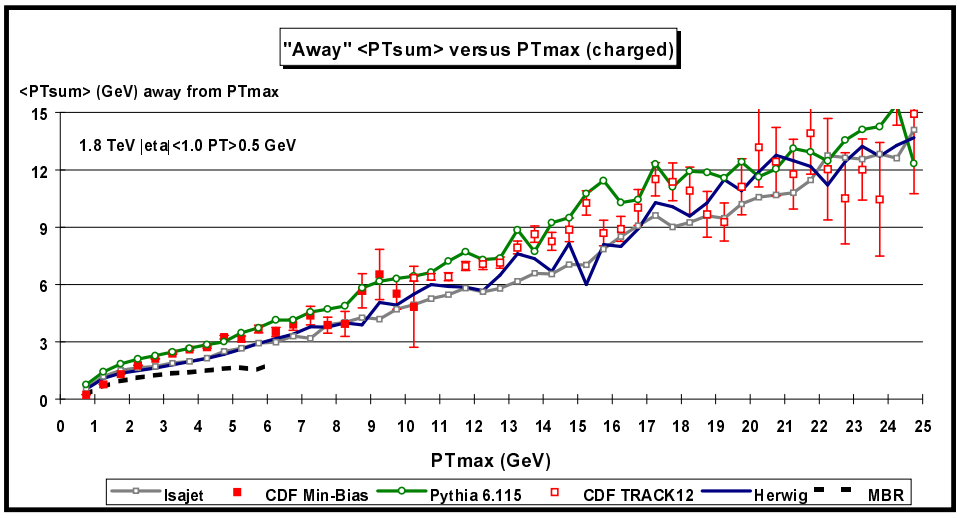

Fig. 3.30. Data from Fig. 3.16 on the average "associated" *scalar* P_T sum of charged particles (P_T > 0.5 GeV and $|\eta| < 1$) as a function of PTmax (*leading charged particle*) for the "away" region defined in Fig. 3.13 compared with the QCD "hard" scattering Monte-Carlo predictions of Herwig 5.9, Isajet 7.32, Pythia 6.115, and the "soft" scattering predictions of MBR. Each point corresponds to the "away" <PTsum> in a 0.5 GeV bin (*not including PTmax*). The theoretical predictions have been corrected for the CTC efficiency.

Fig. 3.25 and Fig. 2.26 compare the "toward" <Nchg> and <PTsum>, respectively, with the theoretical "hard" scattering Monte-Carlo predictions of Herwig 5.9, Isajet 7.32, and Pythia 6.115, and the "soft" MBR predication with the data. Fig. 3.27 and Fig. 3.28 compare the

"transverse" <Nchg> and <PTsum>, respectively, with the theoretical "hard" scattering Monte-Carlo predictions of Herwig 5.9, Isajet 7.32, and Pythia 6.115, and the "soft" MBR prediction with the data. Finally, Fig. 3.29 and Fig. 3.30 compare the "away" <Nchg> and <PTsum>, respectively, with the theoretical "hard" scattering Monte-Carlo predictions of Herwig, Isajet, and Pythia 6.115, and the "soft" MBR prediction with the data.

IV. The Evolution of "Jets" from 0.5 to 50 GeV

The data show clear "jet structure" even at quite low PTmax values (see Fig. 3.5). In this section, we define "jets" and examine the evolution of these "jets" from P_T(jet) = 0.5 to 50 GeV. We will also examine the event "shape" as a function of the P_T(jet#1) (leading jet). As illustrated if Fig. 4.1, "jets" are defined as "circular regions" (R = 0.7) in η-ϕ space and contain charged particles from the underlying event as well as particles which originate from the fragmentation of high P_T outgoing partons (see Fig 1.1). Also every charged particle in the event is assigned to a "jet", with the possibility that some "jets" might consist of just one charged particle.

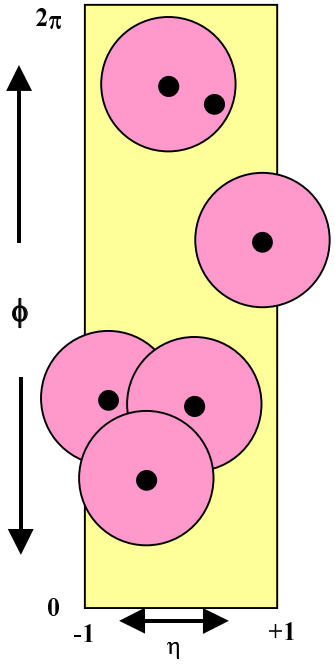

Fig. 4.1. Illustration of an event with six charged particles (P_T > 0.5 GeV and |η| < 1) and five "jets" (circular regions in η-ϕ space with R = 0.7).

(1) Jet Definition

We define jets as circular regions in η-ϕ space with "distance" defined by

$$d = \sqrt{(\Delta\eta)^2 + (\Delta\phi)^2} \ .$$

Our jet algorithm is as follows:

- Order all charged particles according to their P_T.

- Start with the highest P_T particle and include in the "jet" all particles within the "distance" R = 0.7.
- Go to the next highest P_T particle (not already included in a jet) and include in the "jet" all particles (not already included in a jet) within the "distance" R =0.7.
- Continue until all particles are in a "jet".

We consider all charged particles ($P_T > 0.5$ GeV and $|\eta| < 1$) and allow the jet radius to extend outside $|\eta| < 1$. Fig. 4.1 illustrates an event with six charged particles and five jets. Jets have a vector momentum given by the vector sum of all the particles within the jet and a transverse momentum given by

$$P_T(jet) = \sqrt{(P_x(jet))^2 + (P_y(jet))^2} \ .$$

The maximum number of jets is related to the geometrical size of jets compared to the size of the region considered and is given approximately by

$$N_{jet}(\max) \approx 2\frac{(2)(2\pi)}{\pi(0.7)^2} \approx 16 \ .$$

The additional factor of two is to allow for the overlap of "jet" radii as shown in Fig. 4.1.

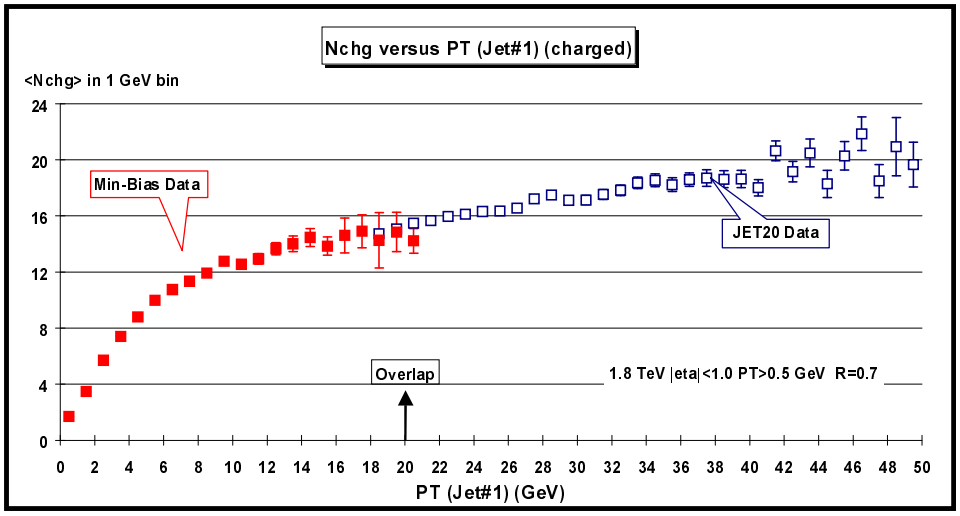

Fig. 4.2. Average number of charged particles ($P_T > 0.5$ GeV and $|\eta| < 1$) as a function of P_T(jet#1) (*leading jet*). Each point corresponds to <Nchg> in a 1 GeV bin. The solid (open) points are the Min-Bias data (JET20 data). The data have not been corrected for efficiency.

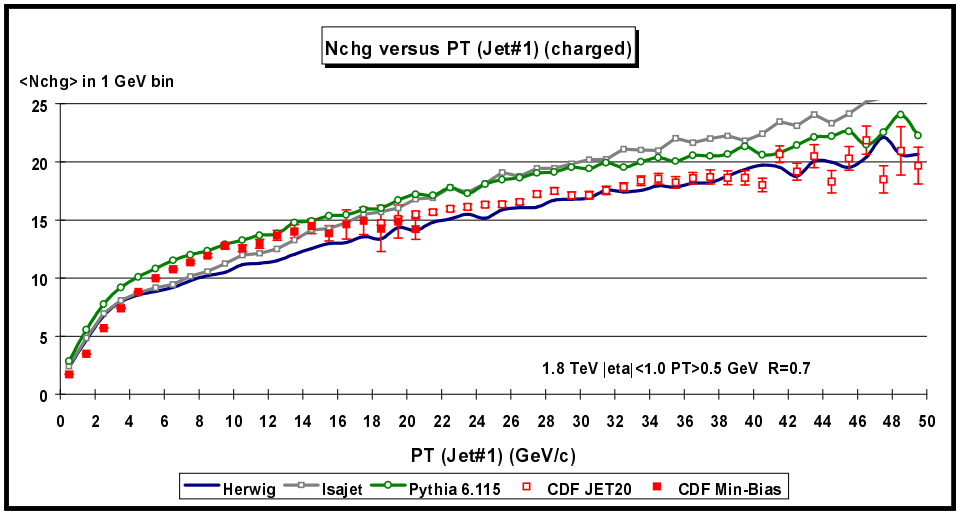

Fig. 4.3. Data from Fig. 4.2 on the average number of charged particles ($P_T > 0.5$ GeV and $|\eta| < 1$) as a function of P_T(jet#1) (*leading jet*) compared with the QCD "hard" scattering Monte-Carlo predictions of Herwig 5.9, Isajet 7.32, and Pythia 6.115. Each point corresponds to $\langle N_{chg} \rangle$ in a 1 GeV bin. The theoretical predictions have been corrected for the CTC efficiency.

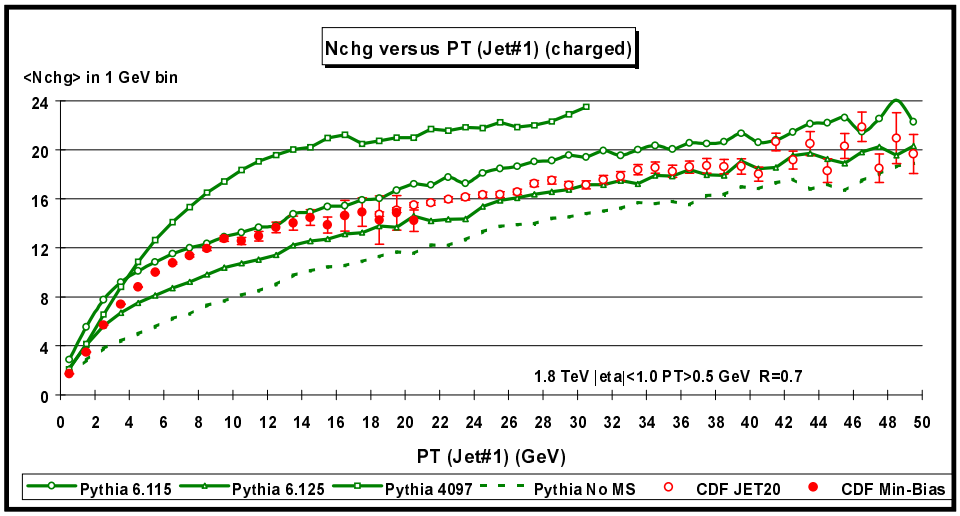

Fig. 4.4. Data from Fig. 4.2 on the average number of charged particles ($P_T > 0.5$ GeV and $|\eta| < 1$) as a function of P_T(jet#1) (*leading jet*) compared with the QCD "hard" scattering Monte-Carlo predictions of Pythia 6.115, Pythia 6.125, Pythia 4097, and Pythia (*no multiple scattering*). Each point corresponds to $\langle N_{chg} \rangle$ in a 1 GeV bin. The theoretical predictions have been corrected for the CTC efficiency.

(2) Nchg and Njet versus P_T(jet#1)

Fig. 4.2 shows the average number of charged particles ($P_T > 0.5$ GeV and $|\eta| < 1$) as a function of P_T(jet#1) (*leading jet*) for the Min-Bias and JET20 data. The JET20 data connect on smoothly to the Min-Bias data and allows us to study observables over the range $0.5 < P_T(\text{jet\#1}) < 50$ GeV.

There is a small overlap region where the Min-Bias and JET20 data agree. The errors are only statistical and the data have not been corrected for efficiency (*the true multiplicities are about 9% larger*). Fig. 4.2 shows a fast rise in the overall charged multiplicity at low P_T(jet#1) and then a flattening out and a gradual rise at high P_T(jet#1). Fig. 4.3 compares the data on <Nchg> as a function of P_T(jet#1) with the QCD "hard" scattering Monte-Carlo predictions of Herwig 5.9, Isajet 7.32, and Pythia 6.115. The Monte-Carlo models agree qualitatively but not precisely with the data. Fig. 4.4 shows the predictions of the four versions of Pythia (Pythia 6.115, Pythia 6.125, Pythia 4097, and Pythia with no multiple scattering).

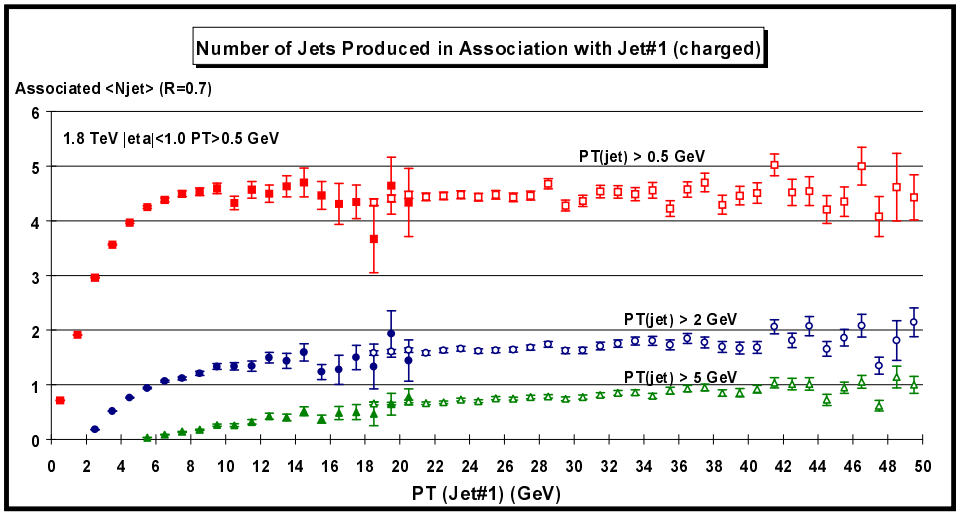

Fig. 4.5. Average number of charged particle jets (R = 0.7) with P_T(jet) > 0.5 GeV, P_T(jet) > 2 GeV, and P_T(jet) > 5 GeV produced in "association" with jet#1 (*leading jet*) as a function of P_T(jet#1). Each point corresponds to average number of jets (*not including jet#1*) in a 1 GeV bin. The solid (open) points are the Min-Bias data (JET20 data) with P_T > 0.5 GeV and $|\eta| < 1$. The data have not been corrected for efficiency. Jets are defined as "circular regions" (R = 0.7) in η-ϕ space (see Fig. 4.1) and contain charged particles from the underlying event as well as particles which originate from the fragmentation of high P_T outgoing partons (see Fig 1.1).

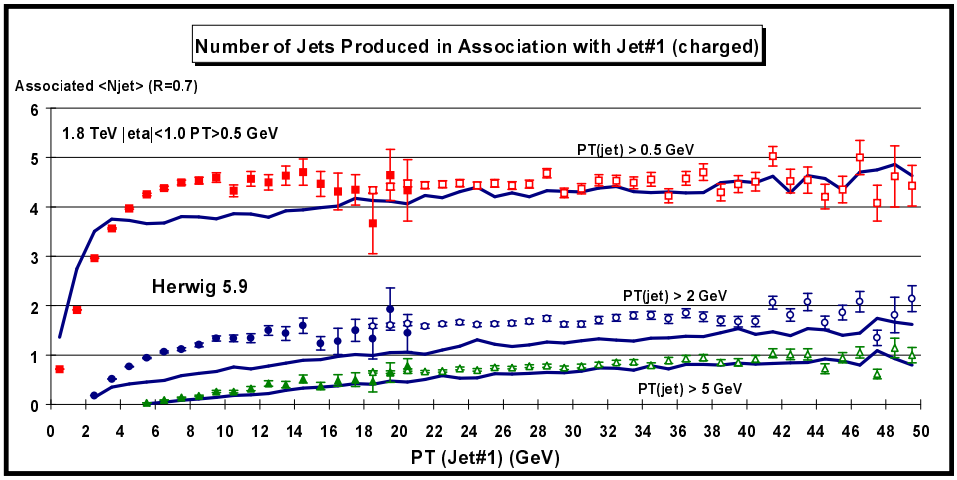

Fig. 4.6. Data from Fig. 4.5 on the average number of charged particle jets (R = 0.7) with P_T (jet) > 0.5 GeV, P_T (jet) > 2 GeV, and P_T (jet) > 5 GeV produced in "association" with jet#1 (leading jet) compared with the QCD "hard" scattering Monte-Carlo predictions of Herwig 5.9. Each point corresponds to average number of jets (*not including jet#1*) in a 1 GeV bin. The theoretical predictions have been corrected for the CTC efficiency. Jets are defined as "circular regions" (R = 0.7) in η-ϕ space (see Fig. 4.1) and contain charged particles from the underlying event as well as particles which originate from the fragmentation of high P_T outgoing partons (see Fig 1.1).

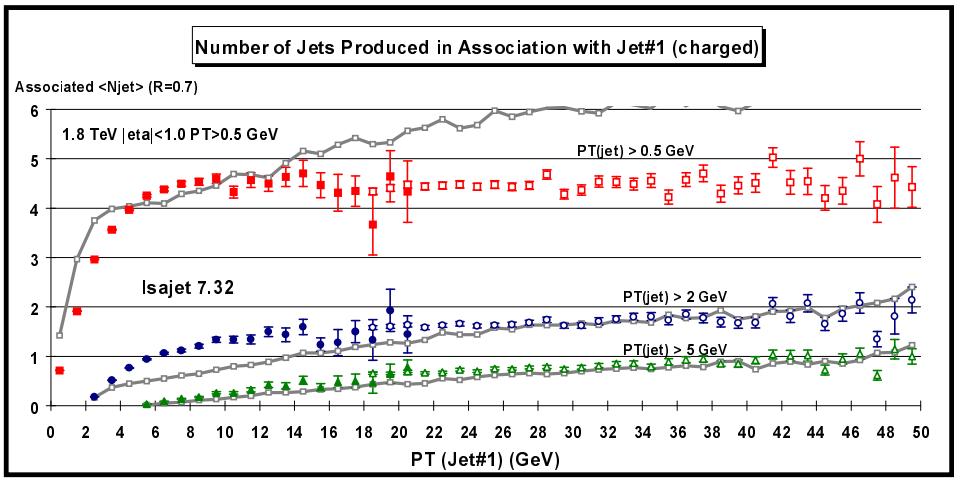

Fig. 4.7. Data from Fig. 4.5 on the average number of charged particle jets (R = 0.7) with P_T (jet) > 0.5 GeV, P_T (jet) > 2 GeV, and P_T (jet) > 5 GeV produced in "association" with jet#1 (leading jet) compared with the QCD "hard" scattering Monte-Carlo predictions of Isajet 7.32. Each point corresponds to average number of jets (*not including jet#1*) in a 1 GeV bin. The theoretical predictions have been corrected for the CTC efficiency. Jets are defined as "circular regions" (R = 0.7) in η-ϕ space (see Fig. 4.1) and contain charged particles from the underlying event as well as particles which originate from the fragmentation of high P_T outgoing partons (see Fig 1.1).

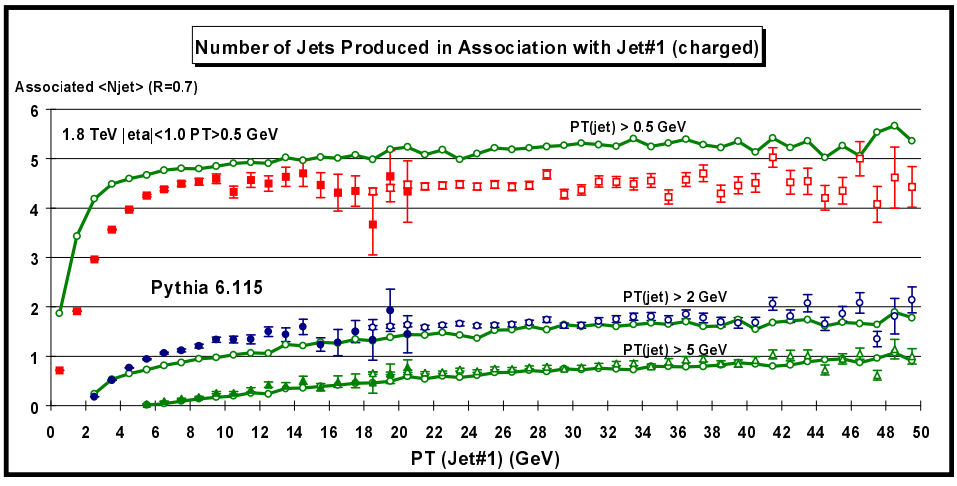

Fig. 4.8. Data from Fig. 4.5 on the average number of charged particle jets (R = 0.7) with P_T (jet) > 0.5 GeV, P_T (jet) > 2 GeV, and P_T (jet) > 5 GeV produced in "association" with

jet#1 (leading jet) compared with the QCD "hard" scattering Monte-Carlo predictions of Pythia 6.115. Each point corresponds to average number of jets (*not including jet#1*) in a 1 GeV bin. The theoretical predictions have been corrected for the CTC efficiency. Jets are defined as "circular regions" (R = 0.7) in η-ϕ space (see Fig. 4.1) and contain charged particles from the underlying event as well as particles which originate from the fragmentation of high P_T outgoing partons (see Fig 1.1).

Fig. 4.5 shows the average number of jets (R = 0.7) with $P_T(jet) > 0.5$ GeV, $P_T(jet) > 2$ GeV, and $P_T(jet) > 5$ GeV produced in "association" with jet#1 (*leading jet*) as a function of $P_T(jet\#1)$. . Here one plots <Njet> not including jet#1. It is the number of jets that are produced in association with jet#1 (*add one to get the total jet multiplicity*). An event with $P_T(jet\#1) = 20$ GeV contains, on the average, 4.5 additional jets with $P_T(jet) > 0.5$ GeV, 1.6 with $P_T(jet) > 2$ GeV, and 0.6 with $P_T(jet) > 5$ GeV. The data on the number of jets produced in "association" with jet#1 (*leading jet*) are compared with the QCD "hard" scattering Monte-Carlo predictions of Herwig 5.9 (Fig. 4.6), Isajet 7.32 (Fig. 4.7), and Pythia 6.115 (Fig.4.8). Herwig produces too few associated jets. Isajet produces too many associated jets at large $P_T(jet)$. Pythia 6.115 does well for associated jets greater than 2 GeV, but produces slightly to many low transverse momentum associated jets.

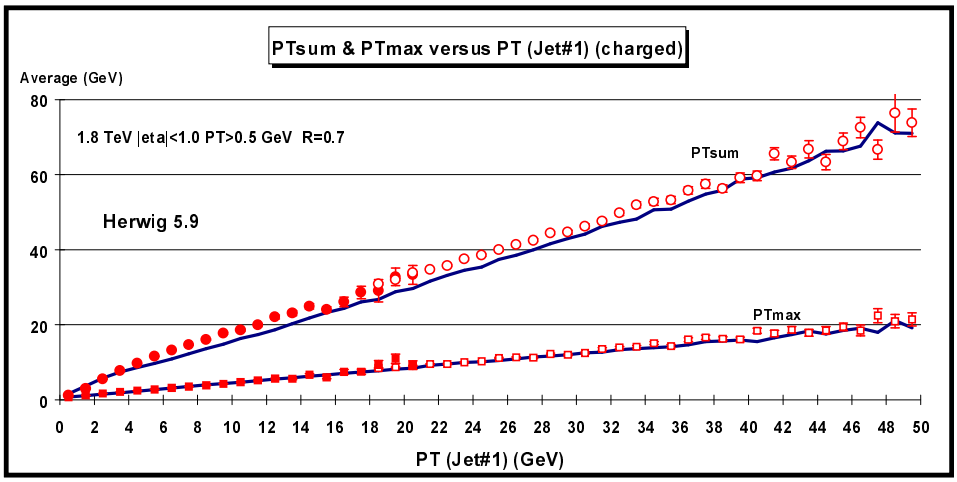

Fig. 4.9. Average *scalar* P_T sum and average maximum P_T for charged particles ($P_T > 0.5$ GeV and $|\eta| < 1$) (*including jet#1*) as a function of $P_T(jet\#1)$. The solid (open) points are the Min-Bias data (JET20 data). The data are compared with the QCD "hard" scattering Monte-Carlo predictions of Herwig 5.9 (*corrected for the CTC efficiency*).

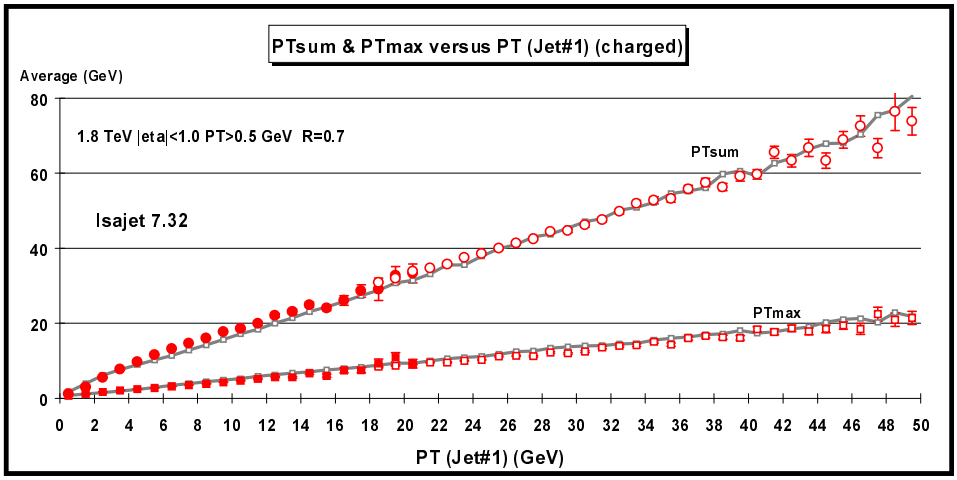

Fig. 4.10. Average *scalar* P_T sum and average maximum P_T for charged particles with $P_T > 0.5$ GeV and $|\eta| < 1$ as a function of P_T(jet#1). The solid (open) points are the Min-Bias data (JET20 data). The data are compared with the QCD "hard" scattering Monte-Carlo predictions of Isajet 7.32 (*corrected for the CTC efficiency*).

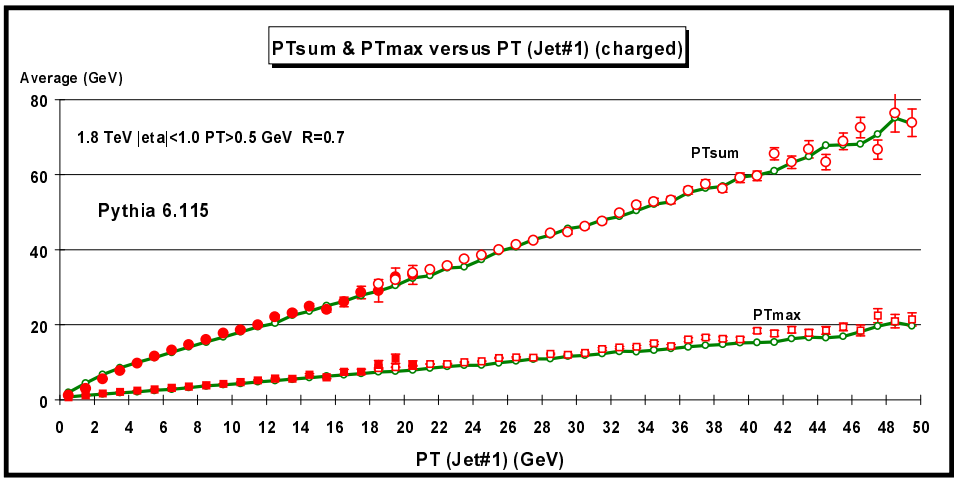

Fig. 4.11. Average *scalar* P_T sum and average maximum P_T for charged particles with $P_T > 0.5$ GeV and $|\eta| < 1$ as a function of P_T(jet#1). The solid (open) points are the Min-Bias data (JET20 data). The data are compared with the QCD "hard" scattering Monte-Carlo predictions of Pythia 6.115 (*corrected for the CTC efficiency*).

(3) PTmax and PTsum versus P_T(jet#1)

The data on the maximum transverse momentum charged particle in the event, PTmax, versus P_T(jet#1) and the *scalar* PT sum of all the charged particles ($P_T > 0.5$ GeV and $|\eta| < 1$) in the event (*including jet#1*) versus P_T(jet#1) are compared with the QCD "hard" scattering Monte-Carlo predictions of Herwig 5.9 (Fig. 4.9), Isajet 7.32 (Fig. 4.10), and Pythia 6.115 (Fig.4.11). An event with P_T(jet#1) = 20 GeV has, on the average, a *scalar* PT sum of about 32 GeV and a leading charged particle with PTmax = 9 GeV. This is quite reasonable since our knowledge of

fragmentation functions tells us that when a parton fragments into hadrons at these energies, the leading hadron, on the average, carries about one-half of the momentum of the jet. Again, the Monte-Carlo models agree qualitatively but not precisely with the data.

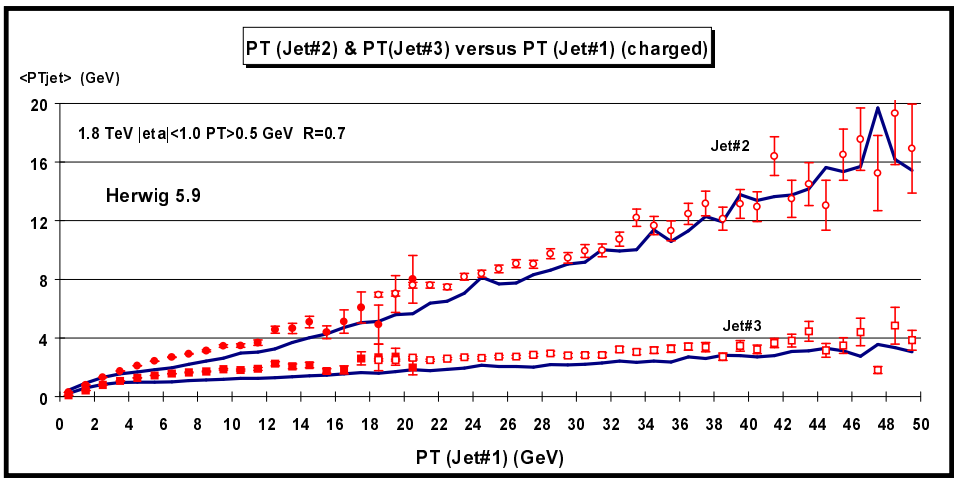

Fig. 4.12. Average transverse momentum of jet#2 (*second highest P_T jet*) and jet#3 (*third highest P_T jet*) for charged particles with $P_T > 0.5$ GeV and $|\eta| < 1$ as a function of P_T(jet#1). If jet#2 or jet#3 does not exist then it is assigned zero transverse momentum. The solid (open) points are the Min-Bias data (JET20 data). The data are compared with the QCD "hard" scattering Monte-Carlo predictions of Herwig 5.9 (*corrected for the CTC efficiency*). Jets are defined as "circular regions" ($R = 0.7$) in η-ϕ space (see Fig. 4.1) and contain charged particles from the underlying event as well as particles which originate from the fragmentation of high P_T outgoing partons (see Fig 1.1).

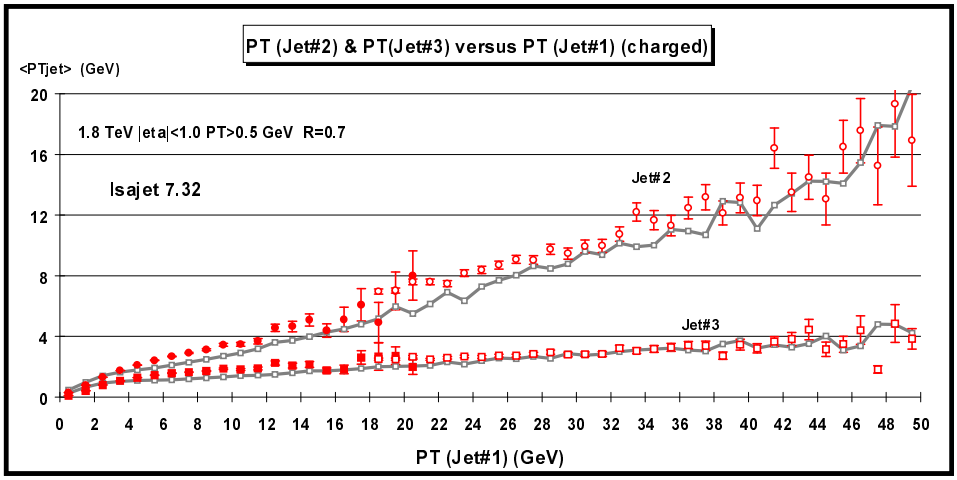

Fig. 4.13. Average transverse momentum of jet#2 (*second highest P_T jet*) and jet#3 (*third highest P_T jet*) for charged particles with $P_T > 0.5$ GeV and $|\eta| < 1$ as a function of P_T(jet#1). If jet#2 or jet#3 does not exist then it is assigned zero transverse momentum. The solid (open) points are the Min-Bias data (JET20 data). The data are compared with the QCD "hard" scattering Monte-Carlo predictions of Isajet 7.32 (*corrected for the CTC*

efficiency). Jets are defined as "circular regions" (R = 0.7) in η-ϕ space (see Fig. 4.1) and contain charged particles from the underlying event as well as particles which originate from the fragmentation of high P_T outgoing partons (see Fig. 1.1).

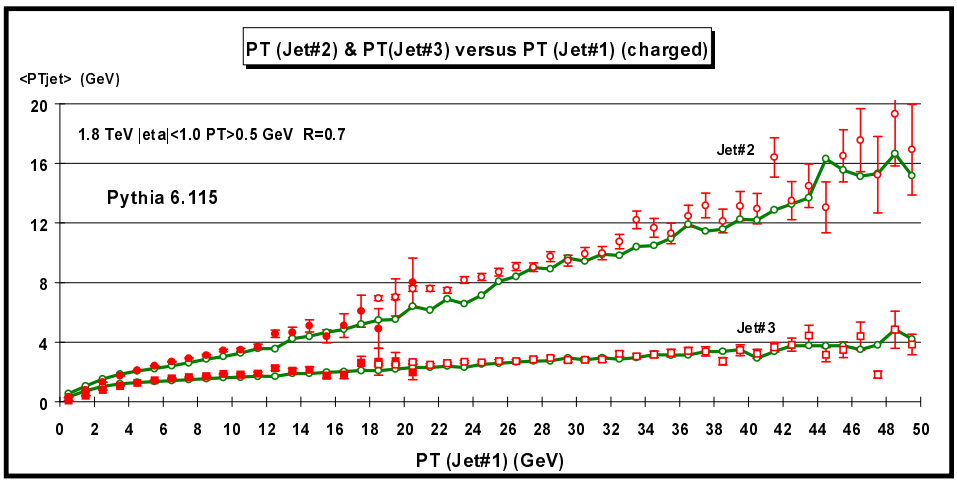

Fig. 4.14. Average transverse momentum of jet#2 (*second highest P_T jet*) and jet#3 (*third highest P_T jet*) for charged particles with $P_T > 0.5$ GeV and $|\eta| < 1$ as a function of P_T(jet#1). If jet#2 or jet#3 does not exist then it is assigned zero transverse momentum. The solid (open) points are the Min-Bias data (JET20 data). The data are compared with the QCD "hard" scattering Monte-Carlo predictions of Pythia 6.115 (*corrected for the CTC efficiency*). Jets are defined as "circular regions" (R = 0.7) in η-ϕ space (see Fig. 4.1) and contain charged particles from the underlying event as well as particles which originate from the fragmentation of high P_T outgoing partons (see Fig. 1.1).

(4) P_T(jet#2) and P_T(jet#3) versus P_T(jet#1)

The leading jet in the event usually results from the fragmentation of a large transverse momentum outgoing parton (see Fig. 1.1), but may also contain some of the underlying event. The second highest P_T jet might contain the fragmentation products of the other high P_T outgoing parton (*when the jets are back-to-back*), but often is composed of the underlying event. The third highest P_T jet can result from gluon radiation off one of the outgoing partons, but at these energies is almost always composed of the underlying event. The data on the transverse momentum of jet#2 and jet#3 versus P_T(jet#1) are compared with the QCD "hard" scattering Monte-Carlo predictions of Herwig 5.9 (Fig. 4.12), Isajet 7.32 (Fig. 4.13), and Pythia 6.115 (Fig.4.14). In these plots if jet#2 or jet#3 does not exist then it is assigned zero transverse momentum. An event with P_T(jet#1) = 20 GeV has, on the average, P_T(jet#2) = 7 GeV and P_T(jet#3) = 2.5 GeV.

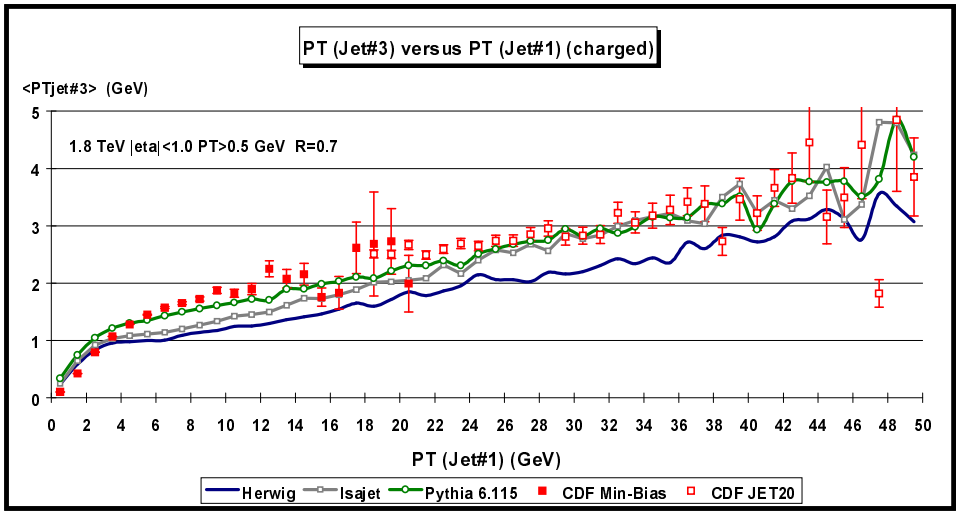

Fig. 4.15. Average transverse momentum of jet#3 (*third highest P_T jet*) for charged particles with $P_T > 0.5$ GeV and $|\eta| < 1$ as a function of P_T(jet#1). If jet#3 does not exist then it is assigned zero transverse momentum. The solid (open) points are the Min-Bias data (JET20 data). The data are compared with the QCD "hard" scattering Monte-Carlo predictions of Herwig 5.9, Isajet 7.32, and Pythia 6.115 (*corrected for the CTC efficiency*). Jets are defined as "circular regions" (R = 0.7) in η-ϕ space (see Fig. 4.1) and contain charged particles from the underlying event as well as particles which originate from the fragmentation of high P_T outgoing partons (see Fig. 1.1).

The transverse momentum of Jet#3 is quite sensitive to the activity of the underlying event. Fig. 4.15 compares the data on $< P_T$(jet#3)$>$ as a function of P_T(jet#1) (*leading jet*) with the "hard" scattering Monte-Carlo predictions of Herwig 5.9, Isajet 7.32, and Pythia 6.115.

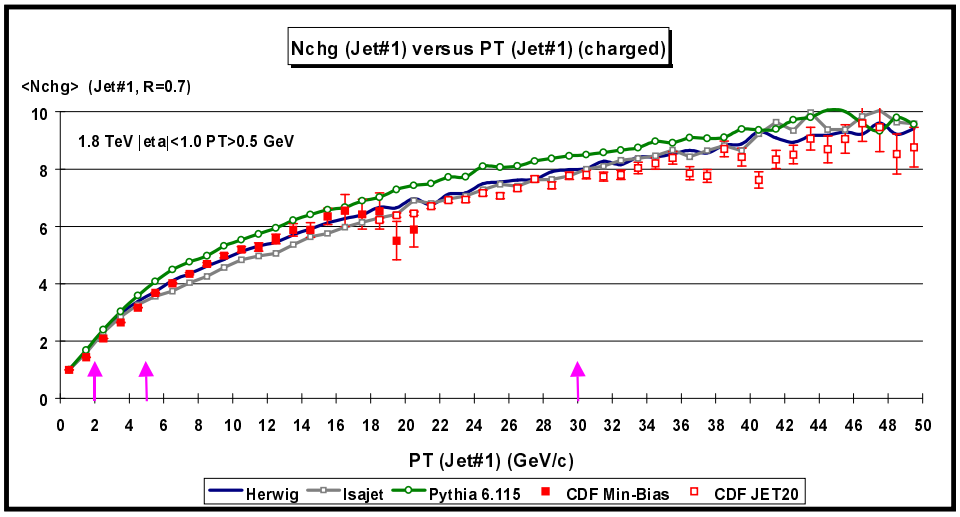

Fig. 4.16. Average number of charged particles in jet#1 (*leading jet*) for charged particles with $P_T > 0.5$ GeV and $|\eta| < 1$ as a function of P_T(jet#1). The solid (open) points are the Min-Bias data (JET20 data). The data are compared with the QCD "hard" scattering Monte-Carlo predictions of Herwig 5.9, Isajet 7.32, and Pythia 6.115 (*corrected for the CTC efficiency*). Jets are defined as "circular regions" (R = 0.7) in η-ϕ space (see Fig. 4.1)

and contain charged particles from the underlying event as well as particles which originate from the fragmentation of high P_T outgoing partons (see Fig 1.1). The arrows correspond the P_T(jet#1) cut-off values for the multiplicity distributions shown in Fig. 4.17, Fig. 4.18, and Fig. 4.19.

(4) Nchg(jet#1) versus P_T(jet#1)

Fig. 4.16 shows the average number of charged particles ($P_T > 0.5$ GeV and $|\eta| < 1$) in jet#1 *(leading jet)* as a function of P_T(jet#1). The solid points are the Min-Bias data and the open points are the JET20 data. The data are compared with the QCD "hard" scattering Monte-Carlo predictions of Herwig 5.9, Isajet 7.32, and Pythia 6.115. Jets are defined as "circular regions" (R = 0.7) in η-ϕ space (see Fig. 4.1) and contain charged particles from the underlying event as well as particles which originate from the fragmentation of high P_T outgoing partons (see Fig 1.1). Fig. 4.17, Fig. 4.18, and Fig. 4.19 show the multiplicity distribution of the charged particles in jet#1 (*leading jet*) for P_T(jet#1) > 2, 5, and 30 GeV, respectively. The QCD Monte-Carlo models agree well with the data even at 2 GeV.

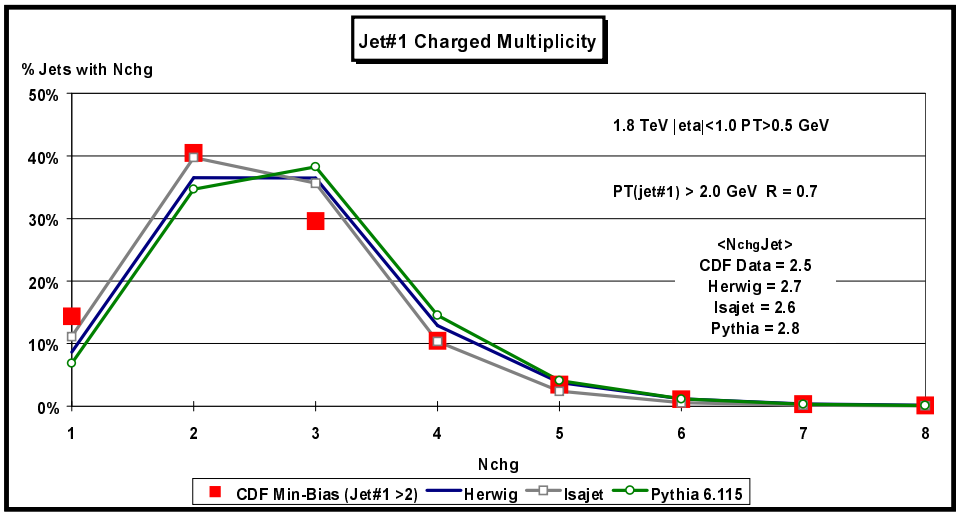

Fig. 4.17. Multiplicity distribution for charged particles in Jet#1 (*leading jet*) with $P_T > 0.5$ GeV and $|\eta| < 1$ when P_T(jet#1) > 2 GeV. Probability of finding N_{chg} charged particles in jet#1 (P_T(jet#1) > 2 GeV, R = 0.7). The solid squares are the Min-Bias data. The data are compared with the QCD "hard" scattering Monte-Carlo predictions of Herwig 5.9, Isajet 7.32, and Pythia 6.115 (*corrected for the CTC efficiency*).

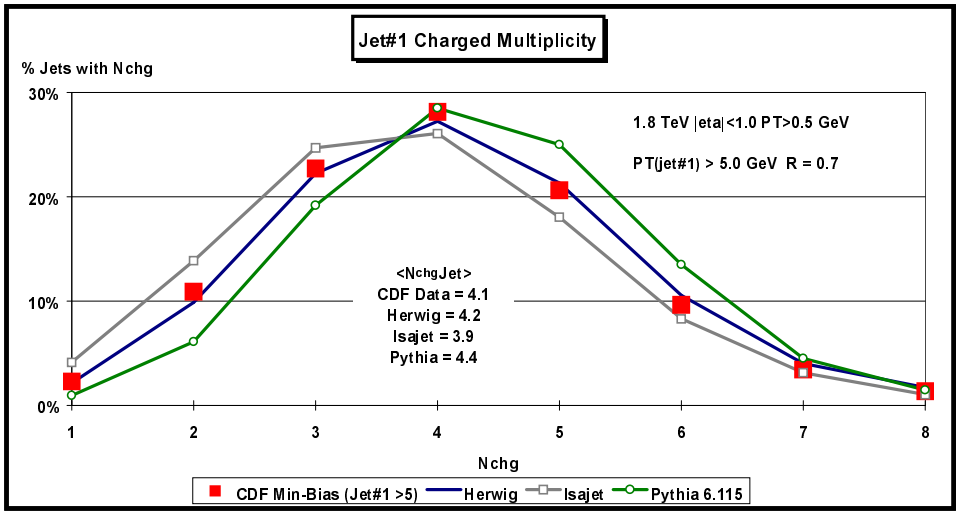

Fig. 4.18. Multiplicity distribution for charged particles in Jet#1 (*leading jet*) with $P_T > 0.5$ GeV and $|\eta| < 1$ when $P_T(\text{jet\#1}) > 5$ GeV. Probability of finding N_{chg} charged particles in jet#1 ($P_T(\text{jet\#1}) > 5$ GeV, R = 0.7). The solid squares are the Min-Bias data. The data are compared with the QCD "hard" scattering Monte-Carlo predictions of Herwig 5.9, Isajet 7.32, and Pythia 6.115 (*corrected for the CTC efficiency*).

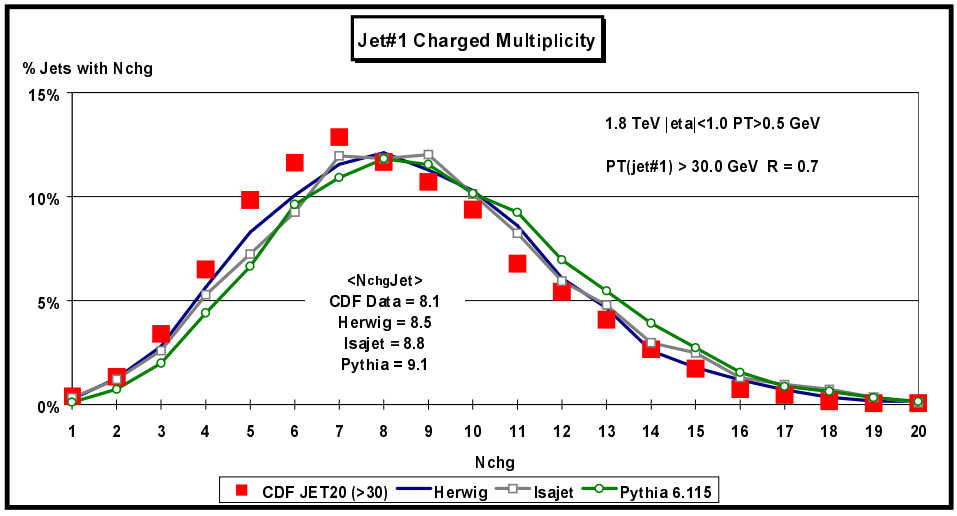

Fig. 4.19. Multiplicity distribution for charged particles in Jet#1 (*leading jet*) with $P_T > 0.5$ GeV and $|\eta| < 1$ when $P_T(\text{jet\#1}) > 30$ GeV. Probability of finding N_{chg} charged particles in jet#1 ($P_T(\text{jet\#1}) > 30$ GeV, R = 0.7). The solid squares are the JET20 data. The data are compared with the QCD "hard" scattering Monte-Carlo predictions of Herwig 5.9, Isajet 7.32, and Pythia 6.115 (*corrected for the CTC efficiency*).

Below 2 GeV the probability that the jet consists of just one particle becomes large. Jets are "born" somewhere around $P_T(\text{jet\#1})$ of about 1.5 GeV with, on the average, about 2 charged particles and grow to, on the average, about 10 charged particles at 50 GeV. The Monte-Carlo models agree as well with the data on 2 GeV jets as they do with the data on 50 GeV jets!

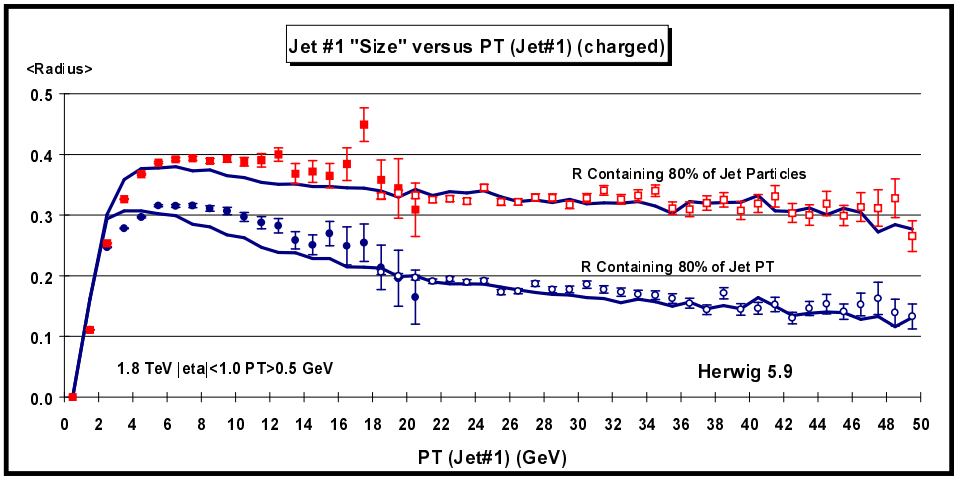

Fig. 4.20. Average "size" of jet#1 *(leading jet)* for charged particles with $P_T > 0.5$ GeV and $|\eta| < 1$ as a function of P_T(jet#1). The solid (open) points are the Min-Bias data (JET20 data). The squares (circles) correspond the radius in η-ϕ space, R, that contains 80% of the charged particles (80% of the P_T) in jet#1. The data are compared with the QCD "hard" scattering Monte-Carlo predictions of Herwig 5.9 (*corrected for the CTC efficiency*).

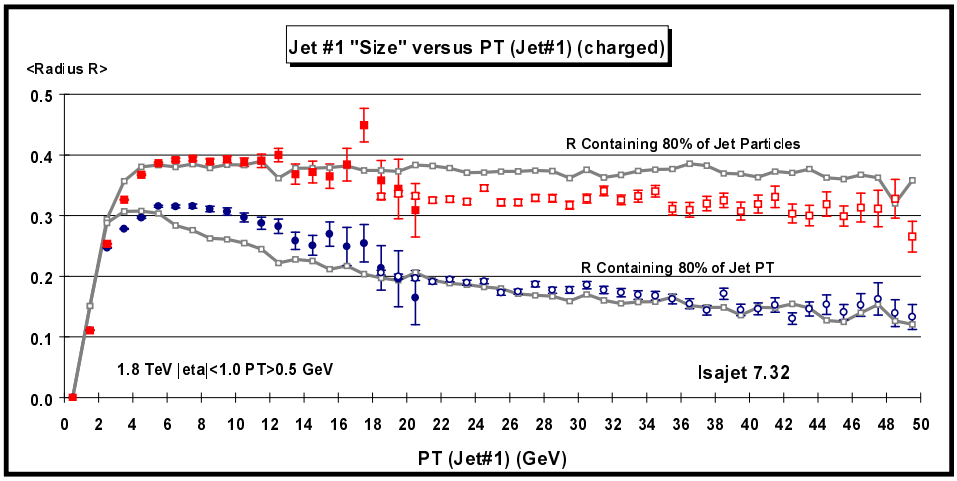

Fig. 4.21. Average "size" of jet#1 *(leading jet)* for charged particles with $P_T > 0.5$ GeV and $|\eta| < 1$ as a function of P_T(jet#1). The solid (open) points are the Min-Bias data (JET20 data). The squares (circles) correspond the radius in η-ϕ space, R, that contains 80% of the charged particles (80% of the P_T) in jet#1. The data are compared with the QCD "hard" scattering Monte-Carlo predictions of Isajet 7.32 (*corrected for the CTC efficiency*).

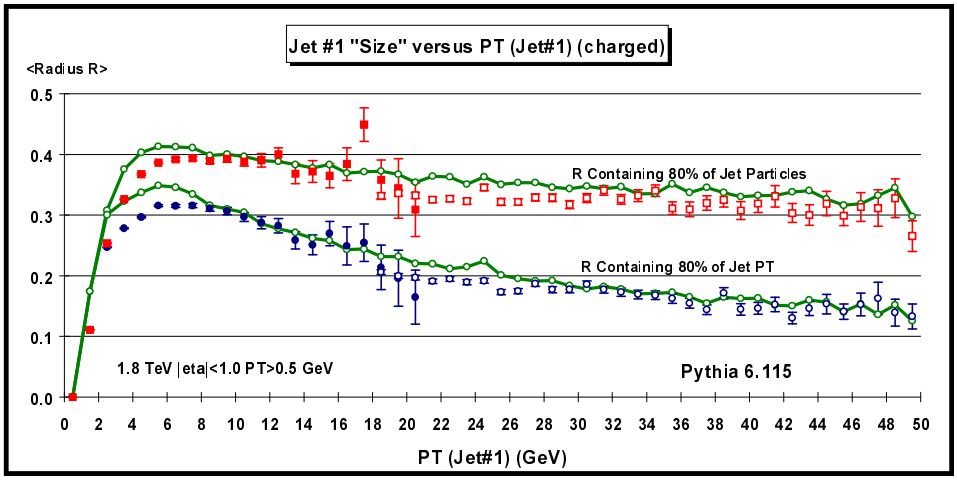

Fig. 4.22. Average "size" of jet#1 *(leading jet)* for charged particles with $P_T > 0.5$ GeV and $|\eta| < 1$ as a function of P_T(jet#1). The solid (open) points are the Min-Bias data (JET20 data). The squares (circles) correspond the radius in η-ϕ space, R, that contains 80% of the charged particles (80% of the P_T) in jet#1. The data are compared with the QCD "hard" scattering Monte-Carlo predictions of Pythia 6.115 (*corrected for the CTC efficiency*).

(5) Jet "Size" versus P_T(jet#1)

Although jets are defined as circular regions in η-ϕ space with R = 0.7, this is not the "size" of the "jet". We define the "size" of a "jet" in two ways, size in particle number and size in transverse momentum. The first corresponds to the radius in η-ϕ space that contains 80% of the charged particles in the jet and the second corresponds to the radius in η-ϕ space that contains 80% of the jet transverse momentum. The data on the average "jet size" of the leading jet versus P_T(jet#1) are compared with the QCD "hard" scattering Monte-Carlo predictions of Herwig 5.9 (Fig. 4.20), Isajet 7.32 (Fig. 4.21), and Pythia 6.115 (Fig. 4.22). A leading 20 GeV "jet" has 80% of its charged particles contained, on the average, within a radius in η-ϕ space of about 0.3, and 80% of its transverse momentum contained, on the average, within a radius of about 0.2. These plots clearly illustrate the "hot core" of jets. The transverse momentum of jets is located in a small radius that decreases as the "jet" P_T increases.

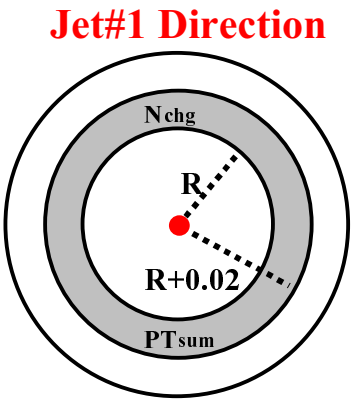

Fig. 4.23. Illustration of correlations in the distance R in η-ϕ space from the direction of the leading jet in the event, jet#1. The distance R is the distance in η-ϕ space between the leading jet and a charged particle with $P_T > 0.5$ GeV and $|\eta| < 1$, $R^2 = (\Delta\eta)^2 + (\Delta\phi)^2$. Plots of <Nchg> and <PTsum> as a function of R are referred to as "multiplicity flow in R" relative to jet#1 and "transverse momentum flow in R" relative to jet#1, respectively.

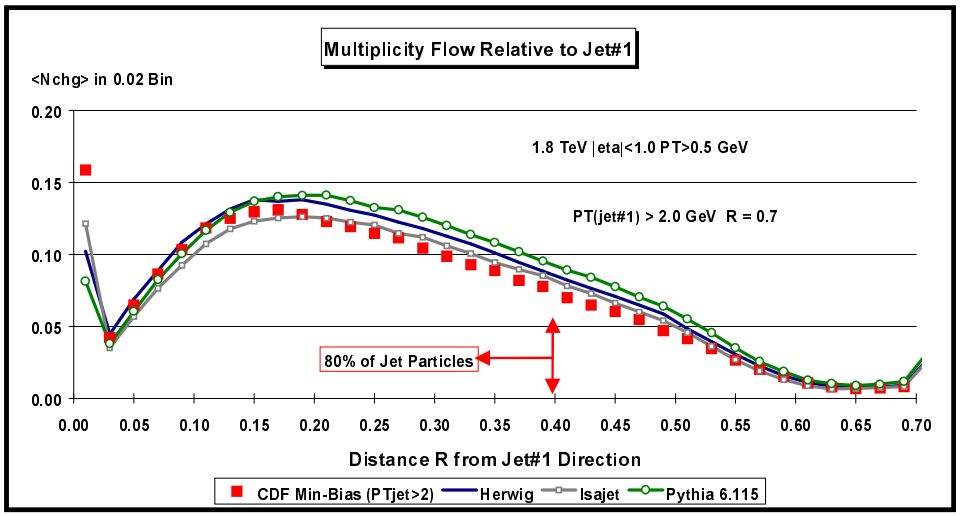

Fig. 4.24. Multiplicity flow in the distance R in η-ϕ space from jet#1 (*leading jet*) for charged particles with $P_T > 0.5$ GeV and $|\eta| < 1$ when P_T (jet#1) > 2 GeV. The points are <Nchg> in a 0.02 bin of R, where R is the distance in η-ϕ space from jet#1. The solid squares are the Min-Bias data. The data are compared with the QCD "hard" scattering Monte-Carlo predictions of Herwig 5.9, Isajet 7.32, and Pythia 6.115 (*corrected for the CTC efficiency*). For an "average jet" with P_T (jet#1) > 2 GeV, 80% of the charged particles are within R = 0.4. The spike at zero correspond to jets with only one charged particle (see Fig. 4.17). (*Note*: the "radius of an average jet" shown here is not the same as the "average jet radius" shown in Fig. 4.20.)

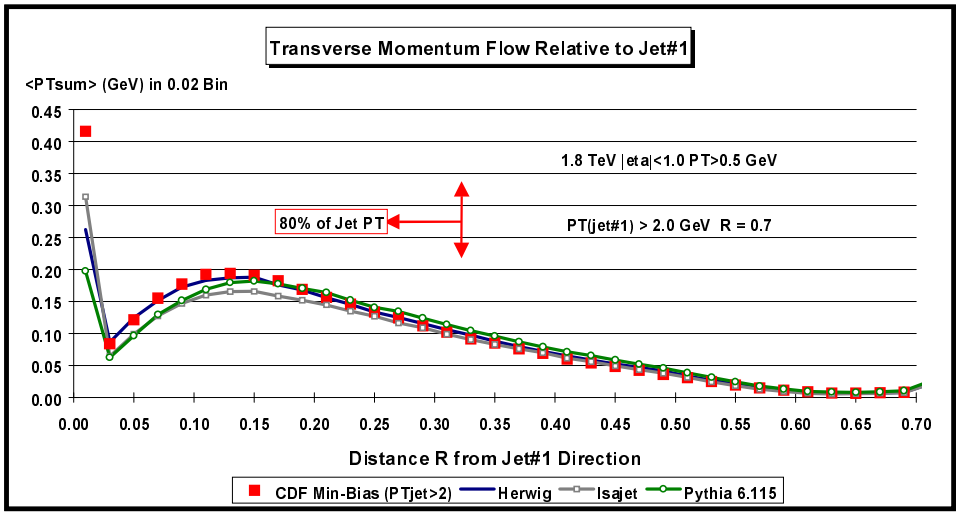

Fig. 4.25. Transverse momentum flow in the distance R in η-ϕ space from jet#1 (*leading jet*) for charged particles with $P_T > 0.5$ GeV and $|\eta| < 1$ when P_T (jet#1) > 2 GeV. The points are <PTsum> in a 0.02 bin of R, where R is the distance in η-ϕ space from jet#1. The solid squares are the Min-Bias data. The data are compared with the QCD "hard" scattering Monte-Carlo predictions of Herwig 5.9, Isajet 7.32, and Pythia 6.115 (*corrected for the CTC efficiency*). For an "average jet" with P_T (jet#1) > 2 GeV, 80% of the jet P_T lies within R = 0.33. The spike at zero correspond to jets with only one charged particle (see Fig. 4.17). (*Note*: the "radius of an average jet" shown here is not the same as the "average jet radius" shown in Fig. 4.20.)

We can study the distribution of charged particles and transverse momentum within the leading jet by examining the distribution of <Nchg> and <PTsum> as a function of the distance in η-ϕ space from the leading "jet" direction as illustrated in Fig. 4.23. Fig.4.24 and Fig. 4.25 compare data on the multiplicity flow and the transverse momentum flow, respectively, in the distance R in η-ϕ space from jet#1 for P_T(jet#1) > 2 GeV compared with the QCD "hard" scattering Monte-Carlo predictions of Herwig 5.9, Isajet 7.32, and Pythia 6.115. The spike at R = 0 correspond to jets consisting of just one charged particle. Fig. 4.26 and Fig. 4.27 show the same distributions for P_T(jet#1) > 5 GeV, while Fig. 4.28 and Fig. 4.29 examine the case where P_T(jet#1) > 30 GeV.

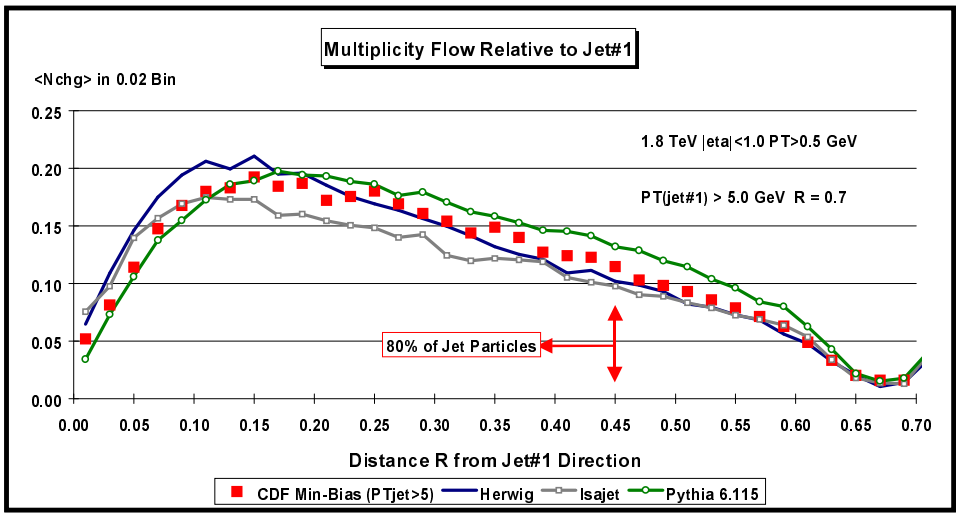

Fig. 4.26. Multiplicity flow in the distance R in η-ϕ space from jet#1 (*leading jet*) for charged particles with $P_T > 0.5$ GeV and $|\eta| < 1$ when P_T (jet#1) > 5 GeV. The points are <Nchg> in a 0.02 bin of R, where R is the distance in η-ϕ space from jet#1. The solid squares are the Min-Bias data. The data are compared with the QCD "hard" scattering Monte-Carlo predictions of Herwig 5.9, Isajet 7.32, and Pythia 6.115 (*corrected for the CTC efficiency*). For an "average jet" with P_T (jet#1) > 5 GeV, 80% of the charged particles are within R = 0.45. (*Note*: the "radius of an average jet" shown here is not the same as the "average jet radius" shown in Fig. 4.20.)

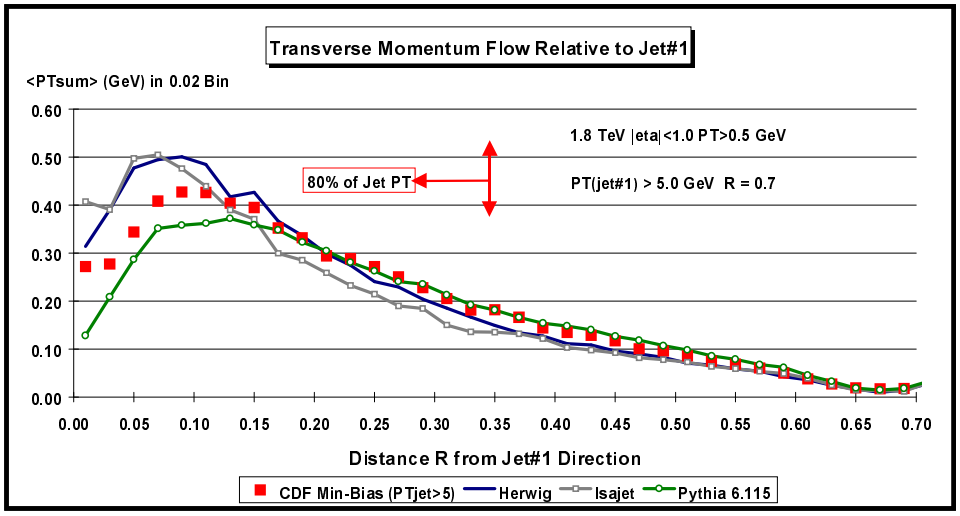

Fig. 4.27. Transverse momentum flow in the distance R in η-ϕ space from jet#1 (*leading jet*) for charged particles with $P_T > 0.5$ GeV and $|\eta| < 1$ when P_T (jet#1) > 5 GeV. The points are $\langle PT_{sum} \rangle$ in a 0.02 bin of R, where R is the distance in η-ϕ space from jet#1. The solid squares are the Min-Bias data. The data are compared with the QCD "hard" scattering Monte-Carlo predictions of Herwig 5.9, Isajet 7.32, and Pythia 6.115 (*corrected for the CTC efficiency*). For an "average jet" with P_T (jet#1) > 5 GeV, 80% of the jet P_T lies within R = 0.35. (*Note*: the "radius of an average jet" shown here is not the same as the "average jet radius" shown in Fig. 4.20.)

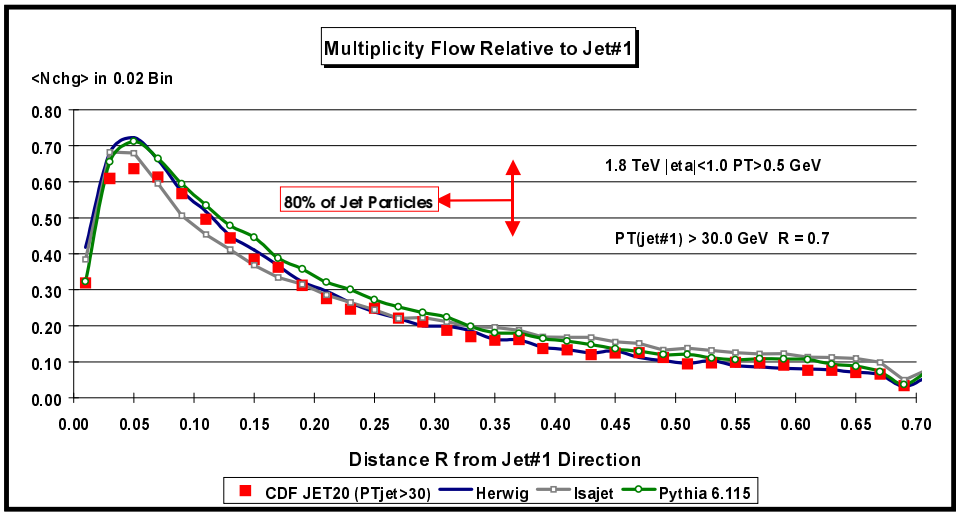

Fig. 4.28. Multiplicity flow in the distance R in η-ϕ space from jet#1 (*leading jet*) for charged particles with $P_T > 0.5$ GeV and $|\eta| < 1$ when P_T (jet#1) > 30 GeV. The points are $\langle N_{chg} \rangle$ in a 0.02 bin of R, where R is the distance in η-ϕ space from jet#1. The solid squares are the JET20 data. The data are compared with the QCD "hard" scattering Monte-Carlo predictions of Herwig 5.9, Isajet 7.32, and Pythia 6.115 (*corrected for the CTC efficiency*). For an "average jet" with P_T (jet#1) > 30 GeV, 80% of the charged particles are within R = 0.37. (*Note*: the "radius of an average jet" shown here is not the same as the "average jet radius" shown in Fig. 4.20.)

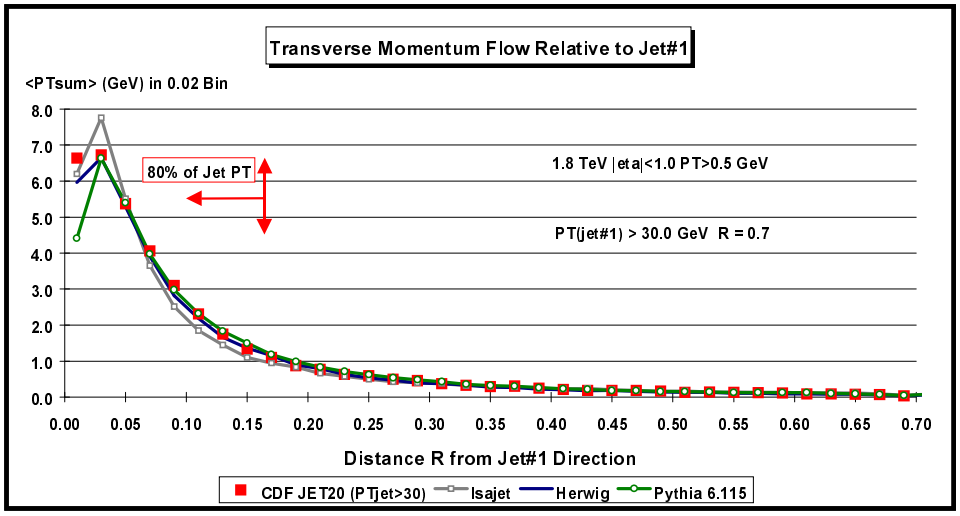

Fig. 4.29. Transverse momentum flow in the distance R in η-ϕ space from jet#1 (*leading jet*) for charged particles with $P_T > 0.5$ GeV and $|\eta| < 1$ when P_T (jet#1) > 30 GeV. The points are $\langle PT_{sum} \rangle$ in a 0.02 bin of R, where R is the distance in η-ϕ space from jet#1. The solid squares are the JET20 data. The data are compared with the QCD "hard" scattering Monte-Carlo predictions of Herwig 5.9, Isajet 7.32, and Pythia 6.115 (*corrected for the CTC efficiency*). For an "average jet" with P_T (jet#1) > 30 GeV, 80% of the jet P_T lies within R = 0.17 (*Note*: the "radius of an average jet" shown here is not the same as the "average jet radius" shown in Fig. 4.20.)

(6) Jet "Charged Fragmentation Function" F(z)

The normal fragmentation function corresponds to the number of particles between z and z +dz (*i.e.* number density), where z = p/P and p is the particle momentum and P is the momentum of the fragmenting parton. Here we define a "charged fragmentation function", F(z), which describes the distribution of charged particles within the leading "charged particle jet". The function F(z) is the number of charged particles between z and z +dz (*i.e.* the charge particle number density), where z = p/Pjet is the fraction of the overall charged particle momentum of the jet carried by the charged particle with momentum p. The fraction z ranges from zero to one. The integral of F(z) over z is the average multiplicity of charged particles within the jet. We refer to this as a "fragmentation function", however it is not a *true* fragmentation function since some of the particles within the leading jets originate from the underlying event and we can never be sure that we have included all the particles that come from the outgoing high P_T parton. Fig. 4.30 shows that data on F(z) for P_T(jet#1) > 2, 5, and 30 GeV. Fig. 4.31 compares data on the "charged fragmentation function" F(z) of the leading "jet" for P_T(jet#1) > 2 GeV with the QCD "hard" scattering Monte-Carlo predictions of Herwig 5.9, Isajet 7.32, and Pythia 6.115. . Fig. 4.32 compares the data on F(z) for P_T(jet#1) > 5 GeV with the QCD predictions, while Fig. 4.33 examines the case P_T(jet#1) > 30 GeV.

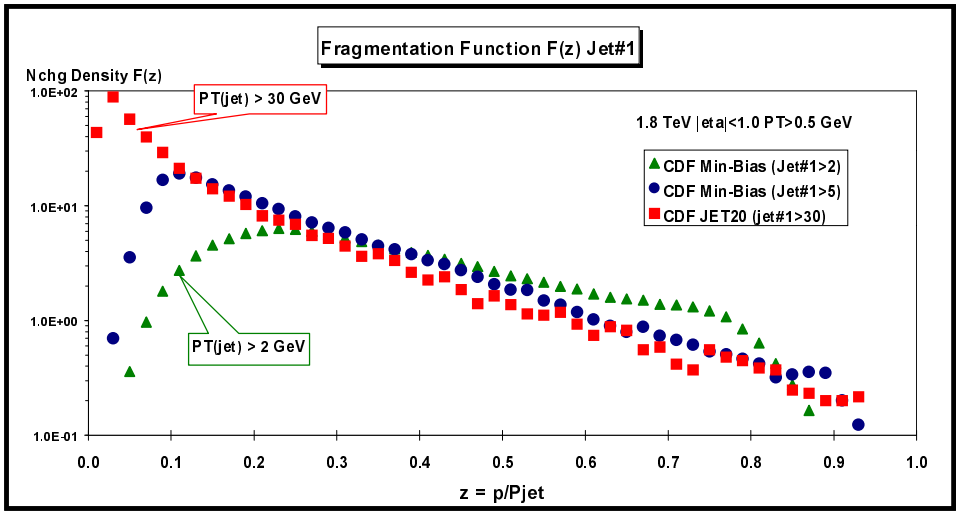

Fig. 4.30. "Charged fragmentation function" F(z) for particles in jet#1 (*leading jet*) with $P_T > 0.5$ GeV and $|\eta| < 1$. The points are the number density, dN_{chg}/dz, for charged particles in jet#1, where z = p/P(jet#1) is the ratio of the charged particle momentum to the charged momentum of jet#1. The integral of F(z) over z gives the number of particles within jet#1. The solid triangles (solid circles) are the Min-Bias data for $P_T(\text{jet\#1}) > 2$ GeV ($P_T(\text{jet\#1}) > 5$ GeV). The solid squares are the JET20 data for $P_T(\text{jet\#1}) > 30$ GeV. Jets are defined as "circular regions" (R = 0.7) in η-ϕ space (see Fig. 4.1) and contain charged particles from the underlying event as well as particles which originate from the fragmentation of high P_T outgoing partons (see Fig 1.1).

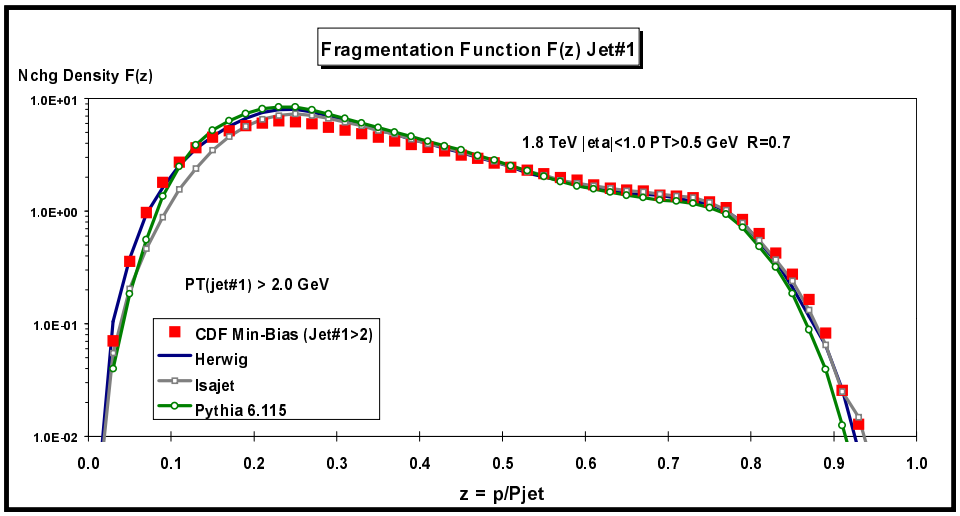

Fig. 4.31. Data from Fig. 4.30 on the "charged fragmentation function" F(z) for particles in jet#1 (*leading jet*) with $P_T > 0.5$ GeV and $|\eta| < 1$ for $P_T(\text{jet\#1}) > 2$ GeV compared with the QCD "hard" scattering Monte-Carlo predictions of Herwig 5.9, Isajet 7.32, and Pythia 6.115 (*corrected for the CTC efficiency*). Jets are defined as "circular regions" (R = 0.7) in η-ϕ space (see Fig. 4.1) and contain charged particles from the underlying event as well as particles which originate from the fragmentation of high P_T outgoing partons (see Fig 1.1).

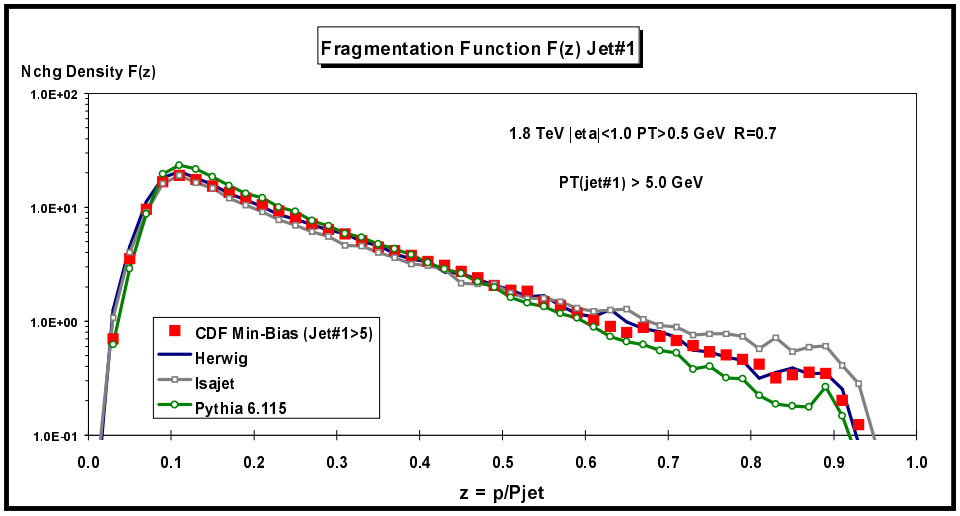

Fig. 4.32. Data from Fig. 4.30 on the "charged fragmentation function" F(z) for particles in jet#1 (*leading jet*) with $P_T > 0.5$ GeV and $|\eta| < 1$ for $P_T(\text{jet\#1}) > 5$ GeV compared with the QCD "hard" scattering Monte-Carlo predictions of Herwig 5.9, Isajet 7.32, and Pythia 6.115 (*corrected for the CTC efficiency*). Jets are defined as "circular regions" (R = 0.7) in η-ϕ space (see Fig. 4.1) and contain charged particles from the underlying event as well as particles which originate from the fragmentation of high P_T outgoing partons (see Fig 1.1).

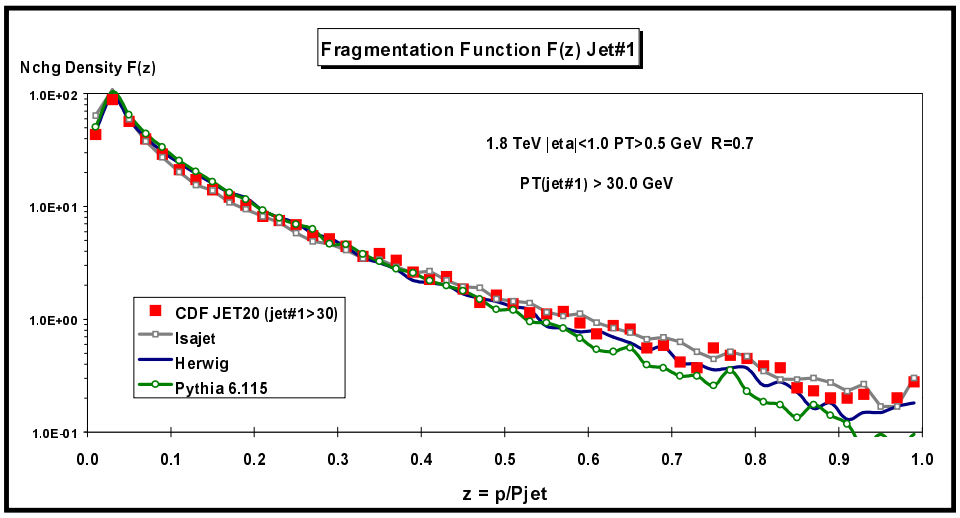

Fig. 4.33. Data from Fig. 4.30 on the "charged fragmentation function" F(z) for particles in jet#1 (*leading jet*) with $P_T > 0.5$ GeV and $|\eta| < 1$ for $P_T(\text{jet\#1}) > 30$ GeV compared with the QCD "hard" scattering Monte-Carlo predictions of Herwig 5.9, Isajet 7.32, and Pythia 6.115 (*corrected for the CTC efficiency*). Jets are defined as "circular regions" (R = 0.7) in η-ϕ space (see Fig. 4.1) and contain charged particles from the underlying event as well as particles which originate from the fragmentation of high P_T outgoing partons (see Fig 1.1).

The QCD "hard" scattering models describe quite well (*although not perfectly*) the multiplicity distribution of charged particles within the leading jet (Fig. 4.17 – Fig 4.19), the "size" of the leading jet (Fig. 4.20 – Fig. 4.22), the distribution of charged particles and transverse momentum as a function of the distance R in η-ϕ space from the leading jet direction (Fig. 4.24 – Fig. 4.29),

and the leading jet fragmentation functions (Fig. 4.31 – Fig. 4.33). We now proceed to study the overall event structure as a function of P_T(jet#1), where the QCD Monte-Carlo models do not do as well.

V. Studying the Event Structure as a Function of P_T(jet#1)

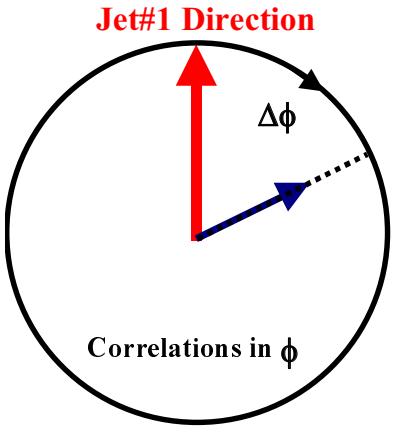

Fig. 5.1. Illustration of correlations in azimuthal angle $\Delta\phi$ relative to the direction of the leading jet in the event, jet#1. The angle $\Delta\phi = |\phi - \phi_{jet\#1}|$ is the relative azimuthal angle between charged particles and the direction of jet#1. Plots of $\langle N_{chg} \rangle$ and $\langle PT_{sum} \rangle$ as a function of $\Delta\phi$ are referred to as "multiplicity flow in ϕ" relative to jet#1 and "transverse momentum flow in ϕ" relative to jet#1, respectively.

(1) Correlations in $\Delta\phi$ relative to P_T(jet#1)

To see overall event structure we examine correlations in the azimuthal angle $\Delta\phi$ relative to the direction of the leading "jet" in the event, P_T(jet#1). As illustrated in Fig. 5.1, the angle $\Delta\phi$ is the relative azimuthal angle between charged particles and the direction of P_T(jet#1). Plots of $\langle N_{chg} \rangle$ and $\langle PT_{sum} \rangle$ as a function of $\Delta\phi$ are referred to as "multiplicity flow in ϕ" relative to P_T(jet#1) and "transverse momentum flow in ϕ" relative to PT(jet#1), respectively. All charged particles ($P_T > 0.5$ GeV and $|\eta| < 1$) are included in these plots (*including those in jet#1*).

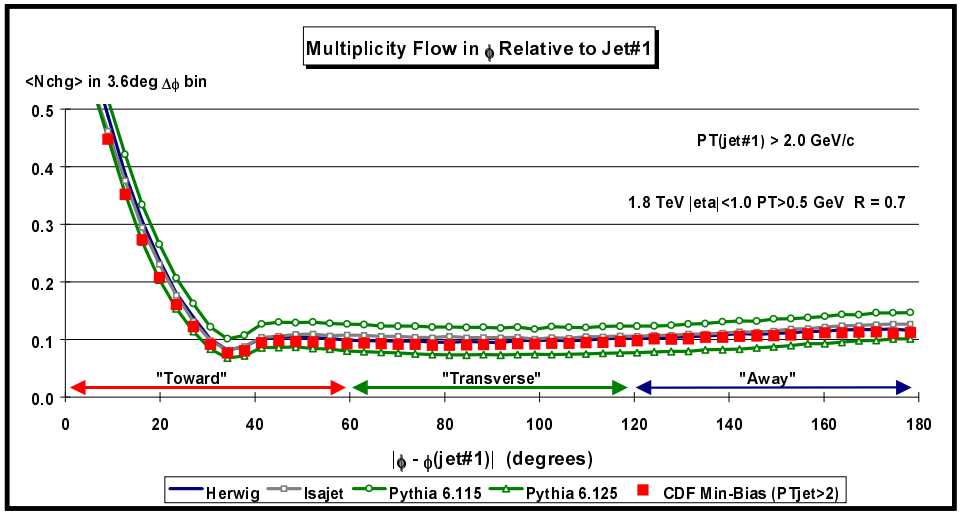

Fig. 5.2. Average number of charged particles as a function of the relative azimuthal angle, $|\phi - \phi_{jet\#1}|$, between the particle and jet#1 (*leading jet*) for $P_T(jet\#1) > 2$ GeV. Each point corresponds to the $\langle N_{chg} \rangle$ in a 3.6^o bin. The solid squares are the Min-Bias data ($P_T > 0.5$ GeV, $|\eta| < 1$) and the curves correspond to the QCD "hard" scattering Monte-Carlo predictions of Herwig 5.9 , Isajet 7.32, Pythia 6.115, and Pythia 6.125. The theoretical predictions have been corrected for the CTC efficiency. The "toward", "transverse", and "away" regions are defined in Fig. 5.8.

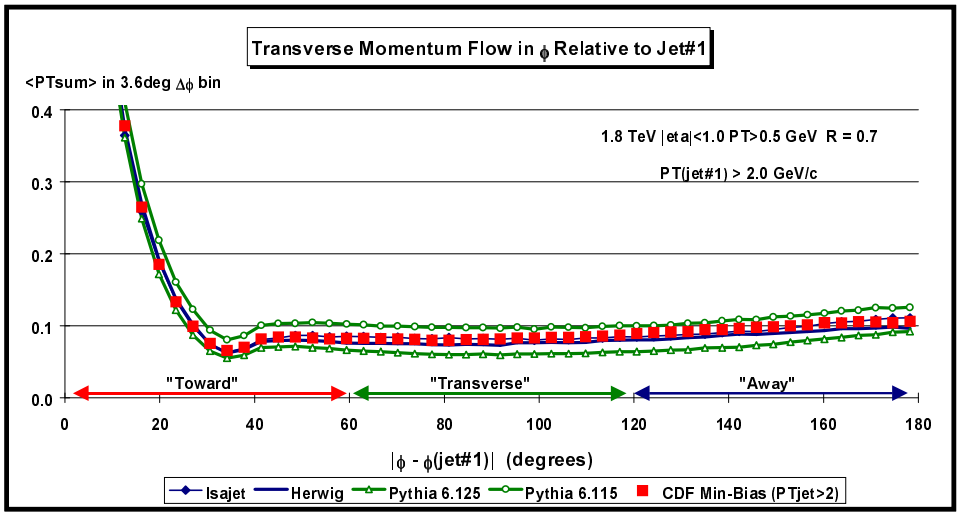

Fig. 5.3. Average scalar sum of charged particles as a function of the relative azimuthal angle, $|\phi - \phi_{jet\#1}|$, between the particle and jet#1 (*leading jet*) for $P_T(jet\#1) > 2$ GeV. Each point corresponds to the $\langle PT_{sum} \rangle$ in a 3.6^o bin. The solid squares are the Min-Bias data ($P_T > 0.5$ GeV, $|\eta| < 1$) and the curves correspond to the QCD "hard" scattering Monte-Carlo predictions of Herwig 5.9 , Isajet 7.32, Pythia 6.115, and Pythia 6.125. The theoretical predictions have been corrected for the CTC efficiency. The "toward", "transverse", and "away" regions are defined in Fig. 5.8.

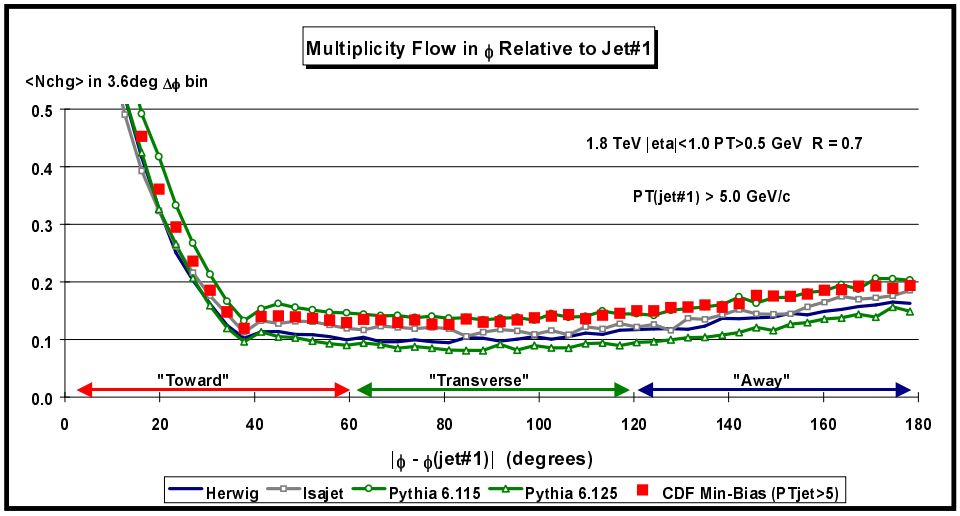

Fig. 5.4. Average number of charged particles as a function of the relative azimuthal angle, $|\phi - \phi_{jet\#1}|$, between the particle and jet#1 (*leading jet*) for P_T(jet#1) > 5 GeV. Each point corresponds to the $\langle N_{chg} \rangle$ in a 3.6^o bin. The solid squares are the Min-Bias data ($P_T > 0.5$ GeV, $|\eta| < 1$) and the curves correspond to the QCD "hard" scattering Monte-Carlo predictions of Herwig 5.9 , Isajet 7.32, Pythia 6.115, and Pythia 6.125. The theoretical predictions have been corrected for the CTC efficiency. The "toward", "transverse", and "away" regions are defined in Fig. 5.8.

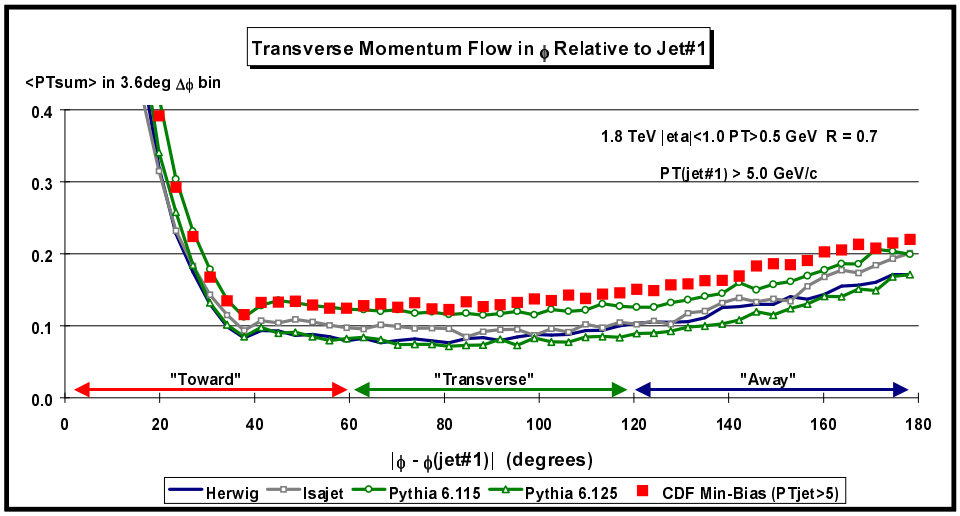

Fig. 5.5. Average scalar sum of charged particles as a function of the relative azimuthal angle, $|\phi - \phi_{jet\#1}|$, between the particle and jet#1 (*leading jet*) for P_T(jet#1) > 5 GeV. Each point corresponds to the $\langle PT_{sum} \rangle$ in a 3.6^o bin. The solid squares are the Min-Bias data ($P_T > 0.5$ GeV, $|\eta| < 1$) and the curves correspond to the QCD "hard" scattering Monte-Carlo predictions of Herwig 5.9 , Isajet 7.32, Pythia 6.115, and Pythia 6.125. The theoretical predictions have been corrected for the CTC efficiency. The "toward", "transverse", and "away" regions are defined in Fig. 5.8.

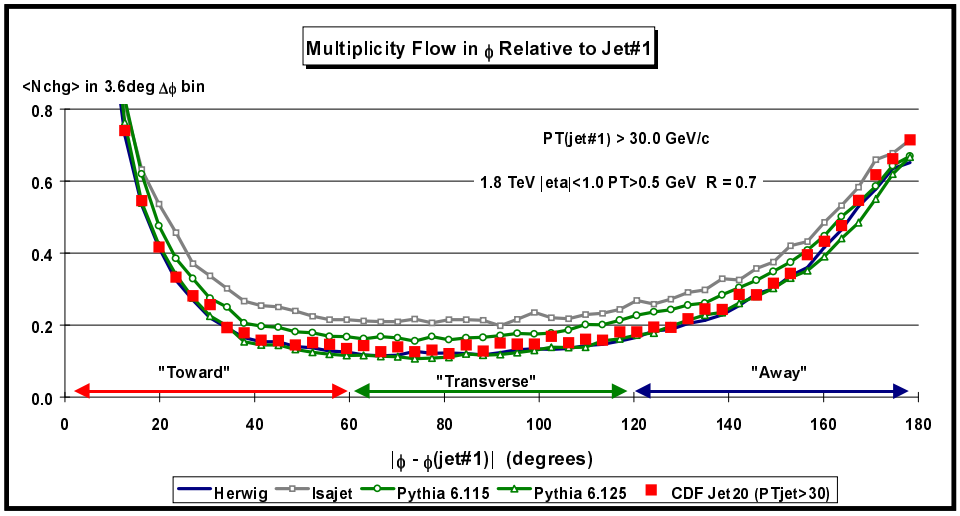

Fig. 5.6. Average number of charged particles as a function of the relative azimuthal angle, $|\phi - \phi_{jet\#1}|$, between the particle and jet#1 (*leading jet*) for $P_T(jet\#1) > 30$ GeV. Each point corresponds to the $\langle N_{chg} \rangle$ in a 3.6^o bin. The solid squares are the Min-Bias data ($P_T > 0.5$ GeV, $|\eta| < 1$) and the curves correspond to the QCD "hard" scattering Monte-Carlo predictions of Herwig 5.9 , Isajet 7.32, Pythia 6.115, and Pythia 6.125. The theoretical predictions have been corrected for the CTC efficiency. The "toward", "transverse", and "away" regions are defined in Fig. 5.8.

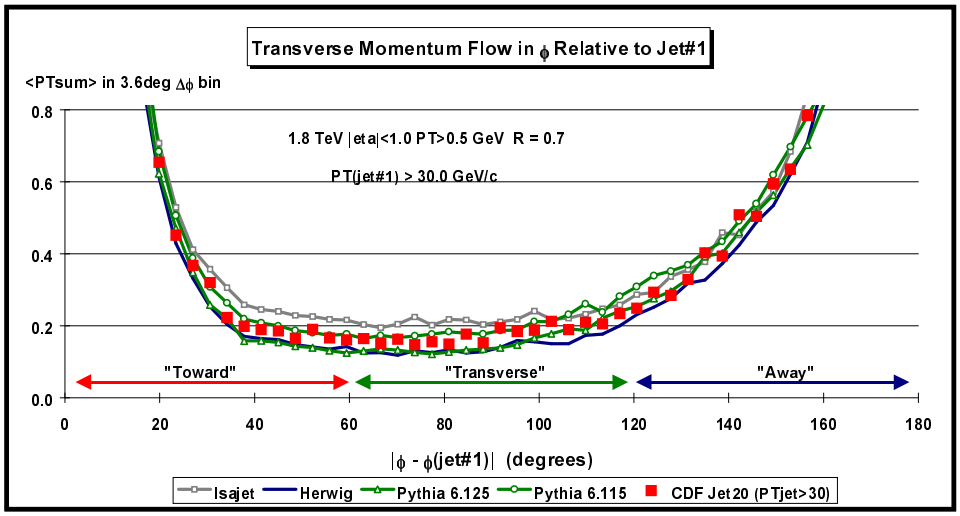

Fig. 5.7. Average scalar sum of charged particles as a function of the relative azimuthal angle, $|\phi - \phi_{jet\#1}|$, between the particle and jet#1 (*leading jet*) for $P_T(jet\#1) > 30$ GeV. Each point corresponds to the $\langle PT_{sum} \rangle$ in a 3.6^o bin. The solid squares are the JET20 data ($P_T > 0.5$ GeV, $|\eta| < 1$) and the curves correspond to the QCD "hard" scattering Monte-Carlo predictions of Herwig 5.9 , Isajet 7.32, Pythia 6.115, and Pythia 6.125. The theoretical predictions have been corrected for the CTC efficiency. The "toward", "transverse", and "away" regions are defined in Fig. 5.8.

Fig. 5.2 and Fig. 5.3 shows the data on the multiplicity flow and transverse momentum flow, respectively, in ϕ relative to P_T(jet#1) for P_T(jet#1) > 2 GeV compared with the QCD "hard" scattering Monte-Carlo predictions of Herwig 5.9, Isajet 7.32, and Pythia 6.115. Fig. 5.4 and Fig. 5.5 examine the case where P_T(jet#1) > 5 GeV, while Fig. 5.6 and Fig. 5.7 have P_T(jet#1) > 30 GeV.

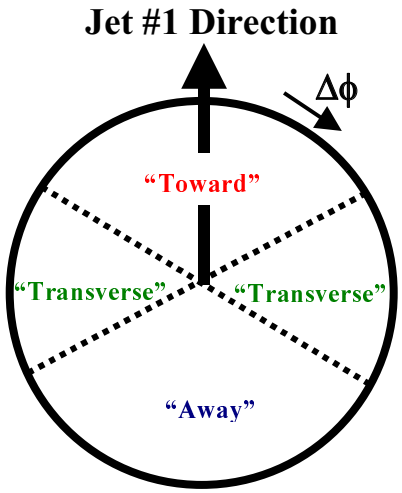

Fig. 5.8. Illustration of correlations in azimuthal angle $\Delta\phi$ relative to the direction of the leading jet in the event, jet#1. The angle $\Delta\phi = |\phi - \phi_{jet\#1}|$ is the relative azimuthal angle between charged particles and the direction of jet#1. The region $|\phi - \phi_{jet\#1}| < 60^o$ is referred to as "toward" jet#1(*includes particles in jet#1*) and the region $|\phi - \phi_{jet\#1}| > 120^o$ is called "away" from jet#1. The "transverse" to jet#1 region is defined by $60^o < |\phi - \phi_{jet\#1}| < 120^o$. Each region, "toward", "transverse", and "away" covers the range $|\Delta\eta| \times |\Delta\phi| = 2 \times 120^o$.

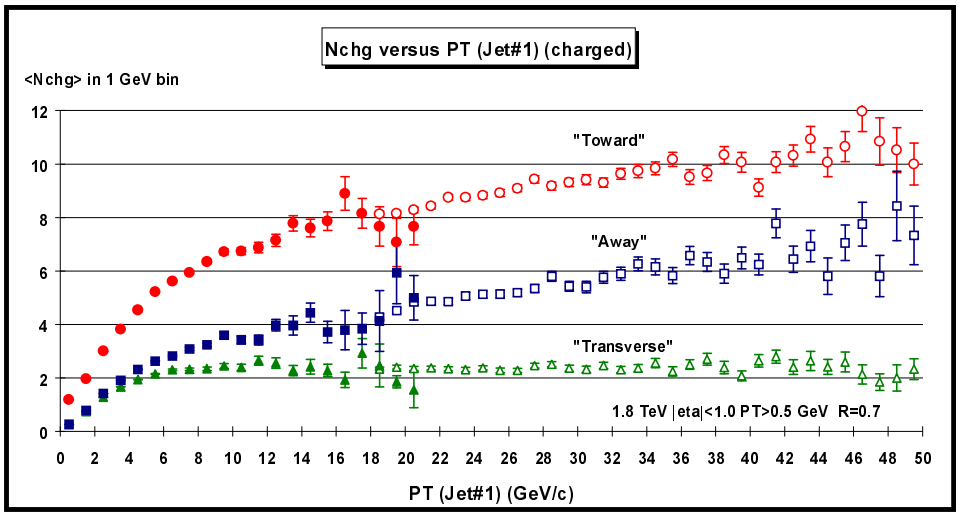

Fig. 5.9. Average number of charged particles (P_T > 0.5 GeV and $|\eta| < 1$) as a function of P_T(jet#1) (*leading jet*) for the three regions defined in Fig. 5.8. Each point corresponds to

the "toward", "transverse", or "away" <Nchg> in a 1 GeV bin. The solid (open) points are the Min-Bias data (JET20 data). The data have not been corrected for efficiency.

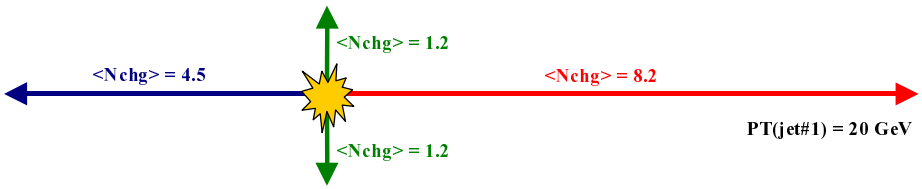

Fig. 5.10. Illustration (*drawn to scale*) of an "average" proton-antiproton event at 1.8 TeV with $P_T(jet\#1) = 20$ GeV. The data in Fig. 5.8 show that the average number of charged particles ($P_T > 0.5$ GeV and $|\eta| < 1$) for the three regions defined in Fig. 5.8 is 8.2 charged particles "toward" jet#1, 2.4 "transverse" to jet#1, and 4.5 "away" from jet#1. The data have not been corrected for efficiency (*the true multiplicities are about 9% higher*).

(2) Event "Shape" versus P_T(jet#1)

In Fig. 5.2 – Fig. 5.7 we have labeled the region $|\phi - \phi_{jet\#1}| < 60^o$ as "toward" jet#1 and the region $|\phi - \phi_{jet\#1}| > 120^o$ is as "away" from jet#1. The "transverse" to jet#1 region is defined by $60^o < |\phi - \phi_{jet\#1}| < 120^o$. As illustrated in Fig. 5.8, each region, "toward", "transverse", and "away" covers the range $|\Delta\eta| \times |\Delta\phi| = 2 \times 120^o$. The "toward" region includes the particles from jet#1 as well as any other charged particles in the region. The "transverse" region is very sensitive to the underlying event. The "away" region is a mixture of the underlying event and the "away-side" jet. Fig. 5.9 shows the data on the average number of charged particles ($P_T > 0.5$ GeV and $|\eta| < 1$) as a function of $P_T(jet\#1)$ for the three regions. Each point corresponds to the "toward", "transverse", or "away" <Nchg> in a 1 GeV bin. The solid points are the Min-Bias data and the open points are the JET20 data. The data in Fig. 5.9 define the average event "shape". This is illustrated in Fig. 5.10 which shows an "average" proton-antiproton collider event at 1.8 TeV with $P_T(jet\#1) = 20$ GeV. There are, on the average, 8.2 charged particles "toward" jet#1 (*including the particles in jet#1*), 2.4 "transverse" to jet#1, and 4.5 "away" from jet#1. The "transverse" and "away" numbers are very similar the those in Fig. 3.15 for PTmax = 10 GeV.

As was the case in Fig. 3.14, there is a lot of activity in the "transverse" region. If we suppose that the "transverse" multiplicity is uniform in azimuthal angle ϕ and rapidity η, the observed 2.4 charged particles translates to 3.9 charged particles per unit rapidity with $P_T > 0.5$ GeV (multiply by 3 to get 360^o, divide by 2 for the two units of rapidity, multiply by 1.09 to correct the CTC efficiency). We know that if we include all P_T then there are roughly 4 charged particles per unit rapidity and here there about the same but with $P_T > 0.5$ GeV! The underlying event has a charge particle density that is at least a factor of two larger than the 4 charged particles per unity rapidity seen in "soft" parton-antiproton collisions at this energy. The charged particle density in the underlying event ("transverse" region) is a function of $P_T(jet\#1)$ and as can be seen in Fig. 5.9 it rises very rapidity as $P_T(jet\#1)$ increases. The "transverse" charged multiplicity doubles in

going from P_T(jet#1) = 1.5 GeV to P_T(jet#1) = 2.5 GeV and forms an approximately constant "plateau" for P_T(jet#1) > 6 GeV. Of course, the "plateau" observed here is essentially the same "plateau" observed in Fig. 3.14.

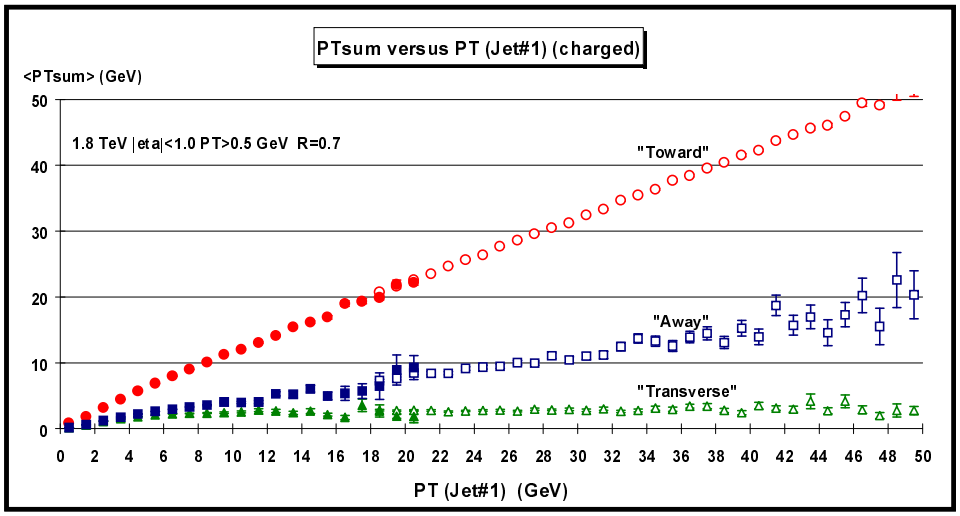

Fig. 5.11. Average *scalar* P_T sum of charged particles with $P_T > 0.5$ GeV and $|\eta| < 1$as a function of PT(jet#1) (*leading jet*) for the three regions defined in Fig. 5.8. Each point corresponds to the "toward", "transverse", or "away" <PTsum> in a 1 GeV bin. The solid (open) points are the Min-Bias data (JET20 data). The data have not been corrected for efficiency.

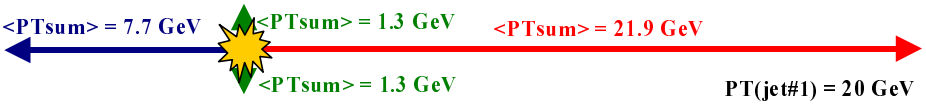

Fig. 5.12. Illustration (*drawn to scale*) of an "average" proton-antiproton collider event at 1.8 TeV with P_T(jet#1) = 20 GeV. The data in Fig. 5.11 show that the average *scalar* PT sum of charged particles with $P_T > 0.5$ GeV and $|\eta| < 1$ for the three regions defined in Fig. 5.8 is 21.9 GeV "toward" Jet#1, 2.6 GeV "transverse" to jet#1, and 7.7 GeV "away" from jet#1. The data have not been corrected for efficiency.

Fig. 5.11 shows the data on the average *scalar* PT sum of charged particles ($P_T > 0.5$ GeV and $|\eta| < 1$) as a function of P_T(jet#1) for the three regions. Each point corresponds to the "toward", "transverse", or "away" <PTsum> in a 1 GeV bin. The solid points are the Min-Bias data and the open points are the JET20 data. Fig. 5.12 illustrates an "average" proton-antiproton collider event at 1.8 TeV with P_T(jet#1) = 20 GeV. There is, on the average, 21.9 GeV "toward" jet#1 (*including the particles in jet#1*), 2.6 GeV "transverse" to jet#1, and 7.7 GeV "away" from jet#1.

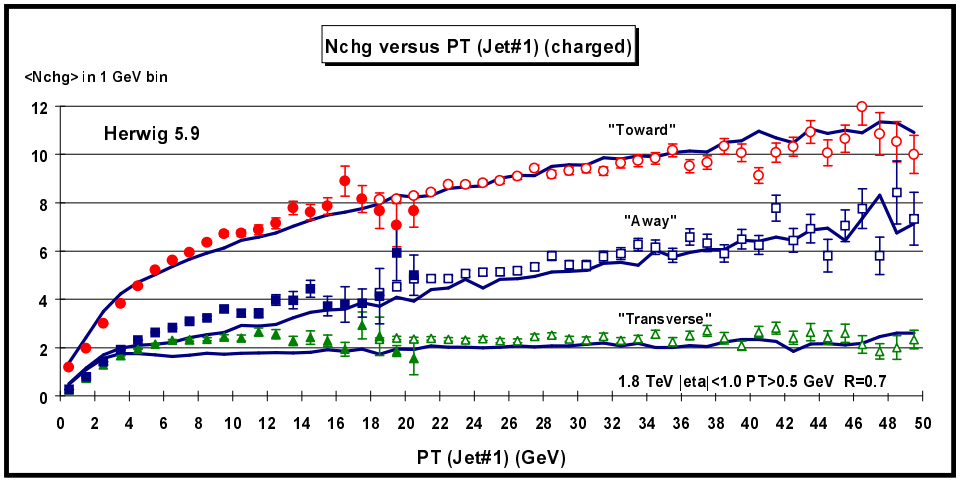

Fig. 5.13. Data from Fig. 5.9 on the average number of charged particles ($P_T > 0.5$ GeV and $|\eta| < 1$) as a function of PT(jet#1) (*leading jet*) for the three regions defined in Fig. 5.8 compared with the QCD "hard" scattering Monte-Carlo predictions of Herwig 5.9. Each point corresponds to the "toward", "transverse", or "away" $\langle N_{chg} \rangle$ in a 1 GeV bin. The theoretical predictions have been corrected for the CTC efficiency.

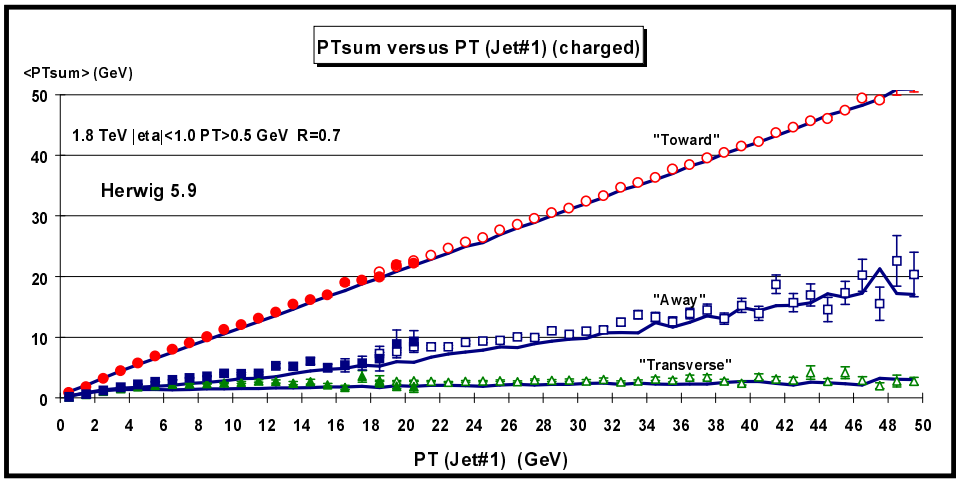

Fig. 5.14. Data from Fig. 5.11 on the average *scalar* P_T sum of charged particles with $P_T > 0.5$ GeV and $|\eta| < 1$as a function of PT(jet#1) (*leading jet*) for the three regions defined in Fig. 5.8 compared with the QCD "hard" scattering Monte-Carlo predictions of Herwig 5.9. Each point corresponds to the "toward", "transverse", or "away" $\langle PT_{sum} \rangle$ in a 1 GeV bin. The theoretical predictions have been corrected for the CTC efficiency.

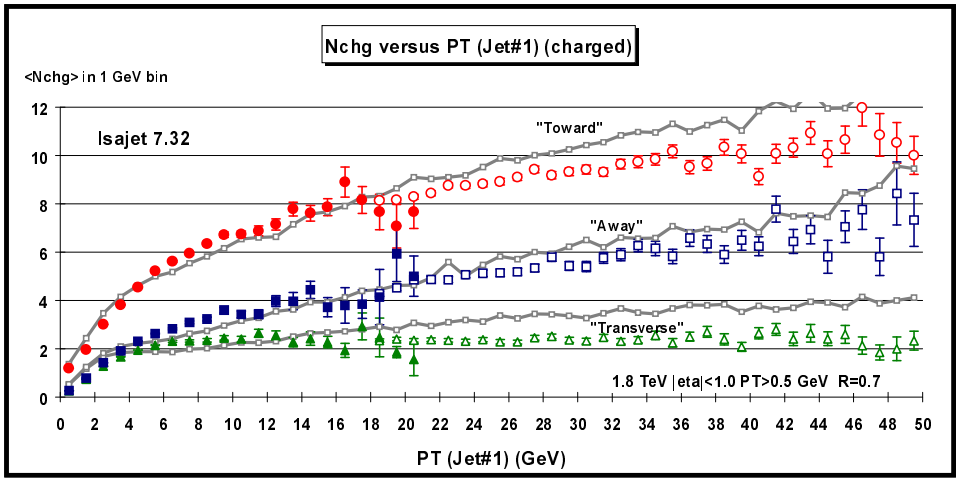

Fig. 5.15. Data from Fig. 5.9 on the average number of charged particles ($P_T > 0.5$ GeV and $|\eta| < 1$) as a function of PT(jet#1) (*leading jet*) for the three regions defined in Fig. 5.8 compared with the QCD "hard" scattering Monte-Carlo predictions of Isajet 7.32. Each point corresponds to the "toward", "transverse", or "away" $\langle N_{chg} \rangle$ in a 1 GeV bin. The theoretical predictions have been corrected for the CTC efficiency.

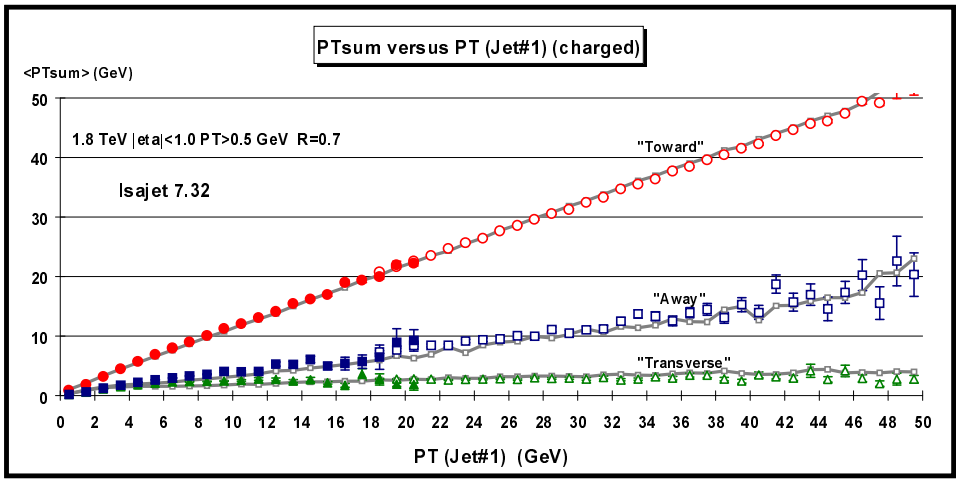

Fig. 5.16. Data from Fig. 5.11 on the average *scalar* P_T sum of charged particles with $P_T > 0.5$ GeV and $|\eta| < 1$ as a function of PT(jet#1) (*leading jet*) for the three regions defined in Fig. 5.8 compared with the QCD "hard" scattering Monte-Carlo predictions of Isajet 7.32. Each point corresponds to the "toward", "transverse", or "away" $\langle PT_{sum} \rangle$ in a 1 GeV bin. The theoretical predictions have been corrected for the CTC efficiency.

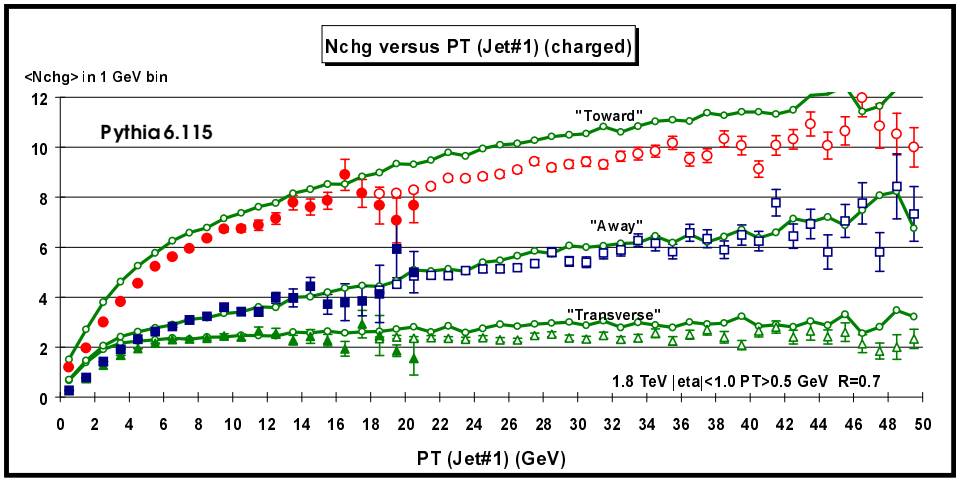

Fig. 5.17. Data from Fig. 5.9 on the average number of charged particles ($P_T > 0.5$ GeV and $|\eta| < 1$) as a function of PT(jet#1) (*leading jet*) for the three regions defined in Fig. 5.8 compared with the QCD "hard" scattering Monte-Carlo predictions of Pythia 6.115. Each point corresponds to the "toward", "transverse", or "away" $\langle N_{chg} \rangle$ in a 1 GeV bin. The theoretical predictions have been corrected for the CTC efficiency.

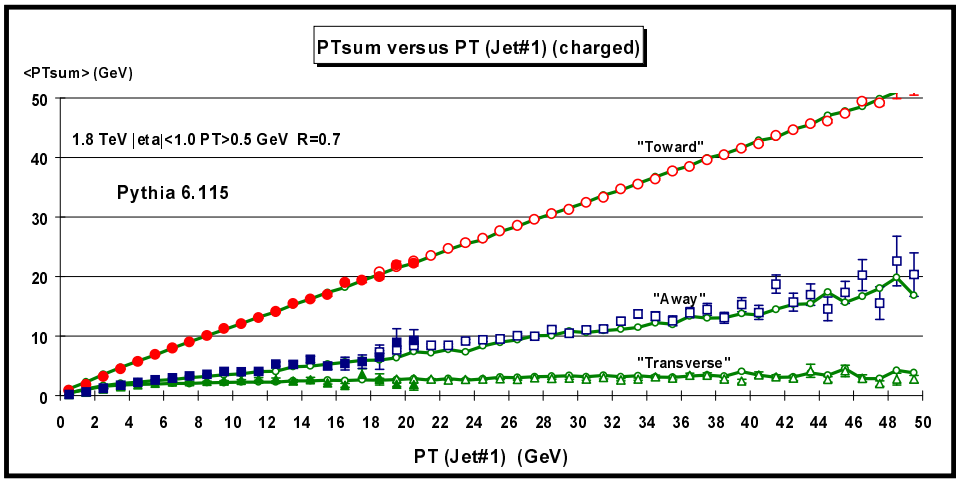

Fig. 5.18. Data from Fig. 5.11 on the average *scalar* P_T sum of charged particles with $P_T > 0.5$ GeV and $|\eta| < 1$ as a function of PT(jet#1) (*leading jet*) for the three regions defined in Fig. 5.8 compared with the QCD "hard" scattering Monte-Carlo predictions of Pythia 6.115. Each point corresponds to the "toward", "transverse", or "away" $\langle PT_{sum} \rangle$ in a 1 GeV bin. The theoretical predictions have been corrected for the CTC efficiency.

In Fig. 5.13 and Fig. 5.14 data on the $\langle N_{chg} \rangle$ and $\langle PT_{sum} \rangle$, respectively, as a function of P_T(jet#1) for the three regions are compared with the QCD "hard" scattering Monte-Carlo predictions of Herwig 5.9. Fig. 5.15 and Fig. 5.16 show the same comparison for Isajet 7.32, while Fig. 5.17 and Fig. 5.18 show the predictions of Pythis 6.115. The wiggles in the theoretical curves are due to the lack of statistics. Each theory curve contains 2,000,000 events corresponding to four 500,000 event runs with P_T(hard) > 3, 5, 10, and 20 GeV which then are

carefully fitted together to form the curves. The QCD Monte-Carlo models agree qualitatively but not precisely with the data. We now look more closely.

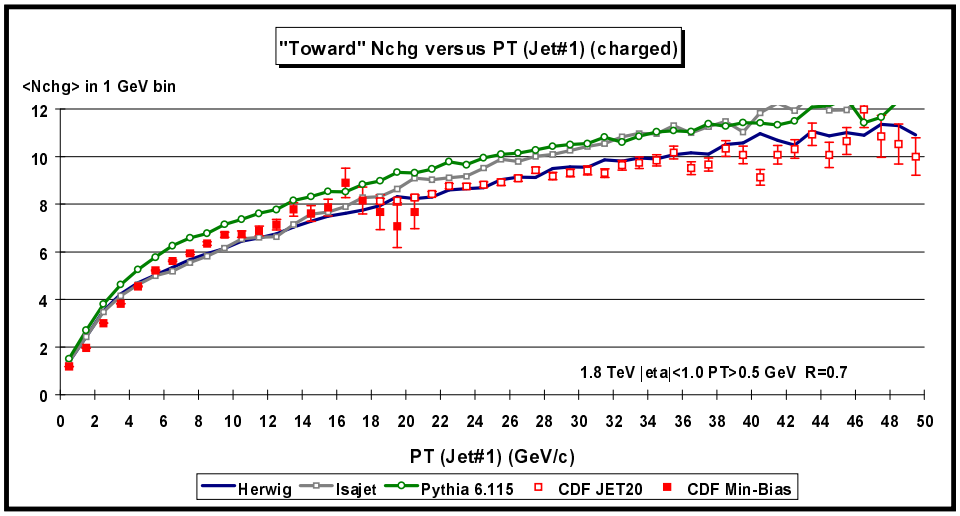

Fig. 5.19. Data from Fig.5.8 on the average number of charged particles ($P_T > 0.5$ GeV and $|\eta| < 1$) as a function of PT(jet#1) (*leading jet*) for the "toward" region defined in Fig. 5.8 compared with the QCD "hard" scattering Monte-Carlo predictions of Herwig 5.9, Isajet 7.32, and Pythia 6.115. Each point corresponds to the "toward" $\langle N_{chg} \rangle$ in a 1 GeV bin. The theoretical predictions have been corrected for the CTC efficiency.

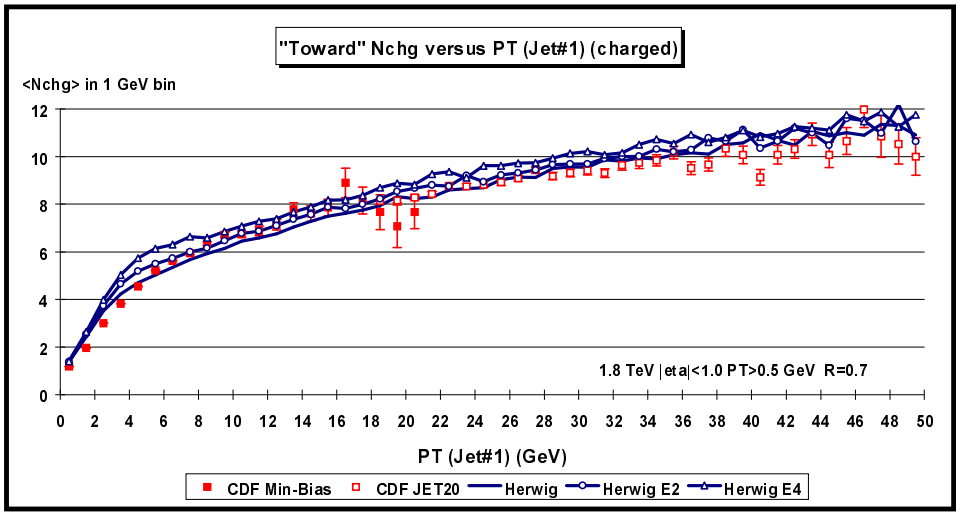

Fig. 5.20. Data from Fig.5.9 on the average number of charged particles ($P_T > 0.5$ GeV and $|\eta| < 1$) as a function of PT(jet#1) (*leading jet*) for the "toward" region defined in Fig. 5.8 compared with the QCD "hard" scattering Monte-Carlo predictions of three versions of Herwig 5.9 (default, ENSOF=2, ENSOF=4). Each point corresponds to the "toward" $\langle N_{chg} \rangle$ in a 1 GeV bin. The theoretical predictions have been corrected for the CTC efficiency.

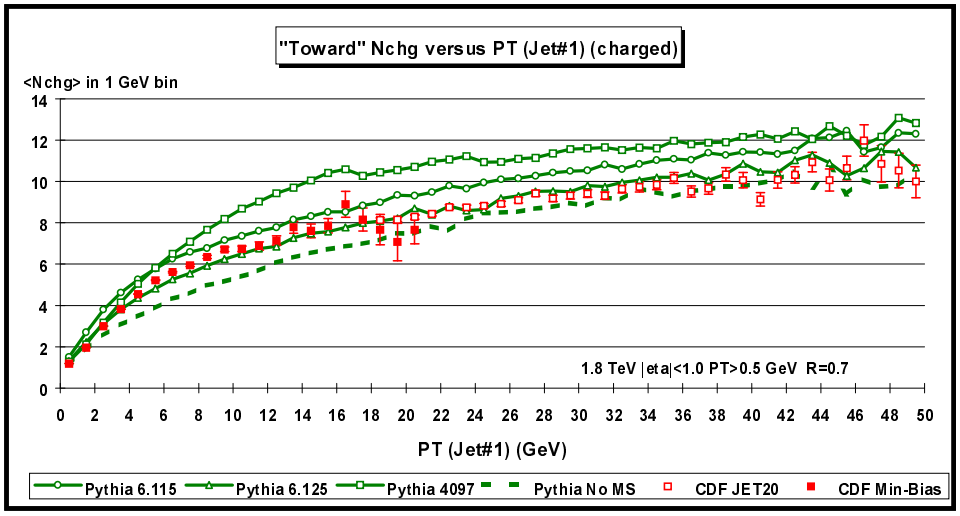

Fig. 5.21. Data from Fig.5.9 on the average number of charged particles ($P_T > 0.5$ GeV and $|\eta| < 1$) as a function of PT(jet#1) (*leading jet*) for the "toward" region defined in Fig. 5.8 compared with the QCD "hard" scattering Monte-Carlo predictions of four versions of Pythia (6.115, 6.125, 4097, and no multiple scattering). Each point corresponds to the "toward" <Nchg> in a 1 GeV bin. The theoretical predictions have been corrected for the CTC efficiency.

Fig. 5.19 compares the "toward" <Nchg> with the theoretical QCD "hard" scattering Monte-Carlo predictions of Herwig 5.9, Isajet 7.32, and Pythia 6.115. Fig. 5.20 compares the "toward" <Nchg> three versions of Herwig (default, ENSOF = 2, and ENSOF = 4, see Table 3). Fig. 5.21 compares the "toward" <Nchg> with four versions of Pythia (6.115, 6.125, 4097, and no multiple scattering, see Table 3).

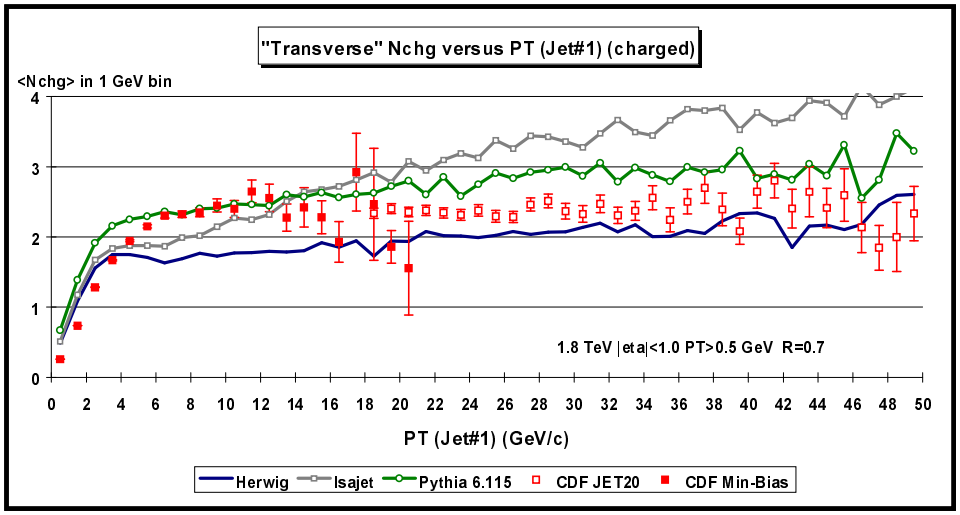

Fig. 5.22. Data from Fig.5.9 on the average number of charged particles ($P_T > 0.5$ GeV and $|\eta| < 1$) as a function of P_T(jet#1) (*leading jet*) for the "transverse" region defined in Fig. 5.8 compared with the QCD "hard" scattering Monte-Carlo predictions of Herwig 5.9, Isajet 7.32, and Pythia 6.115. Each point corresponds to the "transverse" <Nchg> in a 1 GeV bin. The theoretical predictions have been corrected for the CTC efficiency.

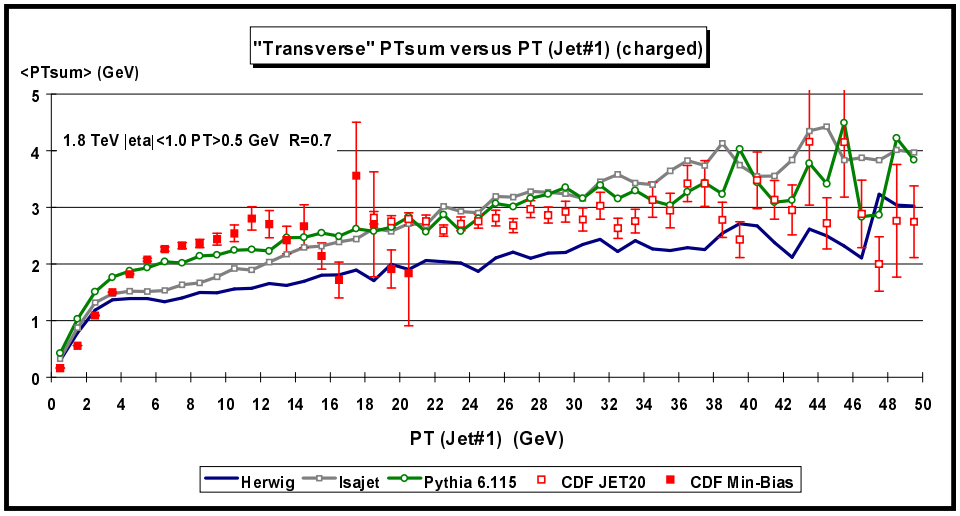

Fig. 5.23. Data from Fig.5.11 on the average *scalar* P_T sum of charged particles with $P_T >$ 0.5 GeV and $|\eta| < 1$as a function of P_T(jet#1) (*leading jet*) for the "transverse" region defined in Fig. 5.8 compared with the QCD "hard" scattering Monte-Carlo predictions of Herwig 5.9, Isajet 7.32, and Pythia 6.115. Each point corresponds to the "transverse" <PTsum> in a 1 GeV bin. The theoretical predictions have been corrected for the CTC efficiency.

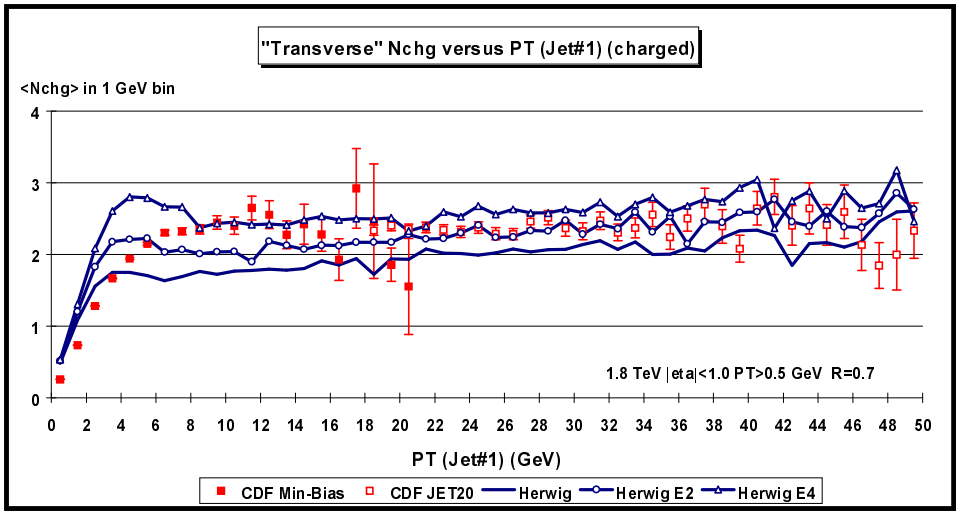

Fig. 5.24. Data from Fig.5.9 on the average number of charged particles ($P_T > 0.5$ GeV and $|\eta| < 1$) as a function of P_T(jet#1) (*leading jet*) for the "transverse" region defined in Fig. 5.8 compared with the QCD "hard" scattering Monte-Carlo predictions of three versions of Herwig 5.9 (default, ENSOF=2, ENSOF=4).. Each point corresponds to the "transverse" <Nchg> in a 1 GeV bin. The theoretical predictions have been corrected for the CTC efficiency.

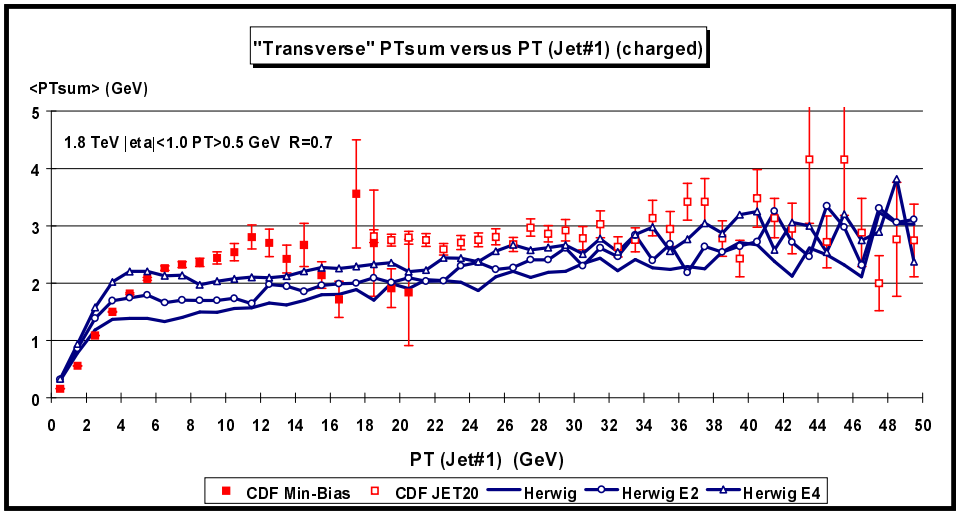

Fig. 5.25. Data from Fig.5.11 on the average *scalar* P_T sum of charged particles with $P_T >$ 0.5 GeV and $|\eta| < 1$as a function of P_T(jet#1) (*leading jet*) for the "transverse" region defined in Fig. 5.8 compared with the QCD "hard" scattering Monte-Carlo predictions of three versions of Herwig 5.9 (default, ENSOF=2, ENSOF=4). Each point corresponds to the "transverse" $\langle PT_{sum} \rangle$ in a 1 GeV bin. The theoretical predictions have been corrected for the CTC efficiency.

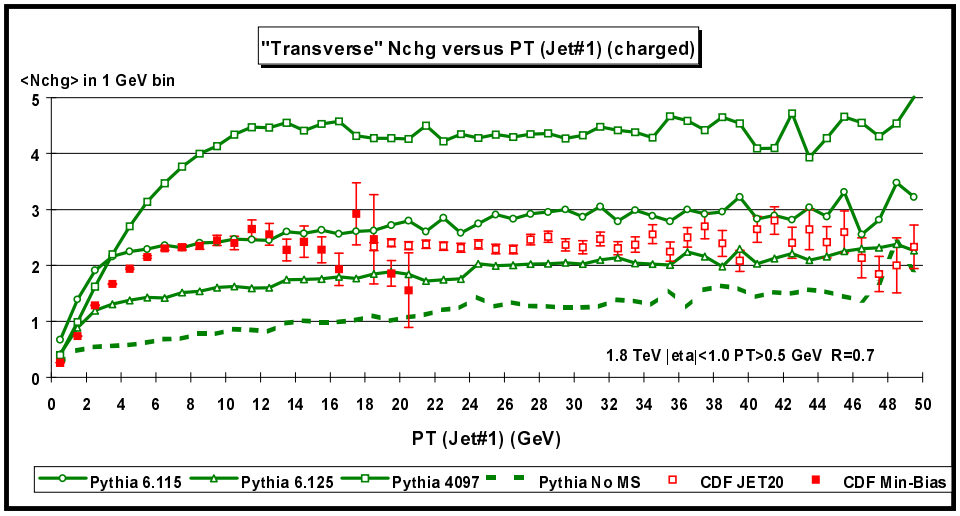

Fig. 5.26. Data from Fig.5.9 on the average number of charged particles ($P_T > 0.5$ GeV and $|\eta| < 1$) as a function of P_T(jet#1) (*leading jet*) for the "transverse" region defined in Fig. 5.8 compared with the QCD "hard" scattering Monte-Carlo predictions of four versions of Pythia (6.115, 6.125, 4097, and no multiple scattering). Each point corresponds to the "transverse" $\langle N_{chg} \rangle$ in a 1 GeV bin. The theoretical predictions have been corrected for the CTC efficiency.

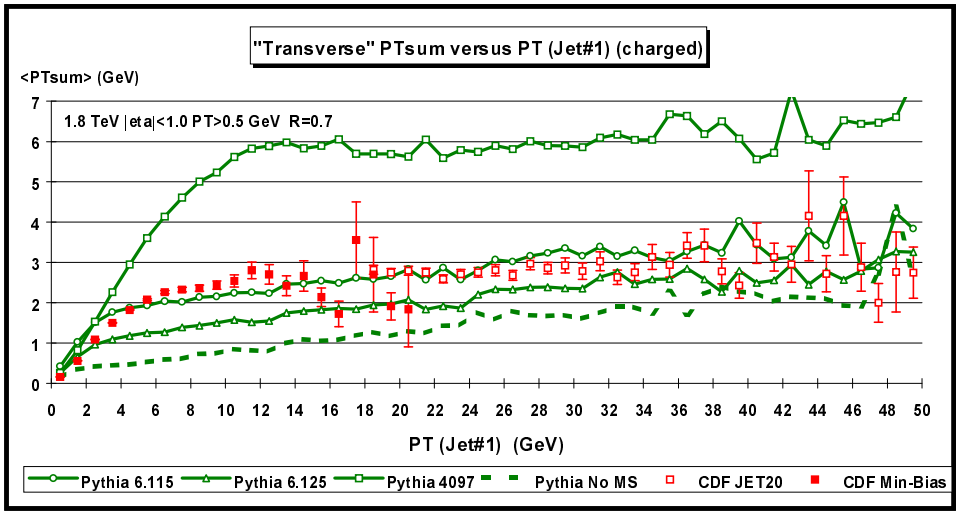

Fig. 5.27. Data from Fig.5.11 on the average *scalar* P_T sum of charged particles with P_T > 0.5 GeV and $|\eta| < 1$ as a function of P_T(jet#1) (*leading jet*) for the "transverse" region defined in Fig. 5.8 compared with the QCD "hard" scattering Monte-Carlo predictions of four versions of Pythia (6.115, 6.125, 4097, and no multiple scattering). Each point corresponds to the "transverse" <PTsum> in a 1 GeV bin. The theoretical predictions have been corrected for the CTC efficiency.

Fig. 5.22 and Fig. 5.23 compare the "transverse" <Nchg> and the "transverse" <PTsum>, respectively, with the QCD "hard" scattering Monte-Carlo predictions of Herwig 5.9, Isajet 7.32, and Pythia 6.115. Fig. 5.24 and Fig. 5.25 compare the "transverse" <Nchg> and the "transverse" <PTsum>, respectively, with three versions of Herwig (default, ENSOF = 2, and ENSOF = 4, see Table 3). Fig. 5.26 and Fig. 5.27 compare the "transverse" <Nchg> and the "transverse" <PTsum>, respectively, with four versions of Pythia (6.115, 6.125, 4097, and no multiple scattering, see Table 3).

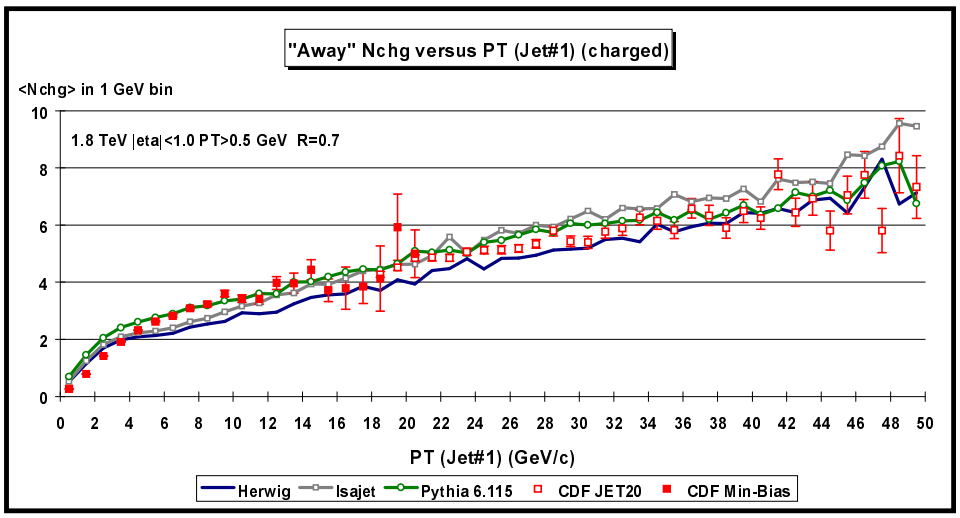

Fig. 5.28. Data from Fig.5.9 on the average number of charged particles (P_T > 0.5 GeV and $|\eta| < 1$) as a function of P_T(jet#1) (*leading jet*) for the "away" region defined in Fig. 5.8 compared with the QCD "hard" scattering Monte-Carlo predictions of Herwig 5.9, Isajet

7.32, and Pythia 6.115. Each point corresponds to the "away" <Nchg> in a 1 GeV bin. The theoretical predictions have been corrected for the CTC efficiency.

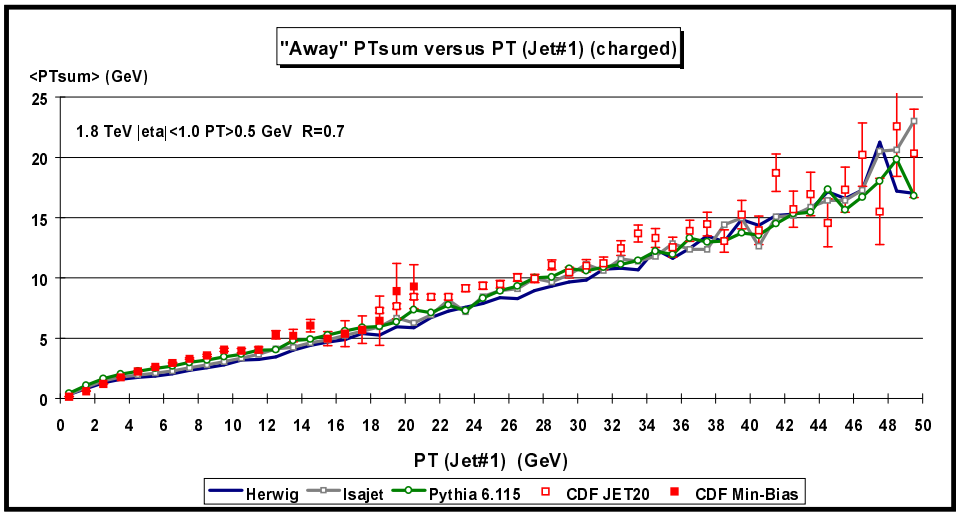

Fig. 5.29. Data from Fig.5.11 on the average *scalar* P_T sum of charged particles with $P_T >$ 0.5 GeV and $|\eta| < 1$as a function of P_T(jet#1) (*leading jet*) for the "away" region defined in Fig. 5.8 compared with the QCD "hard" scattering Monte-Carlo predictions of Herwig 5.9, Isajet 7.32, and Pythia 6.115. Each point corresponds to the "away" <PTsum> in a 1 GeV bin. The theoretical predictions have been corrected for the CTC efficiency.

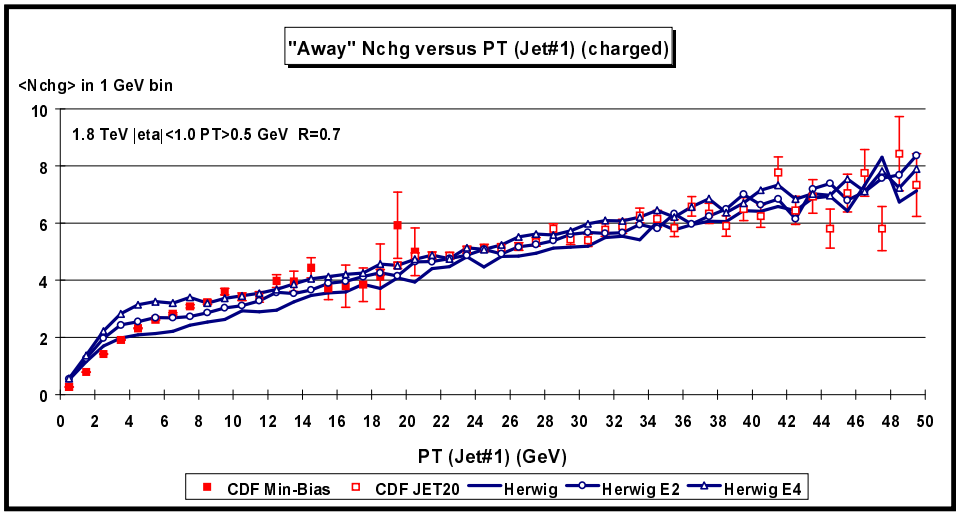

Fig. 5.30. Data from Fig.5.9 on the average number of charged particles ($P_T > 0.5$ GeV and $|\eta| < 1$) as a function of P_T(jet#1) (*leading jet*) for the "away" region defined in Fig. 5.8 compared with the QCD "hard" scattering Monte-Carlo predictions of three versions of Herwig 5.9 (default, ENSOF=2, ENSOF=4). Each point corresponds to the "away" <Nchg> in a 1 GeV bin. The theoretical predictions have been corrected for the CTC efficiency.

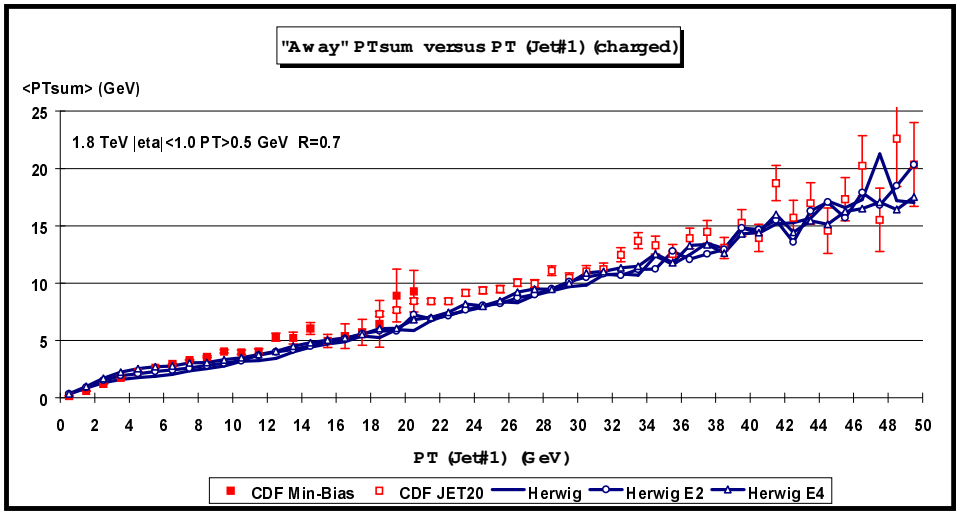

Fig. 5.31. Data from Fig.5.11 on the average *scalar* P_T sum of charged particles with P_T > 0.5 GeV and $|\eta| < 1$as a function of P_T(jet#1) (*leading jet*) for the "away" region defined in Fig. 5.8 compared with the QCD "hard" scattering Monte-Carlo predictions of three versions of Herwig 5.9 (default, ENSOF=2, ENSOF=4). Each point corresponds to the "away" <PT_{sum}> in a 1 GeV bin. The theoretical predictions have been corrected for the CTC efficiency.

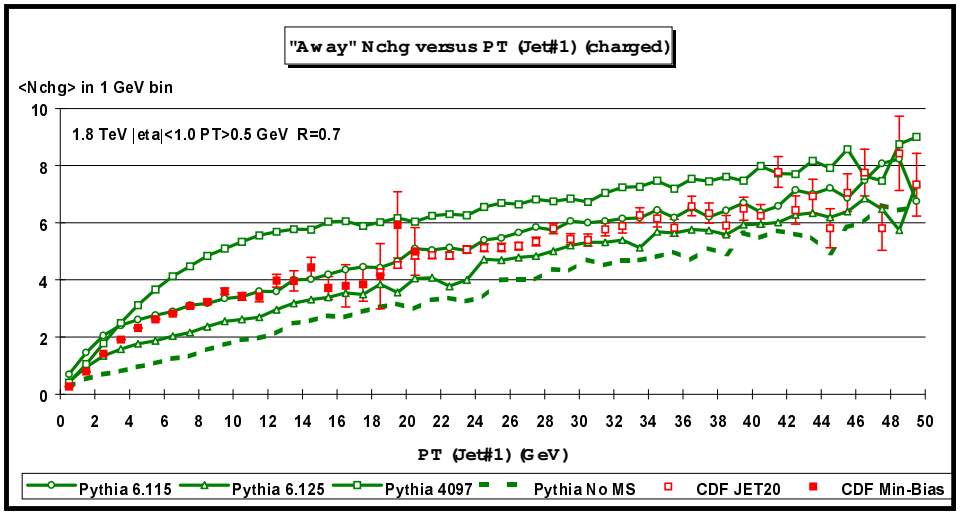

Fig. 5.32. Data from Fig.5.9 on the average number of charged particles (P_T > 0.5 GeV and $|\eta| < 1$) as a function of P_T(jet#1) (*leading jet*) for the "away" region defined in Fig. 5.8 compared with the QCD "hard" scattering Monte-Carlo predictions of four versions of Pythia (6.115, 6.125, 4097, and no multiple scattering). Each point corresponds to the "away" <N_{chg}> in a 1 GeV bin. The theoretical predictions have been corrected for the CTC efficiency.

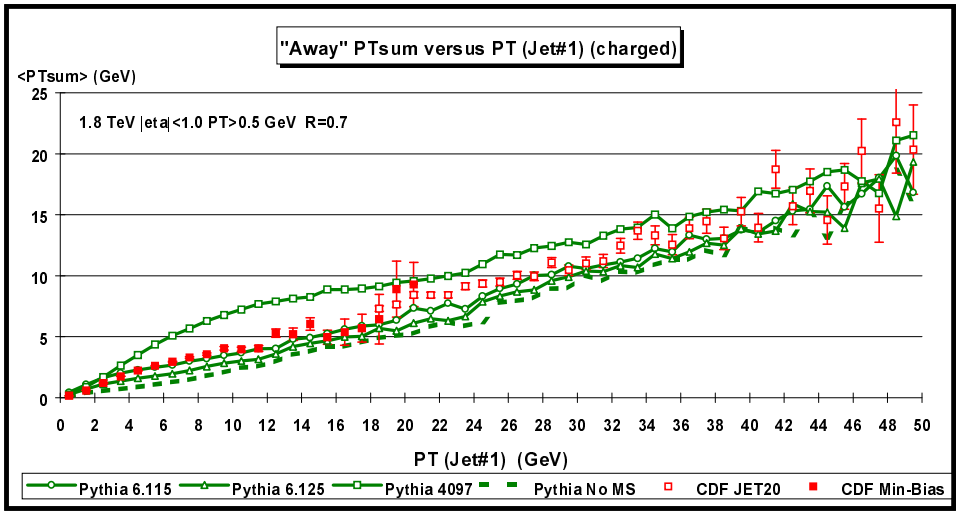

Fig. 5.33. Data from Fig.5.11 on the average *scalar* P_T sum of charged particles with $P_T >$ 0.5 GeV and $|\eta| <$ 1as a function of P_T(jet#1) (*leading jet*) for the "away" region defined in Fig. 5.8 compared with the QCD "hard" scattering Monte-Carlo predictions of four versions of Pythia (6.115, 6.125, 4097, and no multiple scattering). Each point corresponds to the "away" <PTsum> in a 1 GeV bin. The theoretical predictions have been corrected for the CTC efficiency.

Fig. 5.28 and Fig. 5.29 compare the "away" <Nchg> and the "away" <PTsum>, respectively, with the QCD "hard" scattering Monte-Carlo predictions of Herwig 5.9, Isajet 7.32, and Pythia 6.115. Fig. 5.30 and Fig. 5.31 compare the "away" <Nchg> and the "away" <PTsum>, respectively, with three versions of Herwig (default, ENSOF = 2, and ENSOF = 4, see Table 3). Fig. 5.32 and Fig. 5.33 compare the "away" <Nchg> and the "away" <PTsum>, respectively, with four versions of Pythia (6.115, 6.125, 4097, and no multiple scattering, see Table 3).

Clearly the "transverse" <Nchg> and the "transverse" <PTsum> are the most sensitive to the underlying event. Pythia with no multiple scattering does not have enough activity in the underlying event. Pythia 6.115 fits the "transverse" <Nchg> the best, but then overshoots slightly the "toward" <Nchg>. Pythia 4097 has way too many multiple parton interactions and does not agree with the data. Isajet has a lot of activity in the underlying event, but gives the wrong P_T(jet#1) dependence. Instead of a "plateau", Isajet predicts a rising "transverse" <Nchg> and gives too much activity at large P_T(jet#1) values. Herwig does not have enough activity in the underlying event and simply increasing the "underlying event" multiplicity enhancement factor, ENSOF, does not give the correct physics at low P_T(jet#1). It does increase the charged multiplicity in the "plateau", but the "turn on" of the plateau is not correct. If fact, none of the QCD Monte-Carlo models describe correctly the rise of the "transverse" region at low P_T(jet#1) values. Understanding the "turn on" of the underlying event plateau is the key to understanding the physics of what is going on.

VI. Summary and Conclusions

There is a tremendous amount of interesting physics in the Min-Bias data. At 1.8 TeV Min-Bias does not imply "soft" physics! There is a lot of QCD "hard" scattering in the Min-Bias data. Our summary and conclusions are as follows:

1. *"Soft" versus "Hard" Collisions*

The "Soft" Monte-Carlo models do not describe the Min-Bias data for $P_T > 0.5$ GeV and $|\eta| < 1$. This is because the "soft" models have no "hard scattering" and thus no jets and the Min-Bias data show "jet" structure. The QCD "hard scattering" Monte-Carlo models ($P_T(\text{hard}) > 3$ GeV) qualitatively fit the data for PTmax or $P_T(\text{jet\#1})$ greater than about 2 GeV. Below 2 GeV the data are a mixture of "hard" and "soft". To describe this region we will have to combine a model for the "soft" collisions with a QCD perturbative Monte-Carlo model for the "hard" collisions. We hope to present a superposition of "hard" and "soft" models that describes the data at low P_T in a future CDF note.

2. *The Evolution of Jets*

Jets are "born" somewhere around $P_T(\text{jet})$ of about 1 GeV with, on the average, about 2 charged particles and grow to, on the average, about 10 charged particles at 50 GeV. Table 4 summarizes a "typical" parton-antiproton collider events with $P_T(\text{jet\#1}) = 20$ GeV. The QCD "hard" scattering Monte-Carlo models agree qualitatively well with the multiplicity distribution of the charged particles within a "jet", the flow of charged multiplicity and PTsum around the jet direction, the "size" of the jets, and with the jet "fragmentation functions". In fact, the QCD "hard" scattering Monte-Carlo models agree as well with 2 GeV jets as they do with 50 GeV jets! The jets in the Min-Bias data are simply the extrapolation (*down to small* P_T) of the high transverse momentum jets observed in the JET20 data. For a fixed $P_T(\text{hard})$, the QCD "hard" scattering cross section grows with increasing collider energy. As the center-of-mass energy of a proton-antiproton collision grows, "hard" scattering becomes a larger and larger fraction of the total inelastic cross section. Our analysis suggests that at 1.8 TeV "hard" scattering makes up a sizable part of the "hard core" inelastic cross section and a lot of min-bias events have 2 GeV or 3 GeV jets. Scaling up to the LHC energy implies that, at the LHC, a lot of "min-bias" events will contain 20 GeV jets!

Table 4. Summary of a "typical" proton-antiproton collider event (charged particles, $P_T > 0.5$ GeV, $|\eta| < 1$) with $P_T(\text{jet\#1}) = 20$ GeV. Jets are defined as simple circular regions in η-ϕ space with R = 0.7. The numbers have not been corrected for efficiency.

Observable	Average Value
Overall number of charged particles, Nchg	15.1
Nchg "toward" jet#1	8.2
Nchg "transverse" to jet#1	2.4
Nchg "away" from jet#1	4.5
Overall *scalar* PTsum	32.2 GeV
PTsum "toward" jet#1	21.9 GeV
PTsum "away" from jet#1	2.6 GeV
PTsum "away" from jet#1	7.7 GeV
Maximum PT charged particle, PTmax	9.0 GeV
Number of charged particles in jet#1	6.4
Radius R containing 80% of jet#1 particles	0.3
Radius R containing 80% of jet#1 PT	0.2
Number of jets (*excluding jet#1*) with PT(jet) > 0.5 GeV	4.5
Number of jets (*excluding jet#1*) with PT(jet) > 2 GeV	1.6
Number of jets (*excluding jet#1*) with PT(jet) > 5 GeV	0.6
Transverse momentum of jet#2	7.0 GeV
Transverse momentum of jet#3	2.5 GeV

2. *The "Underlying Event"*

A "hard scattering" collider event consists of large transverse momentum outgoing hadrons that originate from the large transverse momentum partons (*i.e.* outgoing jets) and also hadrons that originate from the break-up of the proton and antiproton (i.e. "beam-beam remnants"). The "underlying event" is formed from the "beam-beam remnants", initial-state radiation, and possibly from multiple parton interactions. The Min-Bias data show that the charged multiplicity and PTsum in the "underlying event" grows very rapidity with PTmax or with P_T(jet#1) and then forms an approximately constant "plateau". The height of this "plateau" is at least twice that observed in "soft" collisions at the same corresponding energy. None of the QCD Monte-Carlo models correctly describe the structure of the underlying event seen in the data. Herwig 5.9 and Pythia 6.125 do not have enough activity in the underlying event. Pythia 6.115 has about the right amount of activity in the underlying event, but as a result produces too much overall multiplicity. Isajet 7.32 has a lot of activity in the underlying event, but with the wrong dependence on P_T(jet#1). Pythia 4097 produces way too much activity in the underlying event.

Accurate predictions of detector occupancies and physics backgrounds in Run II depend on the correct modeling of min-bias interactions and the underlying event. This note contains roughly 100 plots! However, there are many more interesting Min-Bias plots to show before one can completely see the overall story. Soon, we hope to write a second CDF note on the physics of the Min-Bias data that examines the differential cross sections in P_T, PTmax, PTsum, PT(jet), and PT(jet#1).

Acknowledgments

The Bologna Group (N. Moggi, F. Rimondi, and Z. Zucchelli) have been very helpful in this analysis.

References

[1] F. Paige and S. Protopopescu, BNL Report, BNL38034, 1986 (unpublished), version 7.32.

[2] G. Marchesini and B. R. Webber, Nucl. Phys **B310**, 461 (1988); I. G. Knowles, Nucl. Phys. **B310**, 571 (1988); S. Catani, G. Marchesini, and B. R. Webber, Nucl. Phys. **B349**, 635 (19991).

[3] Rockefeller Minimum Bias Generator, S. Belforte, J. Grunhaus, and T. Chapin, CDF Note #256.

[4] T. Sjostrand, Phys. Lett. **157B**, 321 (1985); M. Bengtsson, T. Sjostrand, and M. van Zijl, Z. Phys. **C32**, 67 (1986); T. Sjostrand and M. van Zijl, Phys. Rev. **D36**, 2019 (1987).

[5] Paris Sphicas and Dejan Vucinic, "On Using Pythia to Model the Underlying Event in B and W Events", CDF Note, CDF/ANAL/BOTTOM/CDFR/4097, 1998.